Improving Immune Checkpoint Blockade Efficacy Through the Design and Optimization of 5'-Triphosphate RNA Loaded Nanoparticles

By

Max E. Jacobson

Dissertation

Submitted to the Faculty of the

Graduate School of Vanderbilt University

in partial fulfillment of the requirements

for the degree of

DOCTOR OF PHILOSOPHY

in

Chemical and Biomolecular Engineering

May 31st, 2020

Nashville, TN

Approved By:

Prof. John Wilson

Prof. Ethan Lippmann

Prof. Jeffrey Rathmell

Prof. Rebecca Cook

Prof. Scott Guelcher

Acknowledgments

I would like to thank my advisor Professor John T. Wilson for his patience guidance throughout my graduate school career. I appreciate your creative ideas as well as your constant willingness to discuss project progress. I feel privileged to have been able to work in this accepting, supportive environment. I would like to thank the other graduate students in my lab and my year for their collaboration and support. I would like to give a special thanks to the ChBE staff, particularly Angie and Felisha, who have helped me throughout all stages of my graduate career. I would like to thank the Duvall lab as well as the Pyle lab from Yale university for their collaboration to my projects. I would also like to thank my family and friends, particularly a certain James, for supporting me throughout this venture. Finally, I would like to thank the members of my committee, Professors Rebecca Cook, Ethan Lippmann, Jeffrey Rathmell, and Scott Guelcher, for their constant support and crucial advice for my project.

Contents

List of Figures

List of Tables

List of Abbreviations

CTLA-4: cytotoxic T-lymphocyte-associated protein 4

PD-L1: Programmed death-ligand 1

PD-1: Programmed cell death protein 1

TIL: Tumor infiltrating lymphocyte

ICB: Immune checkpoint blockade

CTL: Cytotoxic T Lymphocyte

TME: Tumor microenvironment

TNBC: Triple negative breast cancer

APC: antigen presenting cell

PRR: Pattern recognition receptor

PAMP: Pathogen associated molecular pattern

MHC I/II: Major histocompatibility complex I/II

IFN-I: Type-I IFN

TAM: Tumor-associated macrophage

MDSC: Myeloid derived-suppressor cell

siRNA: Silencing RNA

STING: Stimulator of interferon genes

cGAMP: 2',5-3'5' cyclic guanosine monophosphate–adenosine monophosphate

RIG-I: Retinoic acid inducible gene-I

MAVS: Mitochondrial antiviral signaling protein

IRF: Interferon regulatory factor

ISG: Interferon stimulated gene

TBK1: Serine/Threonine-Protein Kinase

IKKϵ: Inhibitor Of Nuclear Factor Kappa B Kinase Subunit Epsilon

3pRNA/5'ppp RNA: 5'-Triphosphate RNA

OH-RNA: 5'-Hydroxyl RNA control

scrRNA: Scrambled RNA control

PEI: Polyethyleneimine

DMAEMA: Dimethylaminoethyl methacrylate

DEAEMA: Diethylaminoethyl methacrylate

BMA: Butyl methacrylate

PAA: Propylacrylic acid

PEG: Poly(ethylene glycol)

NP: Nanoparticle

NP_c: Control nanoparticle

D-PDB: DMAEMA-b-PAA-c-DMAEMA-c-BMA

TLR: Toll-like receptor

ODN: Oligodeoxynucleotide

BMDM: Bone marrow-derived macrophage

BMDC: Bone marrow-derived dendritic cell

qRT-PCR: Quantitative real-time polymerase chain reaction

IT: Intratumoral

s.c.: Subcutaneous

i.v.: Intravenous

CR: Complete responses

EC_{50}: 50% effective concentration

ANOVA: Analysis of variance

IVIS: *In vivo* imaging system

NMR: Nuclear magnetic resonance

GPC: Gel permeation chromatography

Chapter 1

Introduction

Background and Motivation

In the presence of infection, wounds, or inflammation, cells secrete factors known as cytokines and express surface proteins in order to control immune responses.[1,2] Typically, infection induces the production of pro-inflammatory cytokines to recruit and activate immune cells, resulting in cytoxic lymphocyte (CTL) mediated elimination of pathogens and infected cells, and trauma caused by wounds or inflammation induces the production of anti-inflammatory cytokines to limit deleterious effects of sustained inflammatory signaling.[3] Tumors, however, recruit a milieu of cells to secrete anti-inflamatory, immunosupressive cytokines, disabling immune mediate elimination of cancer through limiting the lymphocyte count in tumors as well as deactivating Tumor specific T cells.[4] Cancer immunotherapies aim to abrogate the anti-(tumor infiltrating Lymphocyte) (TIL) activity or the immunosuppressive signaling of the tumor microenvironment (TME). Upon T cell activation in the TME, T cells bind to cell-intrinsic inhibitory receptors referred to as "immune checkpoints" that signal for apoptosis of any lymphocytes that could eliminate cancer cells.[5] Normally these checkpoints are key for maintaining self-tolerance and controlling the duration of an immune response, however, tumors harness these receptors to develop immune evasion.[6] Immune checkpoint blockade refers to cancer immunotherapies that utilize antibodies to target and neutralize immune checkpoint receptors. These proteins include: Ipilimumab that targets cytotoxic T-lymphocyte-associated protein 4 (CTLA-4), Atezolizumab that targets

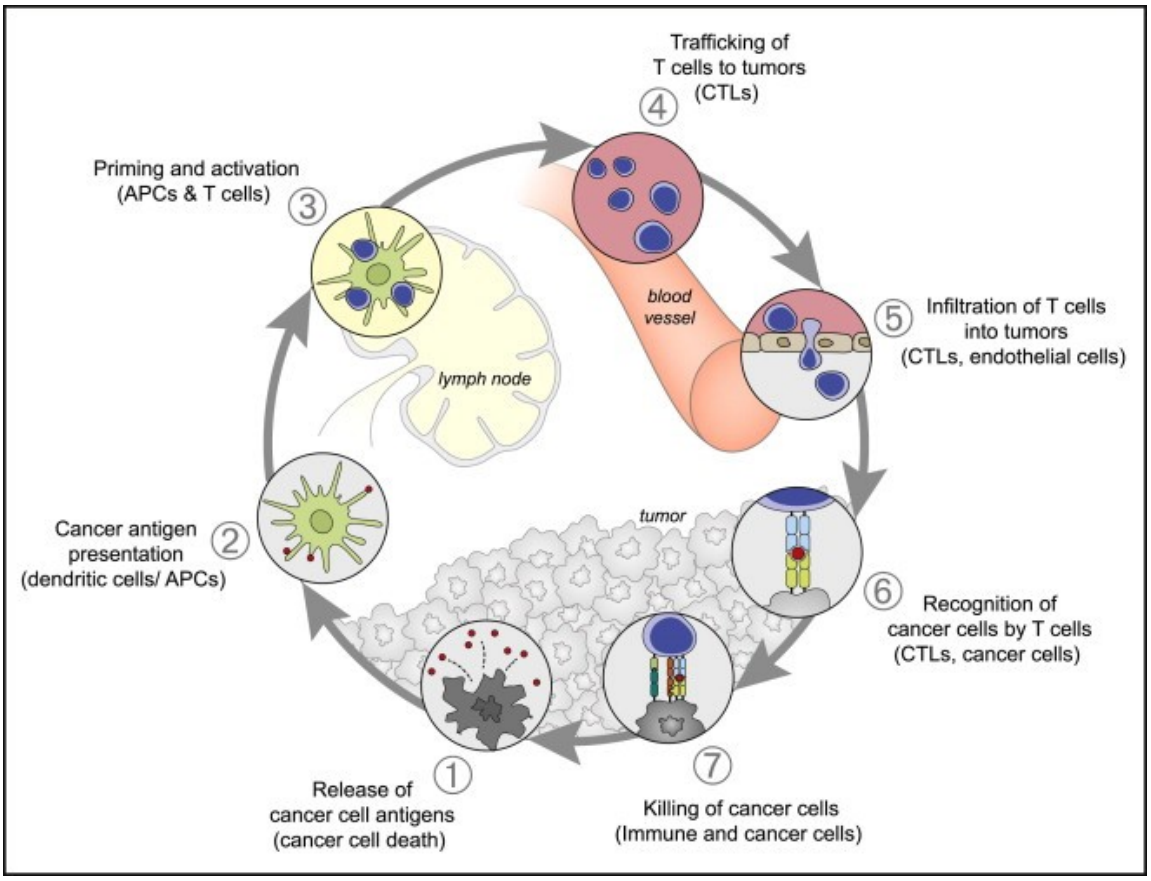

Figure 1.1: **The cancer immunity cycle.**
The generation of immunity to cancer is self-propagating, leading to an accumulation of immune-stimulatory factors that should amplify and broaden T cell responses. The cycle is also characterized by inhibitory factors, including checkpoint inhibitors, that lead to immune regulatory feedback mechanisms which can halt the development or limit the immunity. This cycle can be divided into seven major steps, starting with the release of antigens from the cancer cell and ending with the killing of cancer cells. Each step is described above, with the primary cell types involved and the anatomic location of the activity listed. Reproduced with permission by Cell Press.

programmed death ligand 1 (PD-L1), and Pembrolizumab that targets programmed cell death protein 1 (PD-1).[7] Immune checkpoint blockade therapy (ICB) permits TILs to kill cancer cells, thus enabling the development of anti-tumor immunity as illustrated in the cancer immunity cycle (Figure 1, Figure 2).[8,9] Out of the existing cancer immunotherapies, immune checkpoint blockade (ICB) is the most developed, with checkpoint inhibiting monoclonal antibodies broadly approved across multiple cancer cell types.[10] While ICB is broadly applicable among many different types of cancer, breast cancer showcases its strengths and challenges. Breast cancer is the most commonly diagnosed cancer in the United States for women and the second highest in cancer mortality. In 2012, approximately 1.65 million women were newly diagnosed with breast cancer worldwide and 542,000 women suffered breast cancer related deaths.[11] Breast cancer mortality in the United States has decreased with the development of standardized operative procedures for surgical removal of breast tumors as well as systemic application of radiotherapy, endocrine therapy, and chemotherapy.[12] The suite of developed treatments for breast cancer is expansive because tumors are dynamic and heterogeneous entities that represent a diverse collection of molecular signatures, resulting in widely differential treatment results.[13] Some conditions that may affect treatment efficacy include expression levels of specific receptors (e.g. estrogen, progesterone, and human epidermal growth factor 2), lymphocytes critical for tumor cell killing and development of anti-tumor immunity, and whether the tumor has progressed from the primary cite to form axillary tumors.[14] Tumors expressing increased receptors for these growth factors and hormones may be treated with endocrine and kinase inhibitors. In triple negative breast cancer (TNBC) that lacks over-expression of common endocrine therapy targets tumor treatment may only include extensive radiotherapy and

chemotherapy.[15] The 5-year survival rate for breast cancer patients in the United States was 98.6% for cases where tumors were confined to the primary site and 83.8% if the tumor had spread only to regional lymph nodes. However once metastasized, the 5-year survival rate of patients plummeted to 23.3%.[16] These statistics indicate a worrying trend for all cancer treatments; cancer metastasized beyond the local lymph nodes is rarely treatable. In the United States 90% of cancer related deaths are due to metastatic recurrence.[17] In a randomized study it was shown that in cases where the tumor was contained to the primary site only 11% of patients still developed recurrent breast cancer after breast tumor removal and radiotherapy.[12] Taken together as a whole, these statistics clearly demonstrate a need for a new approach to treating cancer that prevents metastasis and is capable of treating already metastasized tumors.

Treatment of hormone receptor positive or human epidermal growth factor 2 positive breast cancer with targeted endocrine therapies result in robust responsiveness in patients and significantly improved 5-year survival rates.[15] The most practiced treatment for breast tumors with low expression of receptors targeted by endocrine therapies is surgical removal coupled with chemotherapy and radiotherapy; however, this treatment may not prevent recurrence, and relies on specific gene expression in a heterogenous TME for efficacy.[13] RNA immunotherapeutics are promising alternatives and enhancers to chemotherapy, radiotherapy, and ICB therapy.[18] Silencing RNA (siRNA) has the capability to suppress key drivers in immunosuppression in the TME.[19] In addition, virus-mimicking RNA can activate innate immunity to further enhance development of anti-tumor immunity.[20] These and other RNA immunotherapeutics need to reach their targets in the cell cytosol to be effective. Delivery barriers are preventing

therapeutic RNA from reaching their target receptors, limiting relevancy in clinical trials. These include nuclease degradation, low cellular uptake, endosomal recycling, and lysosomal fate.[21] Environmentally responsive polymers – often referred to as 'smart' polymers - formulated with immunotherapeutic RNA can overcome these delivery challenges.[22,23] In order to improve upon the shortcomings of surgical removal coupled with chemotherapy or radiotherapy, immunotherapies are being developed and tested for treating cancer and preventing metastatis.

The Innate Immune Response to the Tumor Microenvironment

The immune system is a powerful tool for eliminating pathogens and establishing a memory response in case of recurrence. The term innate immunity includes general immune responses that are the immediate first line of defense against pathogens. Adaptive immunity describes antigen-specific immunity mediated by T lymphocytes and B lymphocytes.[24] Recognizing signatures of infectious microbes is a key role of the innate immune system. Antigen presenting cells (APCs) can sense invading pathogens using a series of molecular sensors referred to as pattern recognition receptors (PRRs).[25] These signatures are referred to as pathogen associated molecular patterns (PAMPs) and include lipids, lipoproteins, proteins, and nucleic acids.[26] PRRs can be found on cell membranes, endosomal membranes, and inside cell cytosols. Activating PRRs can lead to the production of inflammatory cytokines and chemokines for immunogenic signaling and lymphocyte recruitment, anti-viral type-1 interferons (IFN-I), and activation of pro-apoptotic genes.[27] The production of cytokines triggered by PRR activation is important for maintaining host-microbial homeostasis and inducing anti-microbial defense mechanisms through adaptive immunity.[28] T cells activate upon binding simultaneous T cell receptor and

antigen epitope binding in the major histocompatibility complex (MHC). Cytotoxic CD8+ lymphocytes are activated by MHC-I peptides and CD4+ lymphocytes are activated upon MHC-II binding.[29]

Activation of T cells result in three sequential courses of action: i) antigen specific clonal expansion for the immediate elimination of the pathogen, followed by ii) a contraction phase to lower T cell count and finally, iii) long term maintenance of antigen-specific T cells in the memory phase.[30] The immune system can be harnessed as a powerful tool for cancer elimination through a process known as the cancer immunity cycle, a self-propagating process to develop anti-tumor immunity (Figure 1).[9] Essentially, through detection of pathogenic cancer cells, the immune system begins to mount an innate immune response, producing cytokines and chemokines to activate antigen presenting cells and to recruit lymphocytes to the site of the tumor, respectively, as well as initiating natural killer cell mediated tumor cell death. This allows for the processing and presentation of cancer antigens by activated antigen presenting cells, resulting in the expansion of cytotoxic lymphocytes capable of recognizing and specifically eliminating tumor cells.[9] This process, however, is inhibited at the tumor site by an immunosuppressive TME because of multiple factors including secretion of immune suppressing factors in the TME, a dearth of cytotoxic lymphocytes in the tumor, or an inability to process or detect tumor antigens. These factors render the body's immune system is unable to properly process or eliminate cancer cells without some form of treatment.[31]

Tumors apply an arsenal of immune evasion techniques to avoid detection and processing by cytotoxic lymphocytes. In one example, tumor cells secrete proteins and cytokines that recruit immunosuppressive cells including tumor-associated macrophages (TAMs) and myeloid-derived suppressor cells (MDSCs).[32,33] These

cells secrete immunosuppressive cytokines that induce the production of regulatory T cells and apoptotic-inducing ligands as well as reactive oxygen species that will eliminate any TILs.[34] In addition, the physiological conditions of tumor growth, including rapid angiogenesis for solid tumors, hypoxia, activation of the glycolic pathway, and reduced local pH values promote overexpressed wound healing and immunosuppressive conditions.[35] The tumor often takes advantage of inducible regulatory circuits that control self-tolerance, homeostasis of myeloid cells, wound healing, and responses to dying cells.[36] Cancer immunotherapies aim to eliminate or circumvent the TME to generate anti-tumor immunity. This is generally achieved through two different approaches, which may both be used in tandem: i) elimination of anti-TIL mechanisms or ii) flipping the immunosuppressive TME into an immunosupportive environment.[37] These approaches will promote the CTL mediated elimination of tumor cells and the generation of anti-tumor memory to prevent metastasis.

Immune Checkpoint Blockade

Immune checkpoint blockade is transforming the treatment of an increasing number of cancer cell types. Treatment with checkpoint blockade is associated with longer lasting responses with reduced rates of metastasis and recurrence in preclinical murine models, leading to clinical testing and eventually approval.[38,39] In addition, this therapy is administered systemically, which improves its efficacy for treatment of metastasized tumors.[40] Unfortunately, a number of patients have not responded well to clinical trials for ICB. ICB is associated with immune related adverse events, including fatigue or fever, organ-specific damage leading to rash, colitis, pneumonitis, and adrenal or thyroid insufficiency.[41–43] In addition, a majority

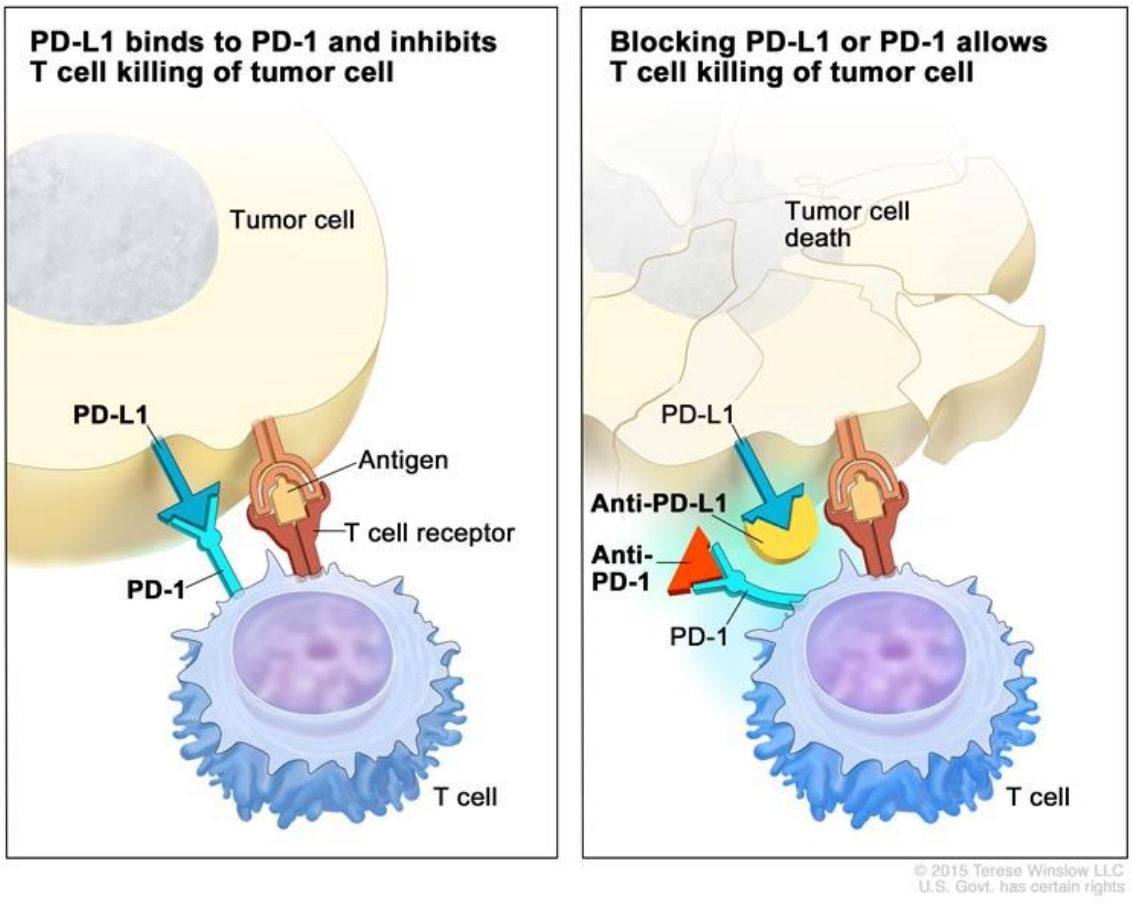

Figure 1.2: **Immune checkpoint blockade.**
Checkpoint proteins, such as PD-L1 on tumor cells and PD-1 on T cells, help keep immune responses in check. The binding of PD-L1 to PD-1 keeps T cells from killing tumor cells in the body (left panel). Blocking the binding of PD-L1 to PD-1 with an immune checkpoint inhibitor (anti-PD-L1 or anti-PD-1) allows the T cells to kill tumor cells (right panel). Reproduced with permission from Teresa Winslow LLC.

of patients do not respond to checkpoint blockade or develop a resistance to ICB therapy over time.[44] This is due to suppression of cytotoxic lymphocyte (CTL) development and count caused by immunosuppressive signaling in the TME of some tumors, resulting in phenotypes including downregulated major histocompatibility complex-I expression, mutation of key co-recognition receptors, and absence of tumor antigen, rendering checkpoint targeting ineffective.[45] To further complicate ICB, key biomarkers for checkpoint blockade efficacy in the tumor microenvironment are still mostly unknown, with the exception of some key genes including PD-L1.[46]

Owing to its ability to treat some solid tumor types, ICB is a very promising treatment for TNBC, which is most commonly treated using tumor excision and chemotherapy. There are several ICBs in clinical development for the treatment of TNBCs (Table 1). May emerging ICBs are currently FDA approved for metastatic melanoma, non-small cell lung cancer, and other solid tumors, Atezolizumab was FDA approved for use in patients diagnosed with early as well as late stage TNBC this year as a monotherapy and in combination with the chemotherapeutic agent nab-paclitxel.[47,48] As interest in immune checkpoint blockade has exponentially increased, a mechanism for the cause of unresponsive patients has been partially elucidated. Specifically, this has led to the understanding that PD-1 and PD-L1 are important targets for TNBC therapies because of a demonstrated increased immune cell infiltration in TNBC tumors.[49] Further, the TME is highly immunosuppressive in patients unresponsive to ICB. This realization has motivated a need for treatments immunotherapies to counter TME immunosuppression and transform the TME into a hotbed of anti-tumor immune activity.

In addition to expanding the reduced treatment options available for TNBC because of low expression of common endocrine therapy targets, ICB has the

potential to affect a greater fraction of patients because of genes targeted by immunotherapies in TNBC tumors.[50] Out of all available ICB, Atezolizumab, a PD-L1 blocking monoclonal antibody, has had the most success in clinical trials and is approved for clinical breast cancer treatment as a monotherapy and in combination with specific chemotherapeutics.[51–54] In addition, phase III clinical trials of Atezolizumab in combination with chemotherapy has been shown to increase median survival of metastatic TNBC patients by 2.6 months for patients with PD-L1 positive tumors and by 1.7 months for patients with PD-L1 negative tumors.[47] Although these results are promising, treatment utilizing Atezolizumab or other monoclonal antibodies for ICB is associated with autoimmune based and occasionally life-threatening side effects.[38] Some of the side effects reported include enterocolitis, gastritis, colitis, arthritis, hypothyroidism, neutropenia, cardio toxicity, peripheral neuropathy, fatigue, anemia, and diarrhea. These side effects were previously reported to be common after treatment with monoclonal antibodies.[55] In the previously mentioned clinical study for Atezolizumab and Abraxane, instances of nausea, coughing, neutropenia, pyrexia, and hyperthyroidism were at least 5% greater than Abraxane alone. In addition, the dual therapy increased the occurrence of serious grade 3 and 4 adverse immune related effects by 6.5%. These immune related effects include increased neutropenia, decreased neutrophil count, peripheral neuropathy, fatigue, and anemia.[47] In order to circumvent the toxic side effects of those ICB therapies, other cancer immunotherapies are currently being developed. Moreover, ICB is only effective in the fraction of patients with already immunogenic tumor microenvironments. For example, in a phase we clinical trial of Nivolumab (anti-PD-1) used to treat advanced solid tumors, 59.5% (25/42) of patients exhibited PD-L1$^+$ tumors and 36% of patients with PD-L1$^+$ tumors responded to treatment,

while 0% of patients bearing PD-L1$^-$ tumors responded to treatment. citetop1 In addition, the presence of TILs is critical for ICB, as illustrated in Figure 1.[9,56] The immunosuppressive milieu of the TME can limit the number and efficacy of TILs, rendering ICB ineffective due to immunosuppressive signaling.[57] Therefore, regimens capable of transforming the TME into an inflammatory, immunosupportive microenvironment could enhance ICB efficacy.

Immunomodulatory Nucleic Acids in Cancer Therapy

In order to utilize cancer immunotherapies to eradicate and prevent metastases, treatments would need to induce anti-tumor immunity and generate memory T-cells through the cancer immunity cycle.[9] This type of treatment consists of viral particles, viral-like particles, or other immune modulators engenders an innate immune response and is referred to as *in situ* cancer vaccination.[63] While traditional vaccines and more recently subunit vaccines utilize viral particles with adjuvant, or carefully crafted delivery vehicles loaded with specific antigens and adjuvants for delivery to antigen presenting cells, *in situ* cancer vaccines aim to harness the immune system using modified virus particles, viral-like particles, or other immunomodulators directly applied to the tumor to change the immunogenic profile of the TME to enable the progression of the cancer immunity cycle.[21,64] As the understanding of immunity expanded, so did vaccine design. The characterization of antigen presentation through the major histocompatibility complex we and II (MHC-I and MHC-II) as well as cellular detection of viral motifs through pattern recognition receptors enabled the development of vaccines that elicit highly specific immune responses.[20,65] Subunit vaccines, typically including a choice antigen, one or more adjuvants to shape the immune response, and a delivery vector, are capable of

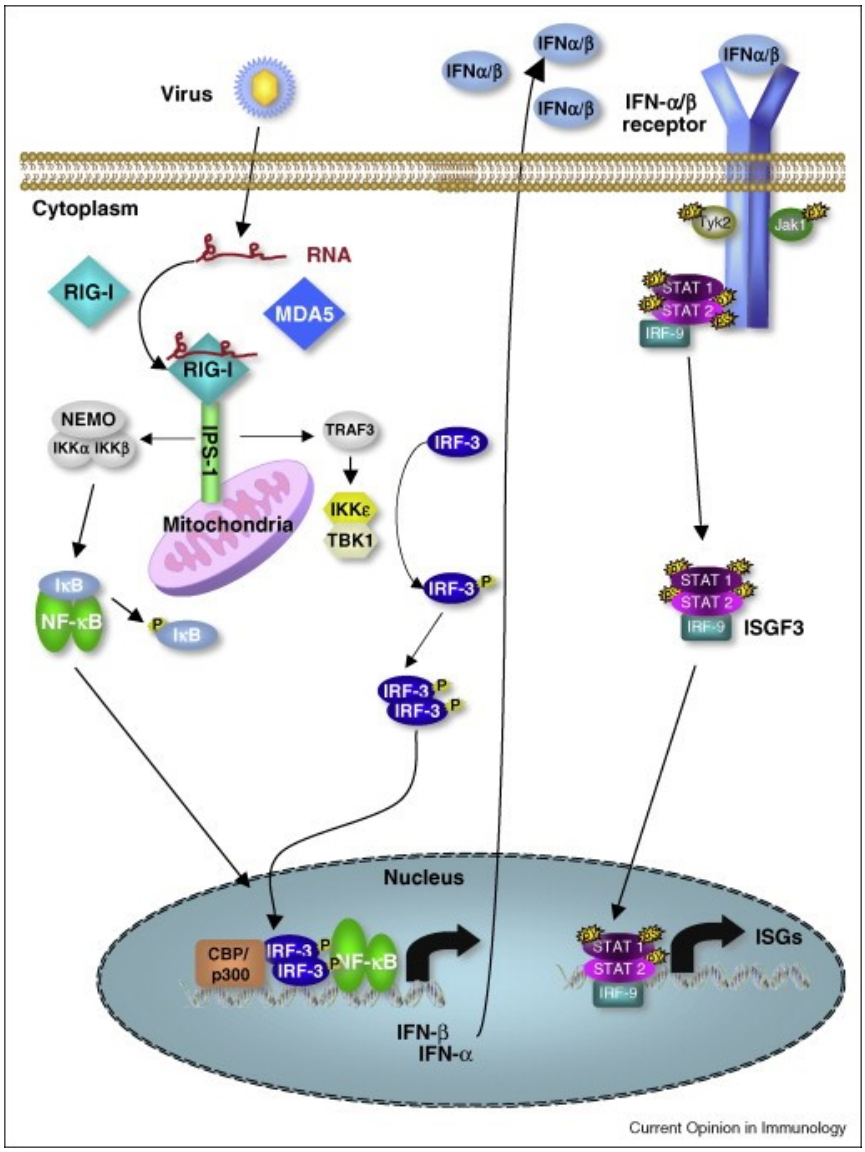

Figure 1.3: **The RIG-I immune surveillance pathway.**
Schematic demonstrating activation of RIG-I through detection of viral 3pRNA. RIG-I activation leads to activation of mitochondrial antiviral signaling protein (MAVS), which begins a signaling cascade, initiating the interaction of Inhibitor Of Nuclear Factor Kappa B Kinase Subunit Epsilon (IKKϵ) and Serine/Threonine-Protein Kinase (TBK1), followed by phosphorylation of the transcription factors Interferon regulatory factors (IRF) IRF3 and IRF7. Phosphorylated p-IRF3 and p-IRF7 are translocated into the nucleus, where they dimerize and bind to transcription factor binding sites of the IFNα and IFNβ. The autocrine and paracrine signaling caused by the production of type-I IFN results in the expression of hundreds of IFN stimulated genes (ISGs) as well as inflammatory genes to signal antiviral resistance.[61,62]

inducing a highly specific immune response.[21] By applying concepts used for subunit vaccine design, including utilizing a delivery vector and a viral-mimicking adjuvant to trigger a specific innate immune response, we can design *in situ* cancer vaccines that elicit a highly specific immune response to improve the efficacy of other established cancer immunotherapeutics, including ICB.

One potentially therapeutic target for *in situ* cancer vaccinations is the stimulator of interferon genes (STING).[66] Upon detection of cytosolic DNA, the enzyme cyclic-GMP-AMP synthase facilitates the synthesis of 2',5-3'5' cyclic guanosine monophosphate–adenosine monophosphate (cGAMP) to activate the STING pathway and initiate a cascade of pro-inflammatory, anti-viral cytokine signaling, including type 1 IFNs and chemokines.[67,68] STING activation is integral to developing anti-tumor immunity during cancer therapies.[69] Briefly, killed cancer cell debris is endocytosed by antigen presenting cells, as illustrated in the cancer immunity cycle steps 1 and 2 (Figure 1). Through this process, killed cancer cell DNA in the cell cytosol is detected, resulting and production of cGAMP and activation of the STING pathway. Activation of STING during this step enables progression of this cycle by secreting factors to activate APCs and both prime and later recruit Tumor-specific T cells, thereby enabling immunotherapies.[70] The role of STING activation in transforming the immunosupressive TME is highlighted by studies demonstrating STING-deficient mice exhibiting higher susceptibility to spontaneous formation of tumors, reduced antitumour T-cell immunity, as well as reduced efficacy of immunotherapies.[71,72] Our group has recently demonstrated that delivery of cGAMP improves checkpoint blockade treatment efficacy in a poorly immunogenic murine melanoma model.[44]

Retinoic acid inducible gene (RIG-I), as well as other similar RIG-I like receptors

(RLRs), are promising therapeutic targets for *in situ* cancer vaccinations. These receptors are cytosolic pattern recognition receptors that usually engage viral RNA to mount an innate immune response. RIG-I induction can initiate caspase recruitment domain mediated programmed cell death.[73] In addition, upon ligand binding RIG-I interacts with interferon-β promotor stimulator 1, promoting an inflammatory response through the downstream activation of the nuclear factor NF-κB and an anti-viral response through activation of interferon regulatory factor 3/7 (IRF 3/7) (Figure 3).[61,74] This response includes the production of type-1 IFNs, the production of Th1 cytokines, and chemokine production for the recruitment of T-cells directly to the tumor site, supporting three steps of the cancer immunity cycle: activation and priming of antigen presenting cells, CTL recruitment to the tumor site, and infiltration of CTLs into tumors.[9,75] Activating RIG-I also induces apoptosis in melanoma, lung, breast, and prostate cancer cells through the upregulation of TNF-related apoptosis inducing ligand and Noxa.[76,77] RIG-I is robustly expressed in most tissues, including cancer cells, and therefore can be targeted in almost any TME..[78,79] Recent studies have also shown that endogenous RIG-I activation is a critical pathway for immune mediated cell death of cancer cells, and that ICB loses efficacy in treated RIG-I deficient mice.[80] RIG-I and RLRs, as well as their downstream receptors, can be targeted using multiple nucleic acid or small molecule agonists. RIG-I and other RLRs are activated after binding short RNAs with a viral 5' Triphosphate motif (5'ppp RNA), a similar 5' diphosphate motif, or various lengths of poly(I:C) RNA.[20] In addition, IRF3 downstream of RIG-I can be directly activated through the delivery of hydroxyquinoline-like small molecules.[81] The nucleic acid agonists are more commonly utilized as RIG-I agonists for *in situ* cancer vaccinations, and are currently in phase I/II clinical trials for solid tumors (e.g. NCT03721679

and NCT03065023).[82,83] However, this class of therapeutic currently has multiple delivery challenges that need to be addressed before using nucleic acid RIG-I agonists as an immunotherapeutic.

RNA immunotherapeutics are promising alternatives and enhancers to ICB therapy.[18] Silencing RNA (siRNA) has the capability to suppress key drivers in immunosuppression in the TME.[19] These and other RNA immunotherapeutics need to reach their targets in the cell cytosol to be effective. Delivery barriers are preventing therapeutic RNA from reaching their target receptors, limiting relevancy in clinical trials. These include nuclease degradation, low cellular uptake, endosomal recycling, and lysosomal fate.[21] Environmentally responsive polymers – often referred to as 'smart' polymers - formulated with immunotherapeutic RNA can overcome these delivery challenges.[22,23]

Smart Nanoparticle Design for RNA Delivery to Tumors

There exist several challenges for successful delivery of RIG-I agonist nucleic acid immunotherapeutics. These include nuclease degradation, poor cell uptake, endosomal recycling, and lysosomal degradation, and are shared with other nucleic acid therapeutics.[84,85] Polyplexes, inorganic nanoparticles, and lipid-based nanomaterials have been developed as delivery systems for siRNA and other nucleic acid cargo; however, there has been minimal investigation into delivery systems for RIG-I agonists.[86–88] Many studies exploring mechanisms or applications of RIG-I ligands, in addition to the few phase I/II clinical trials, have utilized commercial *in vitro* lipid-based transfection agents, like 1,2-dioleoylsn-glycero-3-phosphatidylcholine and 1,2-dioleoyl-3-trimethylammonium-propane, or polyethyleneimine (PEI) to quickly form active NPs.[89–92] However, PEI is a large

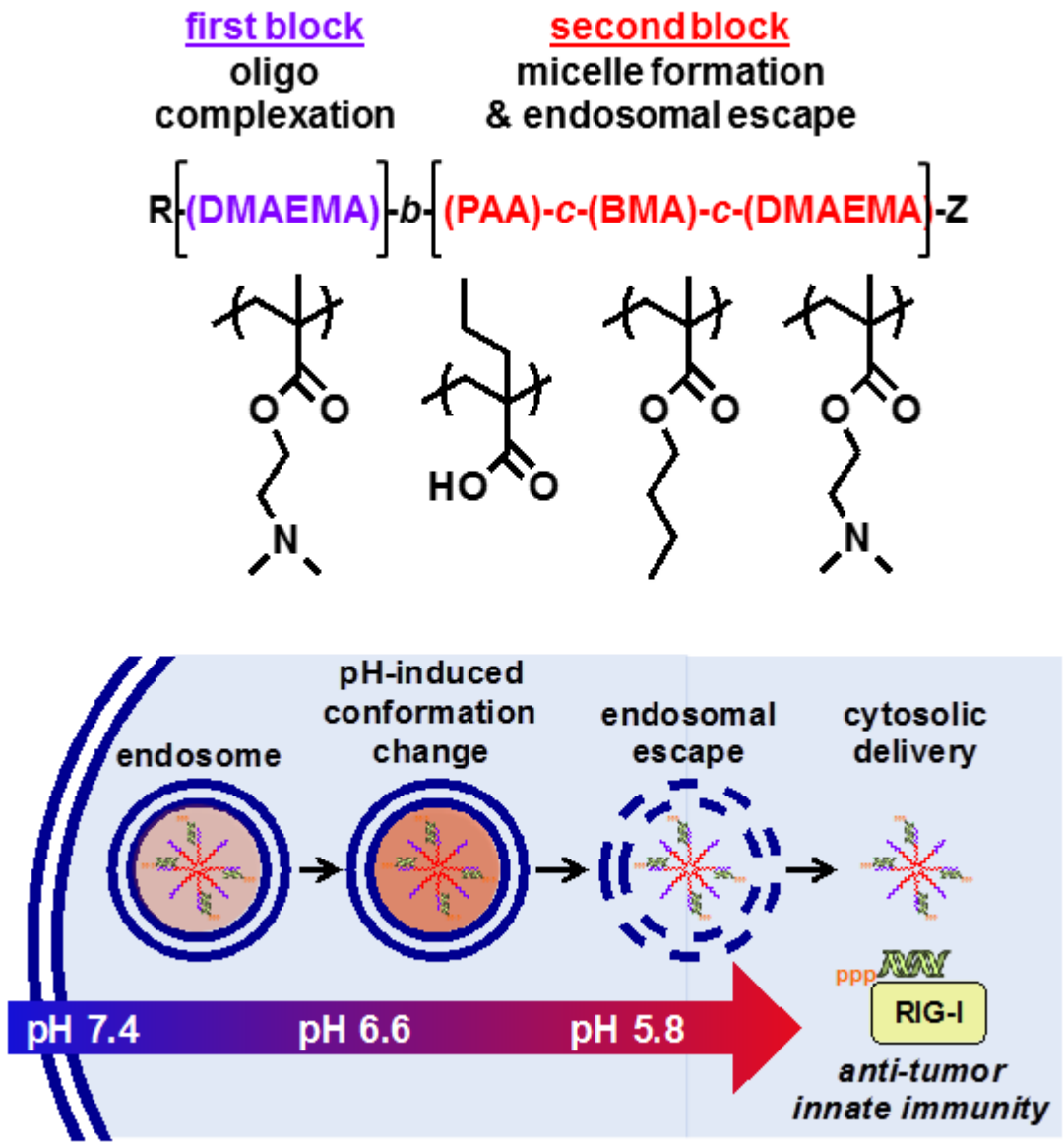

Figure 1.4: **Cytosolic Delivery of 3pRNA using amphiphilic diblock copolymer D-PDB.**
Visual representation of 3pRNA delivery capabilities of amphiphilic diblock copolymers. After endocytosis, low pH values trigger a conformation shift, exposing membrane disruptive polymer side chains to the endosomal wall. This promotes endosomal escape, leading to delivery of cargo to its cytosolic target RIG-I.

polycation and therefore exhibits significant size-dependent toxicity.[93–95] In addition, while this vector is confirmed to be an option for forming nucleic acid / PEI polyplexes for enhanced delivery, it has not been optimized for 2p- or 3pRNA delivery or poly-ICLC delivery nor has it yet been approved for human use. Finally, PEI activates the inflammasome, resulting in immune related adverse effects as well as recruitment of immunosuppressive molecules to the tumor site.[96] Hence, there is both a need develop new delivery platforms for RIG-I agonists as well as to establish carrier design criteria for this unique and emergent class of RNA therapeutic.

A new generation of drug carriers employs amphiphilic diblock pH-responsive co-polymers to form polyplexes. These materials electrostatically complex to nucleic acids to form nanoparticles for cytosolic delivery of siRNA and other cytosolically active RNA (Figure 4).[22,23,97,98] These "smart" nanoparticles, containing a hydrophilic shell to stabilize the particle in aqueous media and a core that can be switched from hydrophobic to hydrophilic, improve drug delivery. At physiological pH (7.4) this core is hydrophobic; however, at endosomal pH values, the core is hydrophilic. This exposes membrane destabilizing groups to the core and enables cytosolic delivery of complexed RNA cargo. These polymers have a few distinct improvements from PEI: i) the polymers comprise less positively charged monomer side chains, and therefore may exhibit reduced cytotoxicity , ii) the second block of polymers carriers in these studies contains membrane disruptive hydrophobic groups that are only exposed to the endosomal membrane upon entering the low pH environment of the endosome, enhancing cytosolic delivery, and iii) the polymers form well-defined, uniform sub 100 nm particles.[97] For example, the Stayton lab designed polymeric carriers for a subunit vaccine comprising antigen and nucleic acid adjuvant. These carriers were amphiphilic diblock copolymers composed

of a cationic dimethylaminoethyl methacrylate (DMAEMA) first block for facile electrostatic complexation and protection of nucleic acid cargo, and an endosome-destabilizing terpolymer block comprising DMAEMA, butyl methacrylate (BMA), and propylacrylic acid (PAA), referred to as D-PDB, that act cooperatively to mediate efficient cytosolic delivery.[97,99,100] The Duvall lab has designed amphiphilic diblock copolymers with a first block comprising a biocompatible, hydrophilic corona of either polyethylene glycol (PEG), 2-methacryloyloxyethyl phosphorylcholine, or poly(oligo(ethylene glycol) methyl ether methacrylate, and a second block comprising 50% DMAEMA and 50% BMA..[88,101] The first block of these polymers forms a hydrophilic corona to reduce NP toxicity, and the second block is responsible for both RNA complexation and cytosolic delivery. This class of polymer represents unexplored potential for enabling RIG-I activation through cytosolic delivery of 5'ppp RNA (3pRNA).

In my research, we investigate combining ICB with activation of RIG-I through efficient delivery of 3pRNA. To overcome these barriers, we decided to investigate using nanoparticles to deliver 3pRNA to the TME. These nanoparticles comprised of 3pRNA and the polymeric carrier D-PDB, a previously established amphiphilic diblock copolymer. Here, polymer complexes with 3pRNA to form 3pRNA/NPs that can overcome nuclease degradation, low cellular uptake, endosomolytic recycling, and lysosomal fates that free 3pRNA experiences, thus allowing exploration of the therapeutic efficacy of PD-1 and PD-L1 checkpoint blockade in combination with 3pRNA/NP delivery. In order to fully investigate this approach, we synthesized and characterized a series of polymeric NPs with systematic variation of polymer architecture and composition. *In vitro* and *in vivo* studies of this series of polymeric NPs complexed with 3pRNA were completed. The results of these studies have

i) improved the understand of nanoparticle drug delivery, ii) delineated polymer structure property relationship between the polymer composition and 3pRNA/NP efficacy, and ii) helped to identify an optimal NP for systemic delivery of 3pRNA. We believe that this work will improve 3pRNA/NPs while also demonstrating their ability to enhance the efficacy of ICB towards building more effective therapies that decrease cancer metastasis.

Aims and Scope

The research detailed in this written work demonstrates the development and testing of nanoparticles (NPs) comprising polymeric carriers complexed with 3pRNA (referred to in this work as 3pRNA/NPs) for local and systemic cancer immunotherapy. Chapter 2 of this these describes our work formulating, 3pRNA/NPs comprising 3pRNA complexed to D-PDB, a polymer previously utilized for subunit vaccine formulation.[97,99] We characterize this formulation and evaluate the anti-tumor effects of 3pRNA/NP treatment in CT26 murine colon carcinoma as well as primary dendritic cells and macrophages. Furthermore, we treat mice expressing CT26 tumors with a combination of PD-1 blockade and local NP mediated delivery of 3pRNA and determine whether 3pRNA/NP treatment can improve the efficacy of PD-1 checkpoint blockade.

In chapter 3, we synthesize a series of amphiphilic diblock copolymers capable of 3pRNA delivery in order to both understand the relationship between polymer structure, pH-responsive polymer properties, and 3pRNA/NP potency as well as to optimize 3pRNA/NPs for intravenous administration routes. We further characterize series polymers that form potent 3pRNA/NPs to better evaluate which polymer should be used for 3pRNA/NP formulations for future intravenous NP

administration. Chapter 4 discusses my attempts to administer 3pRNA/NPs comprising series polymer and 3pRNA using an intravenous route, as well as alternate methods for comparing 3pRNA/NP efficacy for different lead series polymeric carriers. Concluding remarks and future directions for this project are presented in chapter 5.

Table 1: **ICB monotherapy phase III and phase IV clinical trials**

Pembrolizumab (Anti-PD-1)	NCT02819518, NCT03036488, NCT02555657[58–60]
Atezolizumab (Anti-PD-L1)	NCT03197935, NCT02425891, NCT03125902, NCT03281954[51–54]

Chapter 2

Delivery of 5' - Triphosphate RNA with Endosomolytic Nanoparticles Potently Activates RIG-I to Improve Cancer Immunotherapy

Chapter Summary

This chapter is adapted from Jacobson, Max E., *et al.* "Delivery of 5'-triphosphate RNA with endosomolytic nanoparticles potently activates RIG-I to improve cancer immunotherapy." Biomaterials science 7.2 (2019): 547-559 by permission granted under Royal Society of Chemistry (RSC) license policy.

Introduction

Immunotherapy with PD-1 checkpoint blockade (ICB) is transforming the treatment of an increasing number of cancers, resulting in complete and durable responses in a subset of patients.[102,103] However, despite these unprecedented outcomes, the vast majority of patients do not respond to recently approved anti-PD-1 monoclonal antibodies (e.g., Pembrolizumab), motivating significant recent investigation into strategies to increase response rates to ICB.[104,105] Anti-PD-1 antibodies act by blocking the interaction between PD-1 on the surface of tumor infiltrating T cells, and its ligand, PD-L1, expressed primarily on tumor cells and tumor-associated myeloid cells. Disrupting the PD-1/PD-L1 interaction disables this powerful immune checkpoint, reinvigorating anti-tumor T cell effector function and cytotoxic activity.[106] Accordingly, for many cancer types, response to PD-1 antibodies correlates with the relative abundance of tumor infiltrating T cells that are positioned to be reactivated in response to PD-1 blockade.[107,108] However,

many patients and/or cancer types lack this critical T cell-inflamed immunological signature, and instead have tumor microenvironments (TME) that are largely devoid of T cells and highly infiltrated immunosuppressive cell populations.[109,110] This realization has motivated a need for immunotherapeutic modalities that can transform the TME into a hotbed of anti-tumor immune activity.

The innate immune system plays a critical role in mounting and shaping adaptive immune responses.[111] Accordingly, a variety of innate immune activators are now being explored clinically as therapeutics to abrogate immunosuppression in the TME while also creating an immunostimulatory milieu that supports the priming, activation, and infiltration of anti-tumor T cells.[112–115] The majority of these strategies leverage molecularly defined agonists of pattern recognition receptors (PRR), innate immune sensors that recognize unique structural motifs of pathogens or endogenous stress signals.[116] Notable examples include the toll-like receptor (TLR) 7 agonist, imiquimod, which has been approved for topical treatment of superficial basal cell carcinoma,[117] and the TLR-9 agonist, CpG ODN, which is approved as a vaccine adjuvant[118] and is being extensively explored in cancer immunotherapy clinical trials.[119] While promising, the utility and efficacy of TLR ligands may be limited by the expression profile of TLRs, which are typically restricted to leukocytes and, in some instances (e.g., TLR-9), to specific immune cell subsets that may be infrequent or highly heterogeneous within and/or across tumors.[120] Moreover, while many PRRs share common signaling molecules, the molecular phenotype (e.g., cytokine profile) of the resultant innate immune response can vary significantly between PRRs, with attendant consequences on adaptive immunity.[116,121,122] Recent studies have demonstrated that a type-I interferon (IFN) gene expression signature correlates with T cell infiltration into melanoma metastases

and improved response to ICB, providing rationale for design and use of PRR agonists that stimulate type-I IFN and interferon stimulated genes (ISGs) implicated in endogenous anti-tumor immunity (e.g., CXCL9, 10).[113,123,124] Interestingly, anti-tumor innate immunity appears to have considerable homology with innate responses that occur during viral recognition and defense, and indeed, a growing body of evidence now implicates PRR sensing of endogenous retroviral elements in stimulation of anti-tumor immunity.[125,126]

Retinoic acid inducible gene we (RIG-I) is an important PRR for viral sensing that potently activates antiviral innate immunity upon recognition of 5' di- or tri-phosphorylated (2p- or 3pRNA) short, double-stranded RNA in the cytosol.[89,127–129] Unlike the TLRs, RIG-I is present in the cytosol of virtually all cell types, including tumor cells, potentially rendering it a more universal innate immune target for cancer immunotherapy that is less dependent of the presence of specific infiltrating immune cell populations.[130–133] Additionally, activation of RIG-I signaling has been shown to induce preferential apoptosis in several cancer cells, whereas nonmalignant cells, notably antigen presenting cells, are more resistant to RIG-I-mediated apoptosis.[133–135] Therefore, in addition to activating a multipotent IFN-I-driven inflammatory response, cancer cell death triggered by RIG-I signaling could liberate tumor antigen, potentially enhancing cross presentation and priming of anti-tumor T cells.[90,136–138] Consequently, RIG-I has recently emerged as a promising target in immuno-oncology, with 3pRNA RIG-I agonists currently being explored in clinical trials (e.g. NCT03065023).

While RNA RIG-I agonists are a promising class of immunotherapeutic, they face multiple barriers to efficacy that are shared with other nucleic acid therapeutics (e.g., siRNA), including nuclease degradation, poor intracellular uptake, and

critically, endo/lysosomal degradation with minimal cytosolic delivery.[84,85] While there has been extensive work for developing systems for siRNA, mRNA, and DNA delivery,[86,87] including polyplexes, inorganic nanoparticles, and lipid-based nanomaterials, to name few, there has been minimal investigation into delivery systems for RIG-I agonists. Indeed, the majority of studies exploring mechanisms or applications of RIG-I ligands have utilized commercial *in vitro* lipid-based transfection agents or polyethyleneimine (PEI),[89–91] which has been widely explored for nucleic acid delivery, but has not been optimized for 2p- or 3pRNA delivery nor approved for human use, despite decades of research and development. Hence, to harness the immunotherapeutic potential of the RIG-I pathway, there is a need to explore and develop new delivery platforms for 2p- and 3pRNA as well as to establish carrier design criteria for this unique and emergent class of RNA therapeutic.

Owing to the dearth of carrier technologies for 3pRNA, we sought to evaluate the ability of a pH-responsive, membrane destabilizing polymeric nanoparticle (NP) to enhance the cytosolic delivery and immunotherapeutic activity of a synthetic 3pRNA RIG-I ligand.[139–141] These NPs are composed of amphiphilic diblock copolymers with a cationic dimethylaminoethyl methacrylate (DMAEMA) first block for facile electrostatic complexation and protection of nucleic acid cargo, and an endosome-destabilizing terpolymer block comprising DMAEMA, butyl methacrylate (BMA), and propylacrylic acid (PAA), that act cooperatively to mediate efficient cytosolic delivery (Figure 1a). This platform, and variants thereof, has been used previously to enhance intracellular delivery of siRNA and proteins,[139,141–143] but has not been explored for immunotherapeutic applications of 3pRNA delivery. Here, we evaluate the ability of endosomolytic NPs to enhance the immunostimulatory potency of 3pRNA, to stimulate RIG-I activation in the TME, and to improve responses to

PD-1 checkpoint blockade.

Results

Endosomolytic nanoparticles increase the immunostimulatory activity of 3pRNA. Towards developing a nanoparticle platform for potent RIG-I activation, we first evaluated the ability of pH-responsive, membrane destabilizing DMAEMA-b-(DMAEMA-c-BMA-c-PAA) nanoparticles (NP) to enhance the immunostimulatory activity of a synthetic 3pRNA RIG-I ligand (Figure 1a). To determine the charge ratio needed to fully complex 3pRNA, polymeric NPs were complexed with different amounts of 3pRNA corresponding to various charge ratios of positively charged nitrogen to negatively charged phosphate (N:P ratio) ranging from 1:1 to 16:1, and agarose gel electrophoresis was used to evaluate complexation efficiency. Complete RNA complexation was achieved at a charge ratio of 4:1 (Figure 1b), which was selected for all subsequent investigations. We further confirmed assembly of polyplex nanoparticles at this charge ratio via dynamic light scattering, which demonstrated a monodisperse particle size distribution with a median diameter of 108.5 nm and a polydispersity index (PDI) of 1.170 (Figure 1c).

We next evaluated 3pRNA activity in A549 human lung carcinoma cells and THP-1 monocyte ISG reporter cells that express a secreted luciferase downstream of an interferon response element.NPs loaded with control 5'-OH-RNA lacking a triphosphate group (OH-RNA) were used as a control to validate RIG-I dependent expression of ISGs. Additionally, since carriers for 3pRNA explored to date have not utilized an active endosomal escape mechanism, relying primarily on the proton sponge effect, we also sought to determine if the endosomolytic properties of the NP were critical to enhanced activity. To do this, we synthesized a structurally

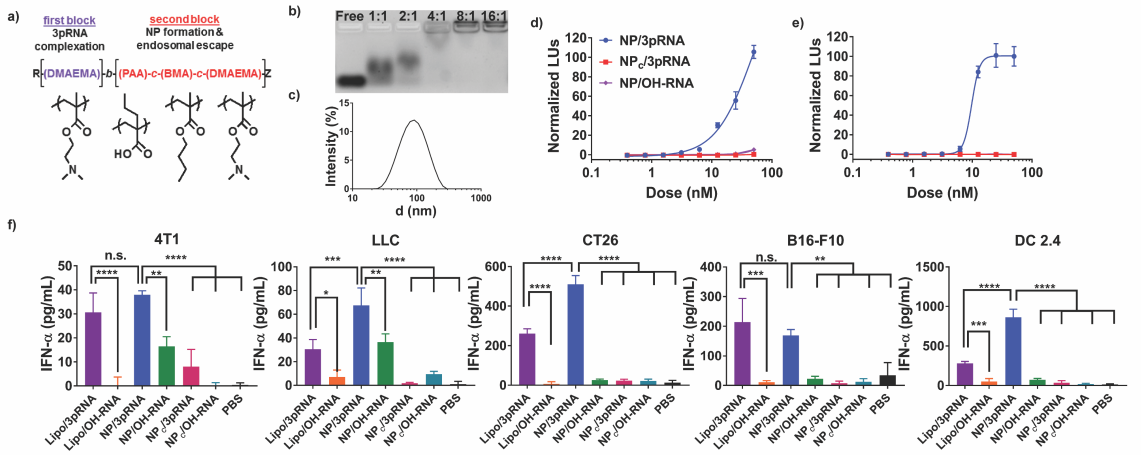

Figure 2.1: **Endosomolytic nanoparticles enhance the delivery of 3pRNA to activate RIG-I pathway.**
(a) Schematic describing the structure and composition of pH-responsive, endosomolytic polymers used for 3pRNA delivery (NPs). The polymer consists of a poly(DMAEMA) first block for electrostatic complexation of 5' triphosphate double-stranded RNA (3pRNA) and a second terpolymer block responsible for assembly of micellar nanoparticles and inducing endosomal escape. (b) 3pRNA was incubated with NP at different charge ratios (N:P) and agarose gel electrophoresis used to evaluate the degree of nucleic acid complexation. (c) Dynamic light scattering analysis of particle size distribution of NP complexed with OH-RNA at N:P 4:1 (n=3). (d) THP1-Dual cells and (e) A549-Dual cells were treated with either NPs loaded with 3pRNA (NP/3pRNA) or OH-RNA (NP/OH-RNA), or non-pH-responsive NPs (NPc) loaded with 3pRNA (NPc/3pRNA) and activation of IRF was measured through secreted luciferase reporter levels. Luminescence was normalized using PBS treated samples and 100 nM NP/3pRNA treated samples (n=4). (f) Different cell types were treated with Lipofectamine (Lipo), NP, or NPc complexed with either 3pRNA or OH-RNA at final RNA doses of 50 nM (n=3) and ELISA used to quantify levels of secreted IFN-α.

analogous diblock polymer with a DMAEMA first block and a poly(BMA) second block that is not pH responsive (Figure A.3a, A.3b) and that lacks hemolytic activity, which has been shown to correspond to endosomolytic activity (Figure A.3c).[144] 3pRNA-loaded NPs (NP/3pRNA) exhibited an EC_{50} between 10 nM and 20 nM for both cell types, while no activity was observed for 3pRNA complexed with the non-pH-responsive control nanoparticle (NP_*c*) over this dose range (Figure 1d, Figure 1e). Free 3pRNA that was not bound to NP or Lipofectamine was inactive over this dose range, consistent with poor cytosolic bioavailability of RNA therapeutics (Figure A.4). In addition, NP delivery of OH-RNA (NP/OH-RNA) did not exhibit activity, confirming the 5'-triphosphate-dependent nature of the response. These findings demonstrate the potential to leverage DMAEMA-b-(DMAEMA-c-BMA-c-PAA) polymeric NPs for 3pRNA delivery and support the importance of a potent endosomal escape mechanism in the design of carriers for RNA RIG-I ligands.

NP delivery of 3pRNA triggers inflammatory cytokine production and immunogenic cell death in cancer cells. Activation of RIG-I in a number of cancer cell types, including melanoma, lung, breast, and prostate cancer cell lines, has been shown to increase tumor immunogenicity via several interconnected mechanisms, including induction of cancer cell-specific death and liberation of tumor antigen, production of anti-tumor cytokines and T cell chemokines, and increased expression of MHC-I.[90,91,135,145–148] We first evaluated the ability of NP/3pRNA to enhance IFN-α secretion in several murine cell lines commonly used in pre-clinical modeling of poorly immunogenic tumors, including CT26 colon carcinoma, B16-F10 melanoma, Lewis lung carcinoma (LLC), and 4T1 breast cancer, as well as in the murine dendritic cell line DC 2.4 (Figure 1f). NP delivery of 3pRNA increased IFN-α production in all cancer cell lines tested, with the largest fold enhancement

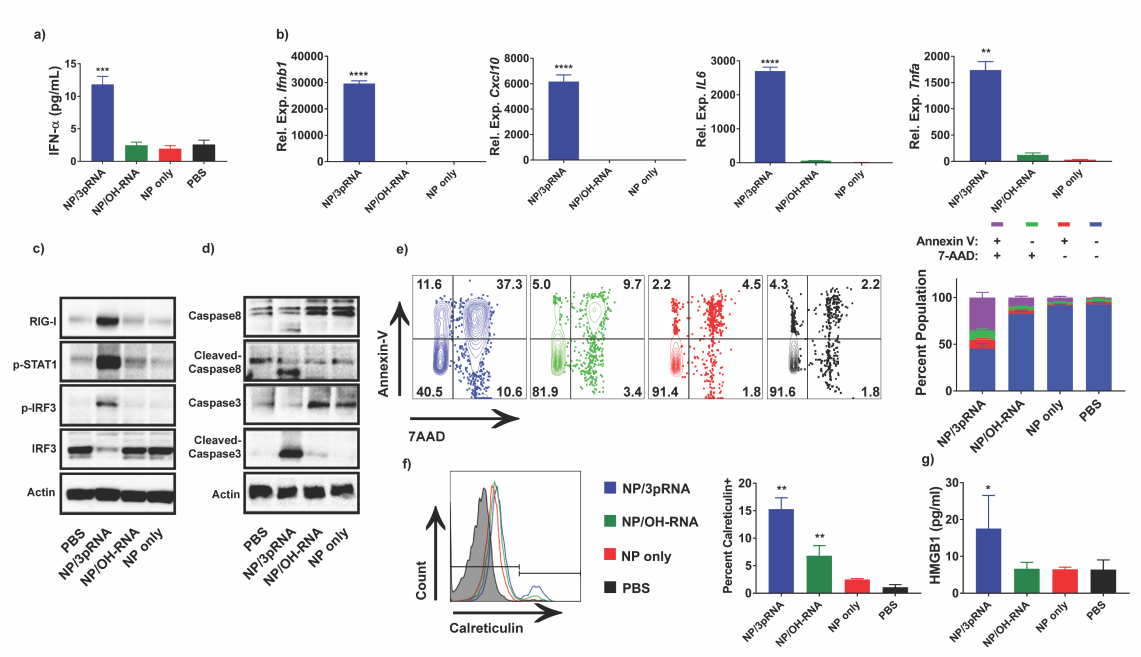

Figure 2.2: **NP delivery of 3pRNA induces production of inflammatory cytokines and mediates immunogenic cell death in CT26 cells.**
(a) Levels of secreted IFN-α measured using ELISA after 24 h treatment of CT26 cells with indicated formulation (n=4). (b) qRT-PCR analysis of *Ifnb1*, *Cxcl10*, *Il6*, and *Tnfa* relative expression (Rel. Exp.) in CT26 cells treated with indicated formulation for 6 h (n=4). Representative images of western blots stained for (c) RIG-I, phosphorylated STAT1 (p-STAT1), and phosphorylated interferon regulatory factor 3 (p-IRF3) and (d) caspase 3 and caspase 8 cleavage in CT26 cells in response to indicated treatment for 24 h (n=3). (e) Representative flow cytometry dots plots and analysis of CT26 cell viability and apoptosis via annexin-V and 7-AAD staining after treatment with indicated formulation for 24 h. (f) Flow cytometry was used to determine cell surface levels of calreticulin on CT26 cells after indicated treatment for 24 h. Representative histogram and analysis of percent calreticulin positive cells are shown (n=4). (g) HMGB1 release from CT26 cells treated for 24 h was determined using ELISA (n=4). For NP/3pRNA, significance is between all other samples, and for NP/OH-RNA significance is between NP only and PBS.

observed in the CT26 and B16 cell lines. In addition, NP delivery of 3pRNA resulted in comparable or improved IFN-α production over delivery of 3pRNA with Lipofectamine 2000, a commercial lipid-based transfection agent used primarily for *in vitro* nucleic acid transfections. As expected, NP delivery of 3pRNA also increased IFN-α production in DC 2.4 cells relative to controls.

Based on these findings, and in light of the modest clinical response rates to PD-1 checkpoint blockade in colorectal cancer,[149] we selected the CT26 model for subsequent investigations into how NP/3pRNA could be used to increase tumor immunogenicity. CT26 cells were treated with multiple doses of NP/OH-RNA to determine the effects of the NP itself on CT26 viability and found that NPs are not toxic at the EC_{50} (Figure A.5a). CT26 cells were treated with NP/3pRNA, NP/OH-RNA, empty particles (NP) or a vehicle control (PBS) at an RNA dose of 50 nM. NP/3pRNA treatment increased secretion of IFN-α (Figure 2a) and gene expression of *Ifnb1* and *Cxcl10*, the latter an ISG and critical T cell chemokine, as well as the NF-κB driven pro-inflammatory cytokines, Il6 and Tnfα, whereas no increases were observed above baseline for all other groups (Figure 2b). This was further supported by protein immunoblots of CT26 cell lysates that indicated that only NP/3pRNA treatment triggered phosphorylation of IRF-3 (pIRF3), a transcription factor downstream of RIG-I that drives expression of type-I IFN and other ISGs (Figure 2c). Additionally, NP/3pRNA resulted in phosphorylation of STAT-1, which occurs downstream of the IFN-α/β receptor, as well as increased expression of RIG-I, itself an ISG, the result of positive feedback after initial RIG-I activation (Figure 2c). Therefore, NP delivery of 3pRNA enhances RIG-I activation in CT26 murine colon carcinoma, resulting in production of type-I IFNs and activating downstream innate immune signaling cytokines.

Previous studies have shown that RIG-I activation in several cancer cell types can lead to induction of immunogenic cell death, an inflammatory form of cell death that has been harnessed to enhance antitumor immunity.[130,138,150–152] In order to determine if NP-mediated RIG-I activation could induce immunogenic cell death in CT26 colon carcinoma, cells were treated with NP/3pRNA, NP/OH-RNA, NP only, or PBS at a final RNA concentration of 50 nM for 24 h. Protein immunoblots of cell lysates indicate that only NP/3pRNA treatment increased caspase 3 and caspase 8 cleavage (Figure 2d), indicated by the appearance of a new lower molecular weight band and decreased intensity of the characteristic caspase 3 and caspase 8 bands, which have been previously implicated in RIG-I- and type 1 IFN-dependent cancer cell death pathways. To evaluate cell viability and apoptosis in response to treatments, cells were stained with annexin-V antibodies and a 7AAD membrane permeability stain and characterized using flow cytometry to determine the percentage of double negative (-/-), annexin-V positive (+/-), 7AAD positive (-/+), and double positive cells (+/+) (Figure 2e). Treatment with NP/3pRNA significantly reduced cell viability relative to all other groups, with a high population of Annexin-V/7AAD double positive cells, indicating a combination of necrotic and apoptotic cell death mechanisms, which is typically more immunogenic than death solely by apoptosis.[152] Additionally, NP/3pRNA resulted in evaluated surface expression of calreticulin, a marker of immunogenic cell death that promotes tumor cell phagocytosis by macrophages (Figure 2f) and secretion of HMGB1, which engages TLR-4 (Figure 2g). Collectively, these data demonstrate that NP delivery of 3pRNA can increase tumor-intrinsic activation of anti-tumor innate immunity and elicit immunogenic cell death, responses with potential to act cooperatively to enhance anti-tumor adaptive immunity.

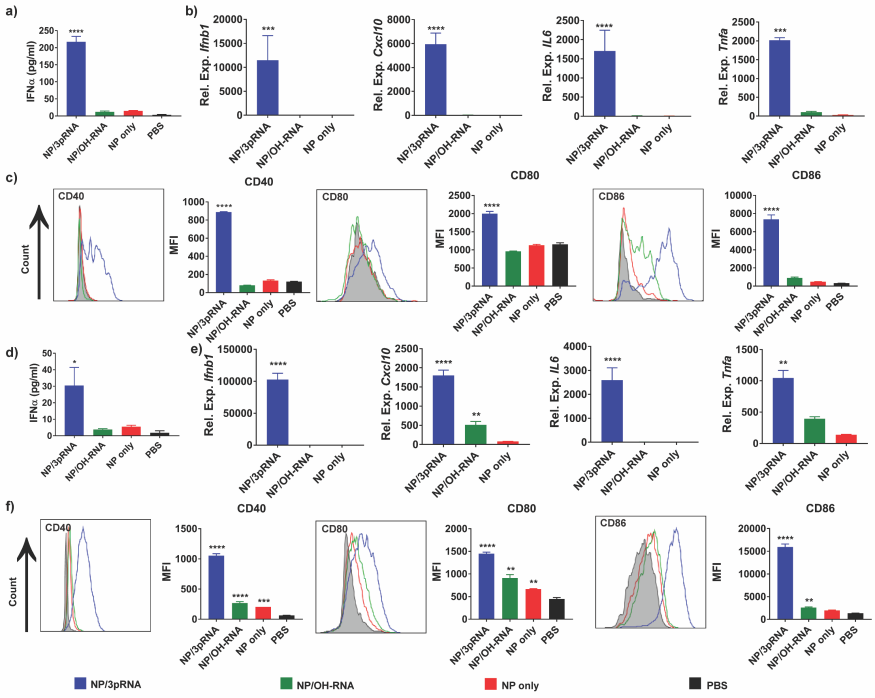

Figure 2.3: **NP delivery of 3pRNA activates myeloid cells and induces production of inflammatory cytokines.**
(a) IFN-α secretion by bone-marrow derived dendritic cells (BMDCs) treated with indicated formulations (n=4). (b) Relative expression of *Ifnb1, Cxcl10, Il6,* and *Tnfa* by BMDCs measured by qRT-PCR (n=4). (c) Representative flow cytometry histograms and average median fluorescence intensity (MFI) values of CD40, CD80, and CD86 on BMDCs in response to indicated treatment (n=4). (d) IFN-α secretion by bone-marrow derived macrophages (BMDMs) treated with indicated formulations (n=4). (e) Relative expression of *Ifnb1, Cxcl10, Il6,* and *Tnfa* by BMDMs measured by qRT-PCR (n=4). (f) Representative flow cytometry histograms and average MFI values of CD40, CD80, and CD86 expression on BMDMs in response to indicated treatment (n=4). For NP/3pRNA, significance is between all other samples, and for NP/OH-RNA and NP only significance is between PBS.

NP delivery of 3pRNA activates primary dendritic cells and macrophages. A variety of different cell populations contribute to propagating immunosuppression in the TME, and therefore immunotherapeutics that are able modulate the immunophenotype of multiple cell types may be more effective for increasing tumor immunogenicity.[109,112,153] Tumor infiltrating myeloid cell populations, including tumor-associated macrophages, myeloid derived suppressor cells, and dendritic cells, are important cell populations in regulating the balance between immunosuppression and effective anti-tumor immunity.[109] We therefore evaluated the capacity of NP/3pRNA to activate RIG-I and trigger anti-tumor innate immune response in bone marrow derived dendritic cells (BMDCs) and bone marrow derived macrophages (BMDMs). As described above, both primary cell types were treated with NP/3pRNA, NP/OH-RNA, NP only, or PBS at a final RNA concentration of 50 nM. We first evaluated the ability of NP/3pRNA to activate BMDCs. Treatment of BMDCs with NP/3pRNA stimulated expression (Ifnb1) and secretion (IFN-α) of type-I IFN, as well as expression of Cxcl10 and the pro-inflammatory cytokines Il6 and Tnfa whereas no increase above background was observed for all control groups (Figure 3a,b). We further analyzed BMDC activation using flow cytometry to measure surface expression of co-stimulatory molecules (Figure 3c). Consistent with gene expression data, only NP/3pRNA resulted in increased expression of CD40 (9-fold), CD80 (2-fold), and CD86 (23-fold).

We next evaluated the ability of NP/3pRNA to activate BMDMs. Results were largely similar to those obtained in BMDCs, with only NP/3pRNA activating production of type-I IFN, IL-6, and TNFα (Figure 3d,e). NP/OH-RNA resulted in a slight, but statistically significant, increase in Cxcl10 expression, potentially a result of intrinsic inflammatory properties of the RNA/NP complex in macrophages.

Similarly, surface expression of CD86, CD40, and CD80 were most significantly increased in response to NP/3pRNA (Figure 3f), though a small but significant increase over background was observed for NP/OH-RNA and NP, potentially reflecting some inherent immunostimulatory properties of the NP, as has been previously described for other cationic and/or endosomolytic materials.[154–157] These effects did not appear to be a result of polymer toxicity, as treatment of DC 2.4 and RAW 264.7 cells with relevant concentrations of NP/OH-RNA did not result in cytotoxicity (Figure A.5b, A.5c). Nonetheless, these data collectively demonstrate that NPs enhance the delivery of 3pRNA to primary macrophages and DCs, resulting in activation of RIG-I and downstream stimulation of type-I IFN, ISGs, and pro-inflammatory cytokines. Given the immunosuppressive capacity of TAMs in many tumor types as well as the importance of DC activation in priming of anti-tumor adaptive immunity and memory responses, these results further support application of NP/3pRNA-mediated activation of RIG-I to increase tumor immunogenicity and improve outcomes of cancer immunotherapy.

NP delivery of 3pRNA activates RIG-I in CT26 tumors and increases CD8+ T cell infiltration. We next evaluated the ability of NP/3pRNA to activate anti-tumor innate immunity in CT26 tumors. Mice with subcutaneous (SC) CT26 tumors were administered NP/3pRNA, NP/OH-RNA, or vehicle (PBS) two times, spaced two days apart via an intratumoral (IT) injection route. Mice did not exhibit weight loss during this treatment, indicating that IT administration of NP/3pRNA results in minimal immune-related adverse events or toxicity (Figure A.6a). Mice were euthanized 24 h after the final injection, and tumors analyzed via qRT-PCR, western blot analysis, and immunohistochemical staining. IT administration of NP/3pRNA significantly increased expression of Ifnb1 and Cxcl10 (Figure 4a,b),

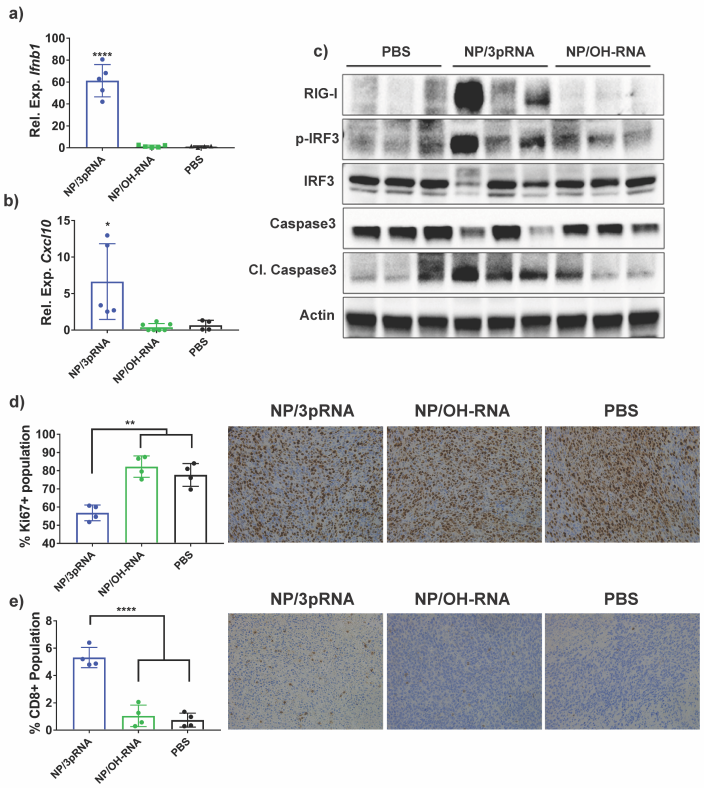

Figure 2.4: **NP delivery of 3pRNA activates RIG-I in CT26 tumors and increases CD8+ T cell infiltration.**
Gene expression of a) *Ifnb1* and b) *Cxcl10* in CT26 tumors treated with indicated formulation was determined using qRT-PCR (n=4). c) Treated tumors were analyzed using a protein immunoblot to determine relative expression of RIG-I, phosphorylated IRF3 (pIRF3), and cleaved caspase 3 (n=3). (d) Sections from CT26 tumors injected with indicated formulation were immunostained for Ki67 and the percentage of Ki67+ was quantified by image analysis (n=4). (e) Sections from CT26 tumors injected with indicated formulation were immunostained for CD8 and the percentage of CD8+ was quantified by image analysis (n=4).

whereas no increase above baseline was observed for NP/OH-RNA. Likewise, western blot analysis demonstrated increased levels of RIG-I and pIRF-3, as well as increased cleavage of caspase 3 (Figure 4c) relative to NP/OH-RNA and vehicle control, further supporting the ability of the NP to enhance cytosolic 3pRNA delivery. Consistent with increased cleaved caspase 3 levels, NP/3pRNA also inhibited cell proliferation as determined by Ki67 staining of tumor sections (Figure 4d). Importantly, immunohistochemical analysis also revealed a significant increase in CD8 staining, likely reflecting infiltration of CD8+ T cells into the TME, consistent with increased expression of Cxcl10, an important T cell chemokine (Figure 4e). While further investigation is necessary to understand the mechanism by which NP/3pRNA activates RIG-I to remodel the TME, these findings demonstrate the ability to leverage endosomolytic NPs to enhance 3pRNA delivery *in vivo*.

NP delivery of 3pRNA increases response rates to PD-1 checkpoint blockade in CT26 model of colon cancer. Based on the capacity of NP/3pNRNA to stimulate RIG-I activation in the TME, we next sought to demonstrate the ability of NP/3pRNA to inhibit tumor growth and synergize with αPD-1 ICB. We evaluated this using an IT administration route that is being explored in clinical trials of immune agonists (e.g., NCT02423863, NCT02834052, NCT01984892, NCT01349959, NCT01928576), including RIG-I agonists.[133,158] BALB/cJ mice bearing subcutaneous CT26 tumors were administered NP/3pRNA or control formulations IT every two days over a two-week period with and without concurrent systemic intraperitoneal treatment with αPD-1 monoclonal antibody (Figure 5a). NP/OH-RNA, αPD-1, and vehicle (PBS) were administered as controls. IT administration of NP/3pRNA resulted in a modest but significant reduction in tumor volume relative to αPD-1 alone, NP/control, and vehicle control, and

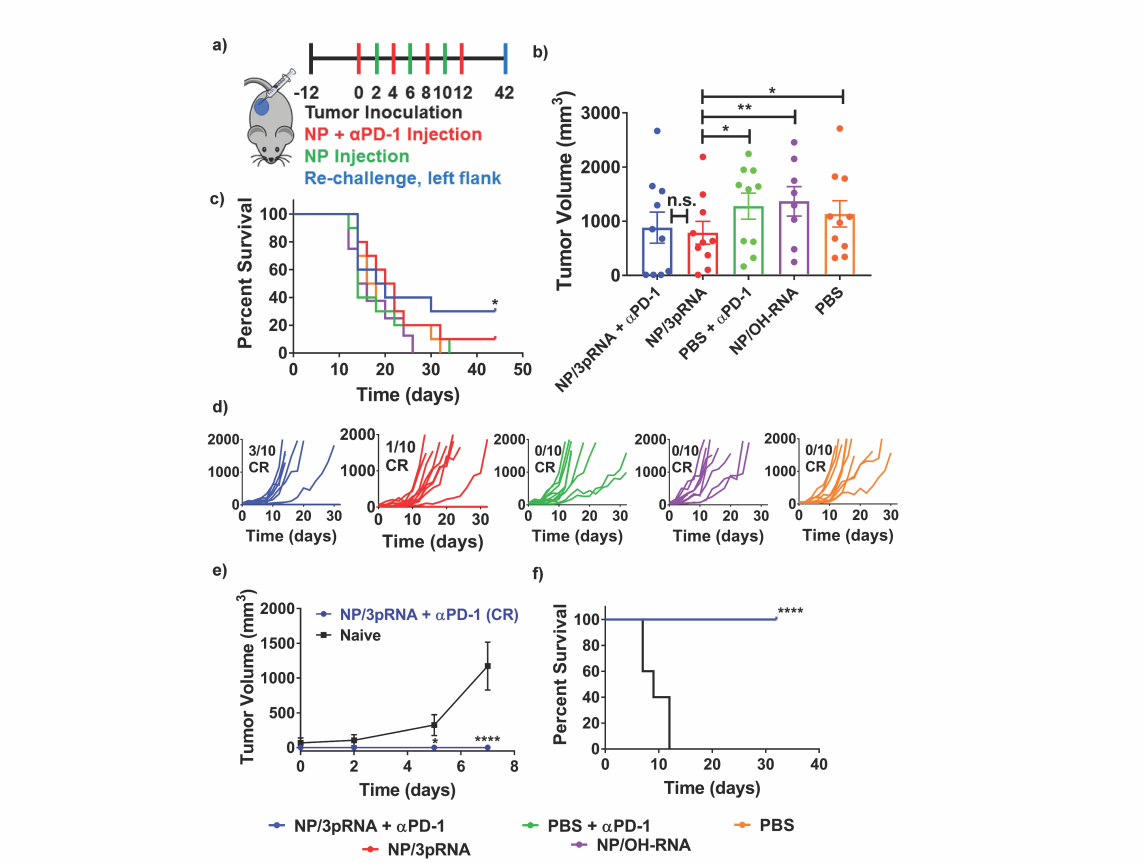

Figure 2.5: **NP delivery of 3pRNA in combination with αPD-1 inhibits tumor growth and extends survival.**
(a) Schematic summarizing tumor formation and treatment schedule used for evaluating efficacy of NP/3pRNA in combination with PD-1 blockade. Mice bearing CT26 tumors were treated intratumorally 5 times spaced two days apart (IT) with NP/3pRNA, NP/OH-RNA, or PBS. Mice were injected with αPD-1 every 4 days intraperitoneally. Mice demonstrating complete responses (CRs) were challenged on the contralateral flank with CT26 tumor cells on day 42. (b) Average tumor volume at day 14, corresponding to the first incidence of euthanize in any treatment or control cohort. Error bars represent S.D. (c) Kaplan-Meier survival curves of mice treated with indicated formulation using 1500 mm3 tumor volume as endpoint criteria (n=10). (d) Spider plots of individual growth curves with the number of CRs at day 42 denoted. (e) Mice exhibiting CRs to NP/3pRNA + αPD-1 treatment were rechallenged with CT26 cells on the contralateral flank without further treatment and tumor growth was compared to treatment-naïve mice inoculated with CT26 cells. Tumor measurements begin two weeks after tumor rechallenge/inoculation, when tumors became palpable (n=3 for CR mice, n=5 for naïve mice). Significance was determined for day 7 between naïve and Cr mice. (f) Kaplan-Meier survival curves for treatment naïve and CRs to NP/3pRNA + αPD-1. Significance was determined using two-way ANOVA with Tukey's multiple comparisons test. Significance for survival was determined using a Mantel-Cox log-rank test.

administration of NP/3pRNA + αPD-1 did not result in significantly reduce tumor volume compared to NP/3pRNA treatment (Figure 5b). In addition, NP/3pRNA administration reduced the average doubling time of CT26 tumors compared to αPD-1 alone, NP/control, and vehicle control (Figure A.7). Importantly, mice did not exhibit weight loss during or after treatment, indicating that IT administration of NP/3pRNA alone or in combination with PD-1 ICB resulted in minimal immune-related adverse effects or toxic effects (Figure A.6b). While the overall effect on average tumor growth was modest, the therapeutic effect of NP/3pRNA was considerably more evident in its ability to decrease the average doubling time of CT26 tumors (Table 6) and overall rates of survival when combined with αPD-1 ICB (Figure 5c). Thirty percent (3/10) of mice treated with NP/3pRNA in combination with αPD1 demonstrated complete responses (CRs) without any evidence of tumor growth for 42 days after cessation of treatment, whereas only 10% (1/10) mice receiving NP/3pRNA monotherapy and none of the mice in control cohorts exhibited complete responses (Figure 5d). To determine if this treatment regimen could stimulate adaptive immunity to protect against tumor recurrence, mice exhibiting complete responses were rechallenged with CT26 cells on the opposite flank. Without any additional treatment, rechallenged mice resisted tumor growth for at least 40 days, whereas age-matched, treatment-naïve controls succumbed to disease within 12 days (Figure 5e). While the immunological mechanisms underlying this response remain to be elucidated, these data provide the first demonstration that carrier-enhanced delivery of a 3pRNA RIG-I agonist can serve as an *in situ* vaccine that can protect against rechallenge.

Discussion

The recent clinical success of ICB has provided a clear testament to the potential for immunotherapies to revolutionize cancer treatment. While some patients respond remarkably to ICB immunotherapies, many do not realize favorable outcomes. In order to improve the efficacy of these treatments a greater appreciation for the importance of the innate immune system in eliciting and supporting effective anti-tumor T cell immunity is needed. This has prompted the expansion of the immunotherapeutic armamentarium to include innate immune agonists. Within this emergent family of immunomodulators, 3pRNA agonists of RIG-I hold considerable promise owing to the robust and ubiquitous expression pattern of RIG-I, their capacity to stimulate a strong type-I IFN-driven inflammatory program, and their ability to induce immunogenic cell death in multiple cancer cell types. However, the clinical potential of 2p- and 3pRNA therapeutics remains limited by poor drug delivery. Therefore, development of new drug delivery systems that can overcome poor cellular uptake, susceptibility to nuclease degradation, and very low cytosolic bioavailability may improve the effectiveness of immunotherapies.

The studies and results of this chapter has demonstrated that polymeric nanoparticles (NP) with pH-responsive, endosome-releasing activity can enhance the intracellular delivery of 3pRNA to potently activate the RIG-I pathway. The importance the pH responsive behavior was demonstrated since a structurally analogous non-pH-responsive carrier did not enhance activity. The data presented in this chapter highlights the importance of an active endosomal escape mechanism in the design of delivery systems for 3pRNA. This work also demonstrates the utility of NPs for 3pRNA delivery, with data indicating that NP/3pRNA can trigger RIG-I signaling and downstream immunostimulatory effects in macrophages, dendritic cells,

and several cancer cell lines. Importantly, *in vivo* studies utilizing NP drug carriers demonstrated enhanced activity of 3pRNA. Here, stimulated expression of type-I IFN and ISGs upon intratumoral administration and increasing the infiltration of CD8+ T cells was observed. Consequently, treatment with NP/3pRNA enhanced the therapeutic efficacy of αPD-1 ICB to yield significant improvement in survival and resulted in a 30% complete response rate in a CT26 murine colon cancer model. While NP properties, RIG-I ligand design, and NP/3pRNA dose and treatment regimen remain to be optimized for maximum therapeutic benefit, these studies demonstrate the importance of carrier design in immunotherapeutic targeting of the RIG-I pathway and set the stage for future investigation into the development of new delivery technologies for this promising class of innate immune agonist.

Materials and Methods

RAFT Polymerization of p(DMAEMA)-b-(DMAEMA-co-BMA-co-PAA). Briefly, Inhibitor was removed from all monomer solutions used for RAFT polymerization using gravity filtration through columns packed with aluminum oxide (Sigma Aldrich). RAFT polymerization of dimethylaminoethyl methacrylate (DMAEMA) (Sigma Aldrich) was conducted under a nitrogen atmosphere in dioxane (40 wt % monomer) at 30^{o}C for 18 h in the presence of 4-cyano-4-(ethylsulfanylthiocarbonyl)sulfanylpentanoic acid (ECT) (Boron Molecular) and 2,20-azobis(4-methoxy-2.4-dimethyl valeronitrile) (V-70) (Wako Chemicals) as the RAFT chain transfer agent and initiator, respectively. The initial monomer (M_o) to CTA (CTA_o) to initiator (I_o) ratio was 100:1:0.05. The resultant p(DMAEMA)) macro-chain transfer agent (mCTA) was isolated by precipitation into cold pentane. The mCTA was transferred to a 3 kDa MWCO snakeskin dialysis membrane (Thermo

Fisher) and exchanged into 2L of molecular grade water (HyClone) twice for 6 h. The solution was frozen, lyophilized, and characterized using ^{1}H nuclear magnetic resonance (NMR) (Bruker AV 400) and gel permeation chromatography (GPC) (Agilent). Propylacrylic acid (PAA) was synthesized as described previously using diethyl propylmalonate (Sigma Aldrich) as the precursor.[159] Purified mCTA was used for block copolymerization of DMAEMA, (PAA), and butyl methacrylate (BMA) (Sigma Aldrich) or BMA only. DMAEMA (30%), PAA (30%), and BMA (40%), or BMA (100%) ($M_o/CTA_o = 0.2$) were added to the mCTA dissolved in dioxane (40 wt % monomer and mCTA) along with the free radical initiator V-70 at a mCTA to initiator ratio ($mCTA_o/I_o$) of 5 and polymerized under a nitrogen atmosphere for 24 h at 30 ^{o}C. The resultant diblock copolymer was isolated using dialysis (3kDa MWCO) against acetone (4 exchanges) with a final dialysis against molecular grade water (HyClone). The same process was used for the synthesis of p(DMAEMA)-b-p(BMA) (D-B), except the monomer feed only contained BMA. The purified polymer was then frozen and lyophilized. The composition and purity of the resultant polymer was analyzed using ^{1}H NMR and GPC. Polymer composition, purity, and molecular weight were determined using ^{1}H NMR (CDCl3) spectroscopy (Figure A.1, A.2), and polymer molecular weight (Mn) and polydispersity (PDI) was determined using GPC using a DMF mobile phase with 0.1 M LiBr with inline light scattering (Wyatt) and refractive index (Agilent) detectors (Table 5).

Synthesis of 5'-Triphosphate RNA. 5'-ppp- CGUUAAUCGCGUAUAAUACGCCUAU-3' was generously synthesized and provided by the laboratory of Dr. Anna M. Pyle at Yale University.[160] 5'-OH-CGUUAAUCGCGUAUAAUACGCCUAU-3' as well as the complement strand 5'-AUAGGCGUAUUAUACGCGAUUAACG-3' was purchased from Integrated DNA

technologies (IDT) and resuspended in RNAse free water. To generate double stranded RNA, equimolar amounts of top strand with a triphosphorylated or OH 5' terminus top strand, and the complement strand were suspended in 0.3 M NaCl, transferred to a 0.25mL PCR tube and annealed using a thermocycler by setting the temperature to 90^{o}C and slowly cooling to 35^{o}C over 1 h. The resulting duplexes were diluted to 100μM RNA in RNAse free water and agarose gel (2%) electrophoresis was used to confirm hybridization.

Formulation of NP/3pRNA complexes for *in vitro* investigations. Amphiphilic diblock copolymer comprising a 10.3 kDa first block of DMAEMA and a 31.0 kDa second block copolymer of 33% DMAEMA, 39% butyl methacrylate (BMA), and 28% propylacrylic acid (PAA) (D-PDB) was synthesized as described above. Lyophilized copolymers were dissolved into ethanol at 50 mg/mL, and rapidly diluted into phosphate buffer (pH 7.0, 100 mM) to a final concentration of 10 mg/mL. This stock was further diluted to 1 mg/mL in phosphate buffered saline (155 mM NaCl, 1.05 mM KH_2PO_4, 3 mM Na_2HPO_4, Gibco), and rapidly mixed with either 3pRNA or OH-RNA at charge ratios (N:P) between 16:1 and 1:1, incubated at room temperature for 30 min, and diluted into PBS (pH 7.4, Gibco) in order to form nanoparticles (NPs). The first block of DMAEMA is estimated to have 50% protonation for the purposes of determining N:P ratios. A charge ratio of 4:1 was selected for all *in vitro* cell culture studies.

Dynamic Light Scattering. D-PDB (1 mg/mL) was mixed with OH-RNA as detailed above at a 4:1 charge ratio, and NP particle size distribution and polydispersity index (PDI) was analyzed via dynamic light scattering (Malvern Zetasizer Nano ZS).

Agarose Gel Electrophoresis. D-PDB (1 mg/mL) was mixed with OH-RNA

as detailed above, except that the components were mixed at charge ratios of either 1:1, 2:1, 4:1, 8:1, or 16:1 resulting in a 15 μL NP solution comprising at least 100 ng RNA. NP/RNA complexes and free RNA were mixed with 5 μL of 30% glycerol and loaded onto a 2% agarose gel. The gel was run in Tris-Borate-EDTA buffer at 100 V for 60 min. The gel was stained with GelRed (Biotium) for 20 min and imaged using a Digital ChemiDoc MP system (Bio-Rad).

Red Blood Cell Hemolysis assay. All experiments using human samples were performed in compliance with United States Federal Policy for the Protection of Human Subjects and guidelines set forth by the Vanderbilt University Human Research Protections Program. These experiments were approved by the Vanderbilt University Institutional Review Board and consent was obtained from human subjects prior to all experimentation. The ability of NPs to disrupt lipid bilayer membranes was performed as previously described.[139] Whole blood from de-identified patients was acquired from the Vanderbilt Technologies for Advanced Genomics (VANTAGE) core. Blood was centrifuged at 500 rcf to pellet erythrocytes, and plasma was aspirated before resuspending erythrocytes in pH 7.4 PBS (Gibco). This process was repeated 3x to isolate erythrocytes, which were ultimately resuspended in pH 7.4, 7.0, 6.6, 6.2, or 5.8 PBS (150 nM) for the hemolysis assay. D-PDB and D-B were mixed with suspended erythrocytes to a concentration of 10 μg/mL in a 96-well V-bottom plate. The plates were incubated for 1 h at 37^{o}C, then centrifuged at 700 rcf to pellet intact erythrocytes. The supernatant was then transferred to a 96-well flat bottom plate and hemoglobin leakage was quantified by measuring absorbance at 575 nm.

Cell lines and Primary Bone Marrow-Derived Cells. The human lung carcinoma IRF and NF-κB reporter cell line A549-Dual (Invivogen) and the

murine macrophage cell line RAW 264.7 (ATCC) was cultured in DMEM (Gibco) supplemented with 2mM L-glutamine, 4.5 g/L D-glucose, 10% heat inactivated fetal bovine serum (HI FBS, Gibco), and 100 U/mL penicillin/100 μg/mL streptomycin (Gibco). The murine colon carcinoma CT26 cell type (ATCC), the murine breast cancer cell line 4T1 (ATCC), the human monocyte IRF and NF-κB reporter cell type THP1-Dual (Invivogen), and the murine melanoma cell type B16-F10 (ATCC) were cultured in RPMI 1640 (Gibco) supplemented with 2 mM L-glutamine, 10% fetal bovine serum (FBS, Gibco), and 100 U/mL penicillin/100 μg/mL streptomycin (Gibco). The murine dendritic cell line DC2.4 (H-2K^b-positive) was kindly provided by K. Rock (University of Massachusetts Medical School) and cultured in RPMI 1640 (Gibco) supplemented with 10% fetal bovine serum (HI FBS; Gibco), 2 mM L-glutamine, 100 U/mL penicillin/100 μg/mL streptomycin (Gibco), 50 μM 2-mercaptoethanol (Gibco), 1 x nonessential amino acids (Cellgro), and 10 mM HEPES (Invitrogen).

Bone marrow cells were isolated from both the femurs and tibias of 8-12 week old female wild-type BALB/cJ mice. After muscle tissue removal and ethanol sterilization of the bones, bone marrow was flushed out over a strainer with Dulbecco's phosphate-buffered saline (DPBS; Corning). Harvested cells were then rinsed with DPBS, erythrocytes were lysed using ACK Lysis buffer, (Gibco) and wells were resuspended in growth medium RPMI-1640 (Gibco) supplemented with 10% FBS (Gibco), 1% Penicillin Streptomycin (Gibco), 10 mM HEPES (Gibco), 1 x nonessential amino acids (Sigma-Aldrich), 1 mM sodium pyruvate (Gibco), 55 μM 2-mercaptoethanol (Sigma-Aldrich), 50 μg/mL Gentamycin (Life Technologies), 2.5 μg/mL Amphotericin B (Corning) and 10 ng/mL Granulocyte-macrophage colony-stimulating factor (GM-CSF, Peprotech) or RPMI-1640 (Gibco)

supplemented with 10% FBS, 1% Penicillin Streptomycin (Gibco), 10 mM HEPES, 1X nonessential amino acids (Sigma-Aldrich), 1 mM sodium pyruvate (Gibco), 55 μM 2-mercaptoethanol (Sigma-Aldrich), 50 μg/mL Gentamycin (Life Technologies), 2.5 μg/mL Amphotericin B (Corning) and macrophage colony stimulating factor (M-CSF, Peprotech). BMDCs and BMDMs emerging from this were cultured and supplemented with additional supplemented RPMI-1640 on days 3 and 7 and were employed in experiments on days 8 to 12 after harvest. All cell types were grown in a humidified atmosphere with 5% CO_2 at 37 ^{o}C.

in vitro Evaluation of NP Delivery of 3pRNA. For all cell lines, 5,000 cells were plated into 96-well plates and were allowed to adhere overnight for reporter cell activity or IFN-α secretion at multiple doses. CT26 cells were plated at 50,000 cells/well for PCR, flow cytometry, and HMGB1 concentration determination experiments. For BMDCs and BMDMs, 500,000 cells were plated in a 6-well plate and were adhered overnight for PCR and IFN-α concentration determination experiments. After letting the cells adhere, cell supernatant was replaced with formulation diluted into fresh media at the indicated concentration. After 6 h or 24 h, the cell supernatant was collected for analysis and stored at -80^{o}C until used. For qRT-PCR analyses, cells were washed and 700 μL of RLT lysis buffer (Qiagen) was added to each well. Lysates were stored at -80^{o}C until used.

To determine the half maximal response concentration (EC_{50}) of indicated formulation, RNA dose sweeps between 0.05-50 nM final RNA concentration were performed in A549-Dual and THP1-Dual cell lines. Values for EC_{50} were extrapolated from dose-response curve fits using GraphPad Prism software. NPs were formulated as detailed above and treated with D-PDB and 3pRNA (NP/3pRNA), D-PDB and OH-RNA (NP/OH-RNA), or D-B and 3pRNA (NP_c/3pRNA).

Luminescent reporter assays were performed using QUANTI-Luc (Invivogen) following the manufacturer's instructions. Luminescence was quantified using a Synergy H1 microplate reader (BioTek, Winooski, VT). All measurements were normalized after baselining to the average value of the PBS-treated negative control group.

All other cell lines, as well as BMDCs and BMDMs, were treated with NPs at a 50 nM final RNA concentration. Cells were treated with NPs formulated as detailed above, consisting of the following groups NP/3pRNA, NP/OH-RNA, D-PDB + PBS (NP only), and PBS. IFN-α concentrations in cell supernatant were determined using a Lumikine mIFN-α kit (Invivogen) according to the manufacturer's instructions. HMGB1 concentrations in cell supernatant were determined using an HMGB1 ELISA mouse kit (Cloud-Clone). mRNA was extracted from cell lysates using an RNA isolation kit (RNeasy mini kit, Qiagen). cDNA was synthesized for each sample using a cDNA synthesis kit (iScript, Bio-Rad) and analyzed using qRT-PCR using SybrGreen (Thermo Fischer) with CFX real time PCR detection system (Bio-Rad) following the manufacturer's instructions. Primers for *Ifnb1* (Mm.PT.58.30132453.g), *Cxcl10* (Mm.PT.58.4357827), *Il6* (Mm.PT.58.10005566), *Tnfa* (Mm.PT.58.12575861), and Ppib (Mm.PT.58.29807961) were purchased from Integrated DNA Technologies.

Protein Immunoblot. Cells were scraped on ice, centrifuged, and pellets were re-suspended in RIPA lysis buffer (Santa Cruz). Cell lysates were placed on ice. Protein concentration was measured using Pierce BCA Protein Assay Kit (Thermo Scientific, Waltham, PA). Equal amount of proteins were subjected to SDS-PAGE and transferred onto nitrocellulose membranes using the semi-dry transfer protocol (Bio-Rad Laboratories, Hercules, CA). After transfer, membranes were probed with

primary antibodies for cleaved caspase 8 (9429T, Cell Signaling Technology), cleaved caspase 3 (9664T, CST), caspase 8 (9427T, CST), caspase 3 (SC 56053, Santa Cruz), phosphor-IRF3 (4997S, CST), IRF3 (4302S, CST), RIG-I (3743S, CST), phospho-STAT1 (9167S, CST), and β-actin (A5411, Sigma-Aldrich) overnight at 4^{o}C. Following incubation, the membranes were probed with anti-mouse (W402B) or anti-rabbit (4401B) HRP-conjugated secondary antibodies (Promega). Protein bands were visualized using the commercial Immobile Western Chemiluminescent HRP Substrate Kit (Millipore, Billerica, MA). Images of immunoblots were obtained using the ChemiDoc XRS+ system (Bio-Rad).

Flow Cytometry. CT26 cells were plated and treated with indicated formulations as described above. After 24 h of treatment, supernatant was collected and cells were removed using 0.05% Trypsin-EDTA (Gibco). Cells and supernatant were spun down and washed 3x in FACS buffer (0.5% BSA in PBS). Cells were stained with anti-calreticulin (AF647, ab196159, Abcam) and analyzed using a Guava easycyte HT benchtop flow cytometer (Millipore).

BMDM and BMDCs were plated and treated with indicated formulations as described above. After 24 h of treatment, cells were washed, removed from the plate using a cell scraper, pelleted via centrifugation (850 rcf, 5 min), and stained with a cocktail of anti-CD40-(FITC), CD80 (APC), and CD-86 (PE/Cy7) antibodies (BioLegend) in FACS buffer (0.5% BSA in PBS). DAPI staining was used to discriminate live from dead cells. Samples were kept on ice and analyzed using a BD-LSR Fortessa flow cytometer. All flow cytometry data were analyzed using FlowJo version 10 (Tree Star Inc).

Preparation of NP/3pRNA for *in vivo* studies. Polymer was dissolved in PBS as described above and subsequently buffer exchanged and concentrated

into phosphate buffered saline (155 mM NaCl, 1.05 mM KH_2PO_4, 3 mM Na_2HPO_4, Gibco) via centrifugal dialysis following the manufacturer's instructions (Ambion, 3kDa MWCO, Millipore) and sterile filtered using a 0.22 μm syringe filter (Pall corporation) to 30-60 mg/mL. Final polymer concentration was determined spectrophotometrically (Synergy H1 microplate reader, BioTek) using an absorbance at 310 nm. Concentrated polymer solution was rapidly mixed with either 3pRNA or OH-RNA at a charge ratio of 4:1 (N:P), incubated at room temperature for 30 min, and diluted into PBS (pH 7.4, Gibco) prior to intratumoral (IT) administration.

Animal Care and Experimentation. Female BALB/cJ mice (7-11 weeks old) were obtained from The Jackson Laboratory (Bar Harbor, ME). All animals were maintained at the animal facilities of Vanderbilt University under specific pathogen-free conditions. All animal experiments were approved by the Vanderbilt University Institutional Animal Care and Use Committee (IACUC). Tumor volume, as well as mouse weight, was measured every other day via caliper measurements and a balance. Tumor volume was calculated using the equation $V = 1/2(L * W * H)$.[161]

qRT-PCR Analysis of CT26 Tumors. Female BALB/cJ mice (11 weeks old mice) were inoculated with 100 μL of CT26 cells suspended in cold PBS (pH 7.4, Gibco), at 2x10^6 cells/mL. Once tumor volumes reached approximately 100 mm^3, Mice were intratumorally administered 50 μL of indicated formulation or vehicle (PBS) containing 25 μg of either 3pRNA or OH-RNA and 400 μg of polymer in PBS using a 0.5 cc syringe and a 29 gauge needle (n=4 for each group). The mice were treated once more 48 h after the first injection with the same formulation. After 24 h, mice from each group were euthanized, and tumors were surgically removed and stored at -20^{o}C in RNA later. Tumors stored in RNA later were transferred into 1 mL of RLT lysis buffer in gentleMACs P tubes (Miltenyi Biotec)

and digested using gentleMACS Octo dissociator (Miltenyi Biotec). Supernatant was transferred to RNeasy mini columns for mRNA purification following the manufacturer's instructions. cDNA synthesis and qRT-PCR was performed as described above.

Immunoblot Analysis of CT26 Tumors. CT26 tumors were established subcutaneously in BALB/cJ mice and treated as described above. After 24 h, mice from each group were euthanized, and tumors were surgically removed and stored at -20^{o}C. For protein isolation, tumors stored dry at -80^{o}C were transferred into 1 mL of RIPA lysis buffer (Santa Cruz) in gentleMACs P tubes (Miltenyi Biotec) and digested using gentleMACS Octo dissociator (Miltenyi Biotec). Following centrifugation (2000 rcf, 3 min), supernatant was transferred to 2 mL microcentrifuge tubes (Eppendorf). Protein immunoblotting was performed following the protocol described above.

Immunohistology of CT26 Tumors. CT26 tumors were established subcutaneously in BALB/cJ mice and treated as described above. After 24 h, mice from each group were euthanized, and tumors were surgically removed and stored in 10% formalin at room temperature. Tumors fixed in 10% formalin were paraffin embedded, sectioned, and sections were stained with hematoxylin and eosin. Immunohistochemistry was performed using the following antibodies: anti-Ki67 (Catalog no. 12202S, Cell Signaling Technology, Danvers, MA) and anti-CD8 (cat no. 14-0808-80, eBioscience Inc, San Diego, CA). Briefly, heat induced antigen retrieval was performed on the Bond Max using their Epitope Retrieval 2 solution for 20 min. Slides were placed in a Protein Block (Ref no. x0909, DAKO, a, CA) for 10 min. The sections were incubated with anti-Ki67 at a 1:300 dilution for 1 h. Sections were incubated with anti-CD8 at a dilution of 1:1500 for 1 h and then incubated in a rabbit anti-rat secondary (BA-4001, Vector Laboratories,

Inc.) for 15 min at a 1:200 dilution. The Bond Refine Polymer detection system was used for visualization. Slides were then dehydrated, cleared and cover-slipped. Tumor sections were processed for this study using the translational pathology shared resource (TPSR) core facility at Vanderbilt University. After processing, a minimum of four images of each sample were taken using a Leica DM2500 microscope. The percent positive cell populations were calculated using ImageJ cell counter tool. The population of Ki67+ and CD8+ cells were compared to the population of hematoxylin and eosin stained cells in each captured slide image.

Evaluation of NP/3pRNA in CT26 colon cancer model. Female BALB/cJ mice (7 weeks old) were inoculated with 100 μL of CT26 cells suspended in cold PBS (pH 7.4, Gibco), at 106 cells/mL on day -12. On day 0, mice were administered 50 μL of NP/3pRNA or NP/OH-RNA at a dose corresponding to 25 μg RNA and 400 μg polymer in PBS every 2 days for 12 days. PBS was used as the vehicle control. In some cohorts, mice were administered 100 μg αPD1 (RMP1-14, BioXCell) in 100 μL PBS intraperitoneally every 4 days for 12 days. The groups for this study were the following: NP/3pRNA + αPD-1 (n=10), NP/3pRNA (n=10), NP/OH-RNA (n=8), PBS + αPD-1 (n=10), and PBS (n=10). Mice were euthanized when tumor volumes exceeded 1500 mm^3.

Statistics. Significance was determined using one-way ANOVA with Tukey's multiple comparisons test unless otherwise noted. Values represent experimental means, and error bars represent S.D. unless otherwise noted. **** p¡0.0001, *** p¡0.005, **p¡0.01, * p¡0.05

Acknowledgements

We gratefully acknowledge Prof. Kenneth Rock (University of Massachusetts Medical School) for providing DC2.4 cells, Prof. Anna M. Pyle and Dr. Olga Fedorova (Yale University) for synthesizing and providing 5' triphosphate RNA, and Prof. Craig Duvall (Vanderbilt University) for use of gel permeation chromatography equipment. We thank the core facilities of the Vanderbilt Institute of Nanoscale Sciences and Engineering (VINSE) for the use of their Malvern Zetasizer for dynamic light scattering, the VUMC Flow Cytometry Shared Resource, supported by the Vanderbilt Ingram Cancer Center (P30 CA68485) and the Vanderbilt Digestive Disease Research Center (DK058404), for the usage of the BD LSR Fortessa flow cytometer, the Vanderbilt Translational Pathology Shared Resource, and the Vanderbilt Technologies for Advanced Genomics (VANTAGE). This research was supported by grants to JTW from the American Cancer Society (Institutional Research Grant IRG-58-009-56), the Alex's Lemonade Stand Foundation (SID924), and the Congressionally-Directed Medical Research Program (W81XWH-161-0063).

Chapter 3

Structural Optimization of Polymeric Carriers to Enhance the Immunostimulatory Activity of Molecularly Defined RIG-I Agonist 5'-Triphosphate RNA

Chapter Summary

The positive corona of the polymer of 3pRNA/NPs comprising 3pRNA and D-PDB utilized in chapter 2 can lead to poor 3pRNA/NP circulation and increased particle toxicity. In this chapter, we show our data regarding the design a novel amphiphilic diblock copolymer for systemic delivery of 3pRNA through the synthesizis and evaluation a series of amphiphilic diblock copolymers with varying second block hydrophobe side chain length and composition. Through these results, we uncover the relationship between these polymer properties and 3pRNA/NP efficacy and ultimate find a single polymer to use for future systemic 3pRNA/NP administration.

Introduction

Without a carrier molecule, 5'ppp dsRNA has limited therapeutic efficacy because of numerous delivery challenges, including nuclease degradation, poor cellular uptake, endosomal recycling, and lysosomal trafficking.[21] However, nanoparticle carriers that complex with nucleic acids can overcome these barriers to improve therapeutic efficacy. Polyethyleneimine (PEI) is a commercially available transfection agent that can be used to enhance nucleic acid delivery.[73] However, PEI is a large polycation and therefore exhibits size-dependent toxicity. Additionally, this polymer is hypothesized to deliver cargo to the cytosol through the proton sponge effect. The

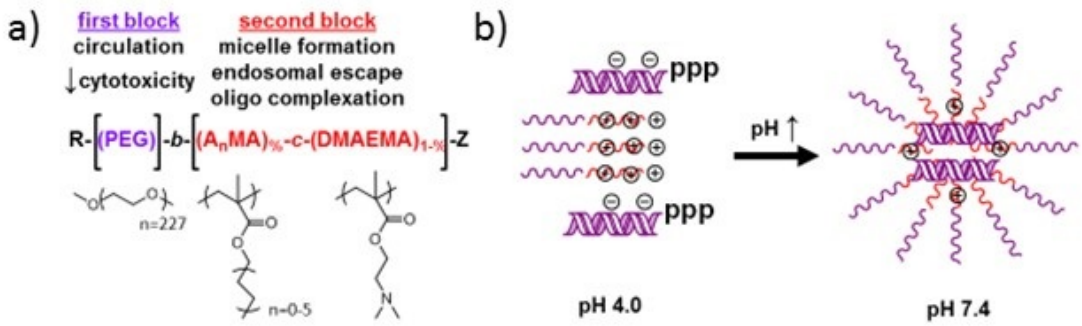

Figure 3.1: **Reversible addition-fragmentation chain transfer polymerization of polymers for 3pRNA/NP formulation.**
a) Schematic demonstrating the structure and purpose of synthesized the polymer series P-b-DA$_n$[%]. n represents the alkyl chain length of the hydrophobic methacrylates incorporated into the polymer second block, and [%] represents the composition of hydrophobic methacrylates incorporated into the polymer. n ranges from 2-12, and [%] ranges from 20-60. b) Schematic for 3pRNA/NP formulation. Polymers are diluted into low pH buffer and complexed with nucleic acid to form polyplexes. pH is raised to physiological value through buffer addition before experimental use.

proton sponge hypothesis suggests that the large buffering capacity of PEI or other cations increases the flow of protons into the endosome, lowering the lysosomal pH. In order to counterbalance the lower pH, water enters the late endosome, causing porous leakage of the nucleic acid cargo. While still generally accepted as the best reason for endosomal escape of cargo to the cell cytosol, there is conclusive proof and some evidence suggesting that this mechanism contributes to the toxicity of PEI.[95] A new generation of amphiphilic diblock pH-responsive co-polymers are currently used to form nanoparticles for cytosolic delivery including 3pRNA as well as other cytosolically active RNA. These polymers improve upon PEI by constraining membrane disruptive hydrophobic groups to the second block of polymer carriers in these studies in order to limit exposure to solely the endosomal membrane upon entering the low pH environment of the endosome.

These polymers, however, usually utilize a positively charged corona for nucleic acid complexation and were not specifically designed for 3pRNA delivery. For example, in chapter one, we weutilized D-PDB for NP delivery of 3pRNA. As another example, Researchers in the advanced therapeutics laboratory at Vanderbilt University utilized polymers with a polyethylene glycol (PEG) first block and a second block of dimethylaminoethyl methacrylate (DMAEMA) and butyl methacrylate (BMA) for delivery of siRNA.[98] Previously synthesized amphiphilic diblock copolymers with either a PEG or zwitterionic corona have been used for delivery of siRNA, and utilize DMAEMA or diethylaminoethyl methacrylate (DEAEMA) as positively charged monomers and only BMA as membrane disruptive hydrophobic monomer.[97,98] While promising and effective for siRNA, this class of polymeric carrier has not been utilized or optimized for 3pRNA, often experiences poor stability for *in vivo* treatments. In addition, very little work towards

optimizing the composition and alkyl chain length of the hydrophobic monomer has been reported. To address the current shortcoming of current strategies for NP-based delivery of RNA, we generated a series of novel amphiphilic diblock copolymers comprised of a 10 kDa first block comprised of PEG and a varied second block composition. The second block is comprised of DMAEMA and a hydrophobic methacrylate monomer with a variable alkyl side chain length (A_nMA) at hydrophobic monomer compositions ranging from 20% to 60% (Figure 1a, Table 2, Table 3). This second block is responsible for RNA complexation, micellar particle formation, inducing endosomal escape, and can complex with nucleic acid at low pH (figure 1b). We evaluate the pH-responsive properties of the series polymers and define a relationship between the hydrophobic monomer alkyl side chain length, the hydrophobic monomer composition, and pH-responsive size change, endosomolytic potential, or 3pRNA/NP activity. Moreover, we wecompare 3pRNA/NPs comprised of polymeric lead carriers to determine which formulation is optimal for 3pRNA/NP *in vivo* treatment.

Results

pH-responsive polymer properties broadly depend on second block composition of P-b-DA$_{[n]}$[%]. To better understand the relationship between series polymer second block composition and 3pRNA/NP efficacy, we we compared each polymer's pH-responsive NP disassembly and membrane disruptive potential. To that end, we we formulated each series polymer at pH 7.4 and 5.8 to mimic the physiological conditions of the bloodstream as well as the endosome and determined whether there was a change of particle size between the two pH values, indicative of micelle disassembly at endosomal pH (Figure 2a-2b). We ratioed volume-

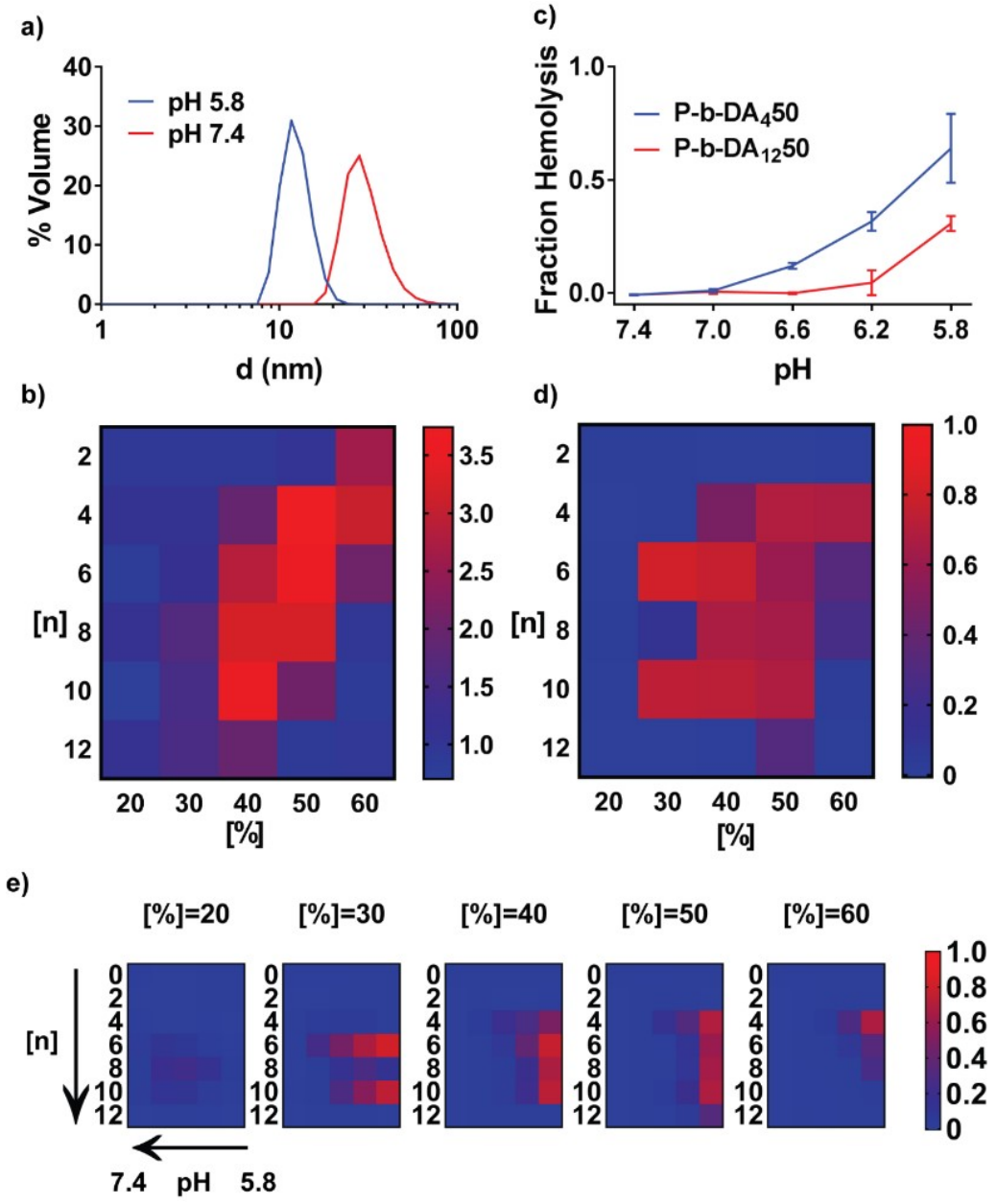

Figure 3.2: **pH-responsive polymer properties broadly depend on second block composition of P-b-DA$_n$[%].**

a) Particle size for P-b-DA$_n$[%] was measured at endosomal and physiological pH at 1 mg/mL in PBS. b) Ratios of particle size for P-b-DA$_n$[%] at physiological pH and at endosomal pH were calculated for P-b-DA$_n$[%]. Color bar indicated particle size ratio. c) P-b-DA$_n$[%] were incubated with erythrocytes at pH 7.4, 7.0, 6.6, 6.2, and 5.8 at 1 μg/mL, and hemoglobin leakage was quantified and normalized to determine the fraction lysis of erythrocytes in the presence of polymers. d) Fraction hemolysis at pH 5.8 was calculated for P-b-DA$_n$[%]. Color bar represents fraction hemolysis. e) Fraction hemolysis at pH 7.4, 7.0, 6.6, 6.2, and 5.8 was determined for P-b-DA$_n$[%] for [%]=20, 30, 40, 50, and 60. Colorbar indicates fraction hemolysis.

average particle size at physiological pH to endosomal pH values to determine a size ratio for each polymer. Size ratios greater than 2 were indicative of polymer instability at lower pH values, which would be beneficial for endosomal escape of the NP RNA cargo. Notably, polymers comprised of second block hydrophobic monomer compositions between [%]=40 and [%]=50 tended to exhibit pH-dependent dissasembly. Moreover, polymers comprised of hydrophobic side chain lengths of n=2 and n=4 tended to exhibit pH-responsiveness at higher hydrophobic monomer compositions between [%]=50 and [%]=60, while polymers with hydrophobic side chain lengths of n=6, n=8, and n=10 demonstrated pH-responsiveness at lower hydrophobic monomer compositions between [%]=30 and [%]=50. Polymers with n=12, were mostly not pH-responsive, remaining in a micellar structure at all pH values.. Moreover, with the hydrophobic monomer composition of [%]=20, no polymers formed micelles, and therefore did not exhibit pH-dependent dissasembly. In addition to these two traits, the heat map visualizes a distribution of pH-responsive series polymers with similar hydrophobic content. In other words, shorter alkyl side chains on hydrophobic monomers in these series polymers can be compensated with a higher hydrophobic monomer composition, and vice versa.

Towards evaluating the membrane disruptive potential of series polymers, we incubated series polymers with erythrocytes suspended at pH 7.4, 7.0, 6.6, 6.2, and 5.8, evaluating hemoglobin leakage as a metric for membrane destabilizing potential, and mapped the polymeric variables of n and [%]to hemolysis at pH 5.8 using a heat map (Figure 2c-2d). While a multitude of the series polymers that previously exhibited pH-responsiveness also exhibit membrane disruptiveness, there are notable exceptions for polymers constituting monomers with alkyl side chain lengths of n=2 and n=12. This phenomenon is most likely due to the mechanics of

membrane disruption for short and long alkyl side chain hydrocarbons. Moreover, series polymers with hydrophobic monomer compositions of [%]=30 appear to exhibit robust membrane lysis, regardless of the low size ratios those polymers tended to exhibit.

In order to further understand the effect of second block composition on membrane disruption, we determined using heat maps for polymers of a particular hydrophobic monomer composition at pH 7.4, 7.0, 6.6, 6.2, and 5.8 (Figure 2e). Series polymers with a hydrophobic monomer composition of [%]=20 exhibit weak hemolysis across pH 7.0, pH 6.6, and pH 6.2. Series polymers with a hydrophobic monomer composition of [%]=30 and a hydrophobic monomer alkyl side chain length of n=10 and n=6 exhibit increasing fraction hemolysis across descending pH values, ranging from pH 7.0 to pH 5.8. Furthermore, as the hydrophobic monomer composition increases for series polymers,two trends were identified. The pH value at which series polymers exhibit hemolysis decreases as the hydrophobic monomer composition of the series polymers increases. Moreover, as the hydrophobic monomer composition increases, series polymers with a shorter hydrophobic monomer alkyl side chain length exhibit increasing fraction hemolysis.

I determine Spearman's rank correlation coefficients for series polymer hydrophobic monomer and alkyl side chain length and composition to fraction hemolysis and size ratio to quantify non-parametric correlations between both pH-responsive polymer properties and series polymer construction . We evaluate linear n and [%], which indicate a singular general trend – e.g. increasing composition of hydrophobic monomer or larger alkyl chain lengths consistently lead to increased or decreased pH-responsive size change and hemolysis. We also evaluate non-linear components of n and [%], which would indicate an active range of n and [%] – e.g. increased pH

responsive size change and hemolysis a corresponds towards composition approaching a small cluster of n and [%], possibly with a peak at a single value. We Wefind that non-linear alkyl side chain length n and hydrophobic monomer composition [%] weakly correlate to size ratio and therefore minimally contribute towards polymeric micelle formation. Moreover, we find that non-linear n and [%] moderately correlate to fraction hemolysis, indicating that series polymer composition and alkyl chain length impact polymeric membrane disruptive potential to a greater extent than pH-responsiveness. We do not find significant dependence on linear n and [%] (Table 4). Here, non-linear dependence on n and [%] indicates that a range of those values, rather than polymers comprised of the highest or lowest n and [%], would exhibit both pH-responsiveness and endosomolytic potential. This corroborates the phenomenon demonstrated for both fraction hemolysis and size ratio, that a range of hydrophobic polymer content exists, provided by either longer alkyl side chain length n or higher hydrophobic monomer composition [%], but not both properties, at which polymers exhibit both endosomolytic potential and pH-responsive size change.

NP delivery of 3pRNA using unique series polymers differentially triggers ISG activation in A549 reporter cells. RIG-I activation has been shown to increase tumor immunogenicity via several connecting mechanisms in multiple cancer cell types, leading to cancer cell death, increased expression of anti-tumor cytokines as well as T-cell chemokines, and processing of tumor antigens by antigen presenting cells, ultimately leading to establishment of anti-tumor immunity.[76,80,162] Here, we demonstrate that 3pRNA/NPs comprised of series polymers and 3pRNA are capable of activating RIG-I in a reporter cancer cell type for two-fold purpose. By comparing 3pRNA/NPs comprised of series polymers containing different second block copolymers, we can determine the effect of the

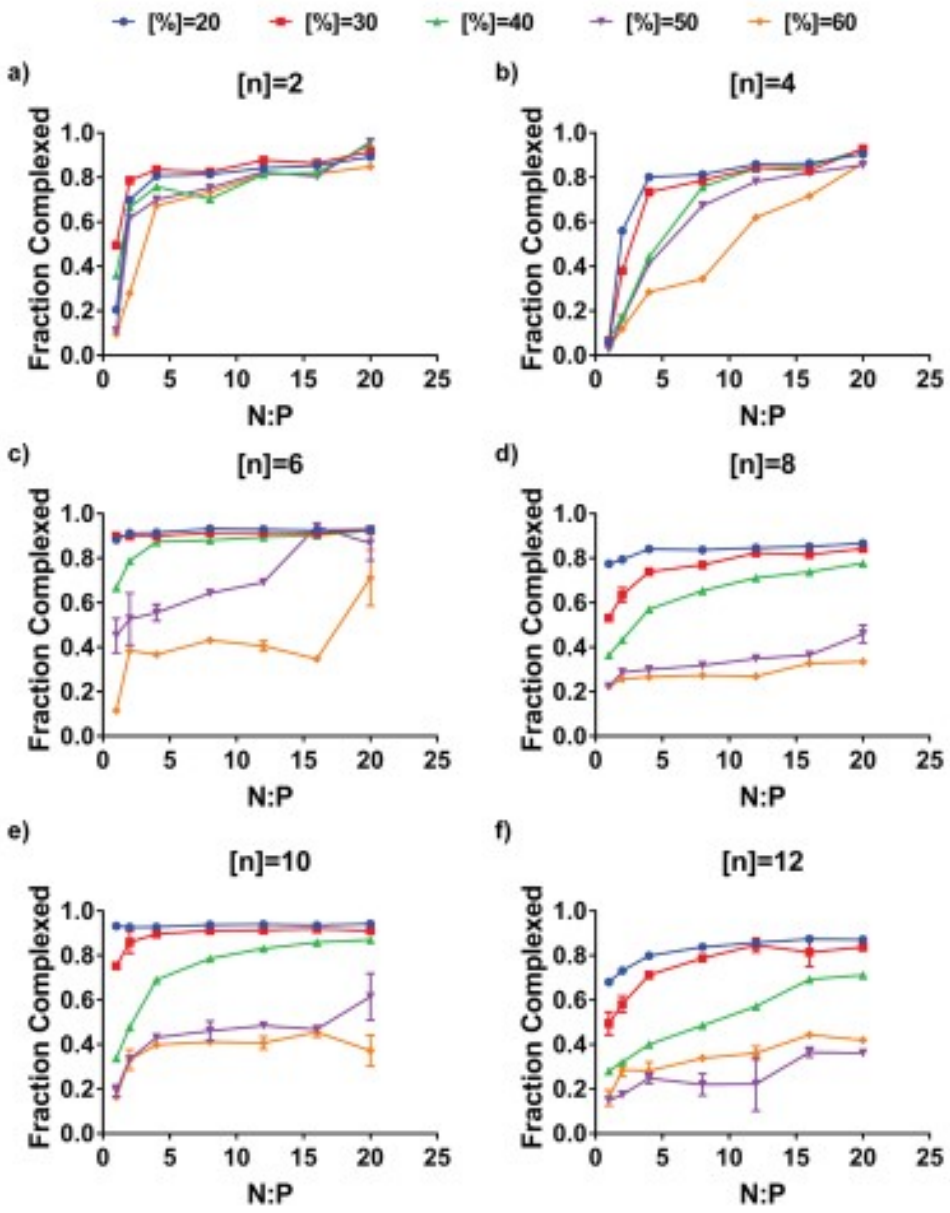

Figure 3.3: **N:P determination for 3pRNA/NP formulation.**
Series polymers comprised of hydrophobic monomer alkyl chain lengths n=2 a), n=4 b), n=6 c), n=8 d), n=10 e), and n=12 f) and hydrophobic monomer compositions ranging from [%]=20 to [%]=60 were complexed with OH-RNA at various N:P ratios and incubated with a Ribogreen intercalating dye to determine the extend that 3pRNA/NPs shield RNA from degradation.

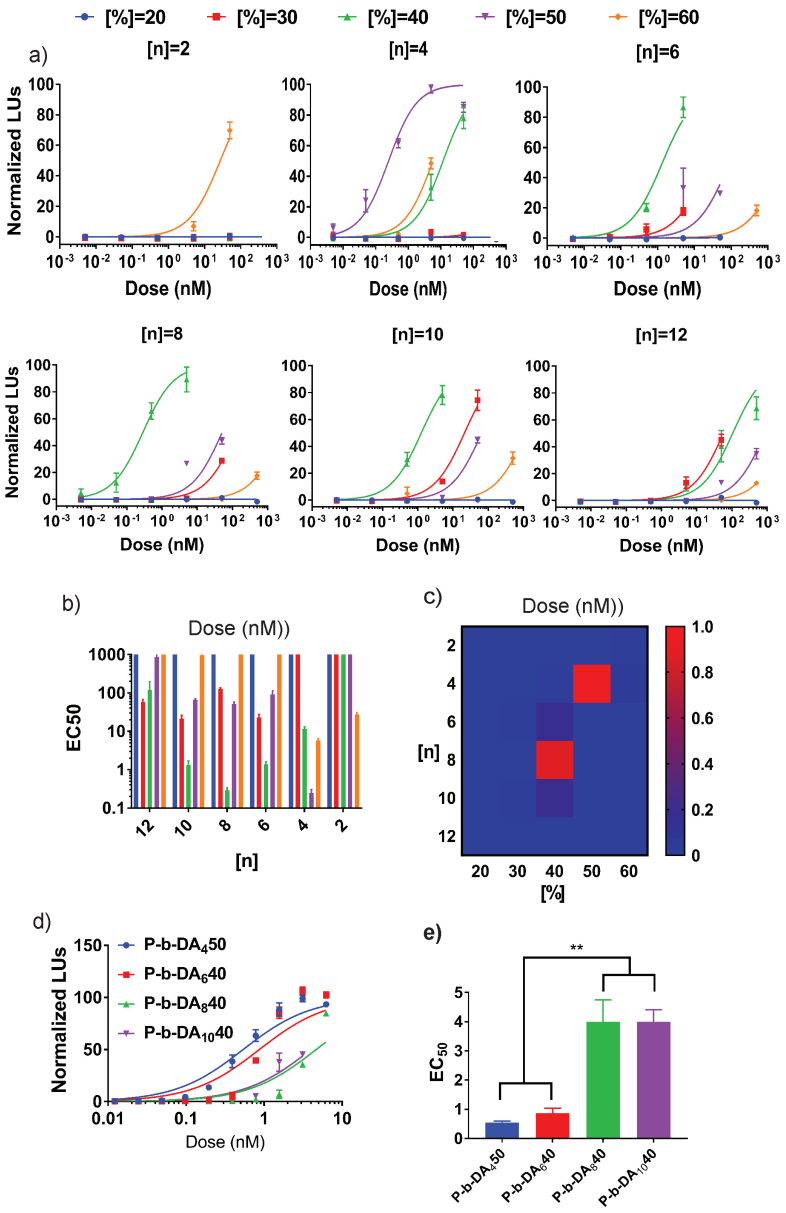

Figure 3.4: **NP delivery of 3pRNA comprised of unique series polymers differentially triggers ISG activation in A549 reporter cells.**
a) Normalized response of luminescent ISG reporter A549 cells after treatment with 3pRNA/NPs comprised of P-b-DA$_n$[%] and 3pRNA, organized by n, at 500 nM, 50 nM, 5 nM, 0.5 nM, and 0.05 nM RNA doses. b) EC_{50} was calculated for each 3pRNA/NP from a). c) Heatmap demonstrating EC_{50} ratios normalized by the lowest EC_{50} value. The colorbar represents EC_{50} ratio. d) Normalized response of luminescent ISG reporter A549 cells after treatment with 3pRNA/NPs comprised of one of the four polymers with the highest EC_{50} ratio, P-b-DA$_4$50, P-b-DA$_6$40, P-b-DA$_8$40, and P-b-DA$_1$040, and 3pRNA. e) EC_{50} was calculated for each 3pRNA/NP from d).

second block hydrophobic monomer alkyl side chain length and composition on 3pRNA/NP efficacy. Furthermore, the most potent 3pRNA/NPs can be used in future studies, contributing to expanding literature on RIG-I activation as a potent target for cancer immunotherapies. We complexed series polymers with OH-RNA at N:P values of 2, 4, 8, 12, 16, and 20 and incubated formulations with an RNA intercalating dye to determine N:P ratios required to form stable 3pRNA/NPs (Figure 3.3). Wefind that carriers with a lower composition of hydrophobic monomer form stable particles at lower N:P ratios. We determined that 3pRNA/NP complexes 3pRNA completely at N:P ratios of 20, and formulated 3pRNA/NPs at that N:P ratio for all studies. We treated A549 reporter cells that express Lucia luciferase downstream of interferon regulatory factor 3 with 3pRNA/NPs comprised of series polymers complexed with 3pRNA at an N:P ratio of 20 at 500 nM, 50 nM, 5 nM, and 0.5 nM final RNA dose (Figure 4a). Utilizing this data, we calculate EC_{50} values for NPs comprised of each series polymer and visualize inverted and normalized EC_{50} values through a heatmap (Figure 4b-4c). We find that four polymers exhibit EC_{50} values between 0.5 nM and 2 nM: P-b-$DA_4$50, P-b-$DA_6$40, P-b-$DA_8$40, and P-b-$DA_1$040. Interestingly, while each of the four lead polymers do demonstrate pH-responsive size change and hemolysis at pH 5.8, they are a small fraction of the series polymers capable of both of these, indicating another property that could be investigated to further understand the relationship between series polymer structure and 3pRNA/NP potency.

Although these data demonstrate that the second block hydrophobic monomer alkyl chain length and composition changes 3pRNA/NP potency, it does not determine the influence of those properties independently. We determined the Spearman's rank correlation coefficient for n, [%], nonlinear n, and nonlinear [%] in

order to understand the direct relationship between these properties and 3pRNA/NP EC_{50} values for various series polymers (Table 2). Interestingly, while there is a weak correlation to nonlinear n, the rank correlation coefficient for nonlinear [%] indicates a moderate correlation. This indicates that while series polymers require a specific hydrophobic monomer alkyl chain length depending on monomer composition, the hydrophobic monomer composition itself may affect critical properties of the formulated 3pRNA/NP.

We further investigate these four carriers using a two-fold dose sweep starting at 5 nM and calculated EC_{50} in order to resolve differences between the EC_{50} values of the lead carriers from the previous study (Figure 4d-4e). Using a more defined EC_{50} curve, we determine that 3pRNA/NPs comprised of P-b-$DA_4$50 or P-b-$DA_6$40 are significantly more potent than 3pRNA/NPs comprised of P-b-$DA_8$40 or P-b-$DA_1$040. Regardless of this significant difference between these four lead carriers, the EC_{50} values are within an order of magnitude. Further studies are needed to determine which 3pRNA/NP formulation would be most effective to activate RIG-I *in vivo* . Here, we investigate 3pRNA/NP stability, inflammasome activation, and ISG activation as well as monocyte activation across multiple cell lines towards this goal.

NP delivery of 3pRNA using lead polymer carriers activates RIG-I in both cancer cells and myeloid cells and induces production of inflammatory cytokines. Since the TME is not solely comprised of cancer cells but rather is populated by a variety of cell types including tumor infiltrating myeloid cells, myeloid-derives suppressor cells dendritic cells, and tumor associated macrophages, an immunosuppressive milieu is necessary that addresses a wide array of cell types. 3pRNA/NPs comprised of lead polymeric carriers need to be able to activate cancer

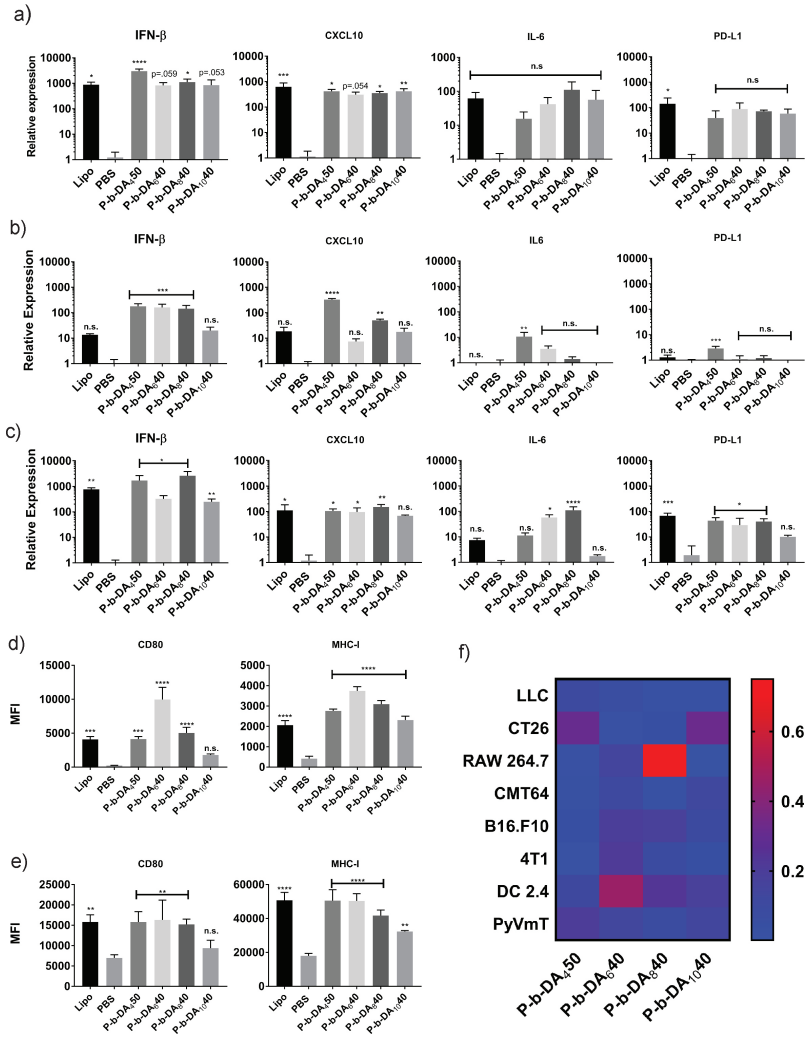

Figure 3.5: **NP delivery of 3pRNA using lead polymer carriers activates both cancer cells and myeloid cells and induces production of inflammatory cytokines.**
Relative expression of *Ifnb1, Cxcl10, Il6,* and *PD-L1* measured by qRT-PCR after treatment of a) 4T1, b) RAW 264.7, and c) DC 2.4 cells with 3pRNA/NPs comprised of 3pRNA and lead carriers or Lipofectamine 2000 (n=3). All statistics are calculated relative to PBS treated cells using one-way ANOVA with post-hoc analysis. Surface expression of costimulatory receptor CD-80 and MHC-I after treatment of d) RAW 264.7 and e) DC 2.4 cells with 3pRNA/NPs comprised of 3pRNA and leads carriers or Lipofectamine (n=3). All statistics are calculated relative to PBS treated cells using one-way ANOVA with post-hoc analysis. f) Relative secreted IFN-α after treating multiple cell types with 3pRNA/NPs comprised of 3pRNA and lead carriers or Lipofectamine 2000. color bar represents relative IFN-α concentration normalized to samples from cells transfected with Lipofectamine 2000 and PBS (n=3). All statistics are calculated relative to PBS treated cells using one-way ANOVA with post-hoc analysis.

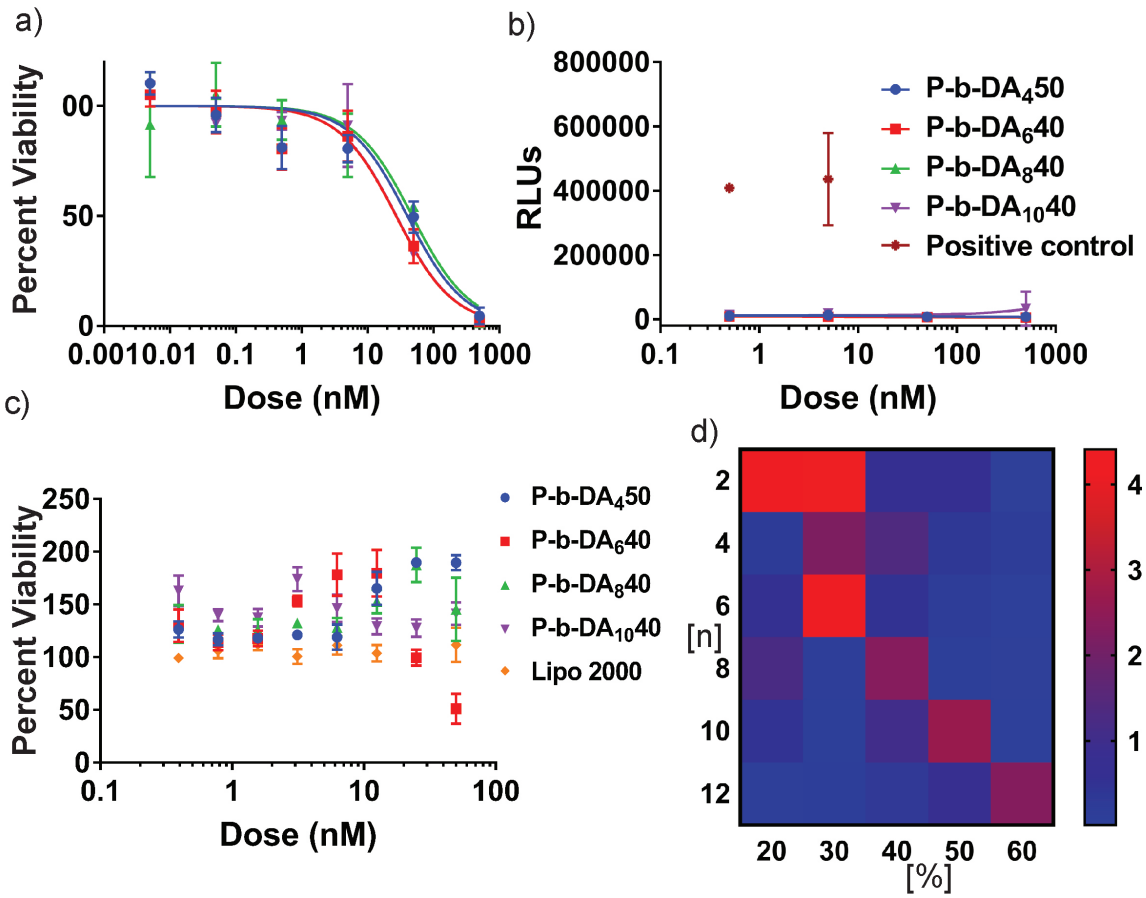

Figure 3.6: **Cells treated with NPs comprised of OH-RNA and series polymers are not toxic or active at relevant concentrations *in vitro*.**
a) A549 reporter cell viability after treating cells with OH-RNA/NPs comprised of RNA and lead carriers at a final RNA concentration of 500 nM, 50 nM, 5 nM, 0.5 nM, or 0.5 nM. b) A549 reporter cell activity after treating cells with OH-RNA/NPs comprised of RNA and lead carriers, compared to one 3pRNA/NP as a positive control. c) MDA constitutive luciferase expression cell viability after treatment with ScrRNA/NPs comprised of ScrRNA and lead carriers, or the commercial transfection agent Lipofectamine 2000 complexed with ScrRNA at a final RNA concentration of 50 nM, 25 nM, 12.5 nM, 6.25 nM, 3.13 nM, 1.56 nM, 0.78 nM, and 0.39 nM. d) Il-1β expression of activated THP-1 human myeloid cells at 6.25 nM final RNA doses for OH-RNA/NPs comprised of P-b-DA$_{[n]}$[%] and 3pRNA. Color bar represents fold increase in Il-1β expression over baseline.

cells as well as these critical myeloid cell populations to effectively immunomodulate the TME. We treated 4T1 murine breast cancer cells (Figure 5a), RAW 264.7 murine macrophages (Figure 5b), and DC 2.4 murine dendritic cells (Figure 5c), with 50 nM final RNA doses of 3pRNA/NPs comprised of lead polymeric carriers and 3pRNA, analyzing the expression of inflammatory and IFN-stimulated genes *IFNβ, CXCL10, IL-6,* and *PD-L1.* All 3pRNA/NPs significantly increase ISG expression, but do not significantly increase the expression of inflammatory genes in 4T1 cells. Interestingly RAW 264.7 cells treated with 3pRNA/NPs comprised of 3pRNA and P-b-$DA_1$040 do not exhibit significant increases in ISG expression over PBS treated cells, though cells treated with 3pRNA/NPs comprised of other lead carriers exhibit significant increases in ISG expression. 3pRNA/NPs formulated using P-b-$DA_4$50 exhibited a significant increase in expression of inflammatory genes *IL-6* and *PD-L1.* Moreover, DC 2.4 cells treated with 3pRNA/NPs experience similar increases in ISG expression to treated RAW 264.7 cells. However, for treated dendritic cells, 3pRNA/NPs comprised of P-b-$DA_1$040 did not result in inflammatory gene expression increases, while all other 3pRNA/NPs did result in expression increases over the baseline. For all three cell types, treatment using 3pRNA/NPs comprised of P-b-$DA_4$50, P-b-$DA_6$40, or P-b-$DA_8$40 complexed with 3pRNA resulted in increased ISG expression, and for all myeloid cells, treatment with P-b-$DA_4$50 also resulted in significantly increased inflammatory gene expression. Overall, 3pRNA/NPs comprised of P-b-$DA_4$50 may be more efficacious *in vivo* because of its ability to better engage both ISGs and inflammatory genes.

Furthermore, we evaluated activation of myeloid cells after 3pRNA/NP treatment. RAW 264.7 (Figure 5d) and DC 2.4 (Figure 5e) cells treated with 3pRNA/NPs were harvested and incubated with fluorescently labeled antibodies for CD80 and MHC-I

and a nucleic acid intercalating dye to confirm cell viability. The surface expression of CD80 and MHC-I on viable myeloid cells was measured using flow cytometry. Following the same trends as the gene expression data, CD80 surface expression is significantly above the baseline except for cells treated with 3pRNA/NPs consisting of P-b-$DA_1$040 while MHC-I surface expression is significantly increased above baseline for all 3pRNA/NPs. We find that 3pRNA/NPs activate myeloid cells, though 3pRNA/NPs comprised of P-b-$DA_1$040 are not as effective as NPs formulated using other polymeric lead carriers. We determined supernatant IFNα concentration of multiple cancer cell types with myeloid cell types being treated using 3pRNA/NPs. IFNα concentrations were measured, and reported as a function of the polymeric variables n and [%] using a heatmap, the color bar representing activity relative to a positive control (Figure 5f). Cells treated with 3pRNA/NPs all exhibit increased IFNα concentrations. Regardless of differences in activity between each cell type, each 3pRNA/NP induces similar IFNα secretion across cell types. Moreover, this activity is not due to off-target polymer-mediated cytotoxicity or inflammation. Multiple cell types were treated with lead carriers complexed with control OH-RNA; these cells did not exhibit cell death below the active doses of 5 nM RNA (Figure 6a,6c). In addition, treating A549 reporter cells with lead carriers complexed with control RNA did not result in activation of ISGs (Figure 6b). We investigated whether treating differentiated human myeloid THP-1 cells, with OH-RNA/NPs comprised of all series polymers, would result in inflammasome activation through indirect measurement of IL-1β, and find that the lead carriers did not induce inflammasome formation at 5 nM RNA dose (Figure 6d).

P-b-$DA_4$50 maintains particle size and activity in serum. RNA degradation is a prominent barrier to 3pRNA *in vivo*. In order to evaluate the ability

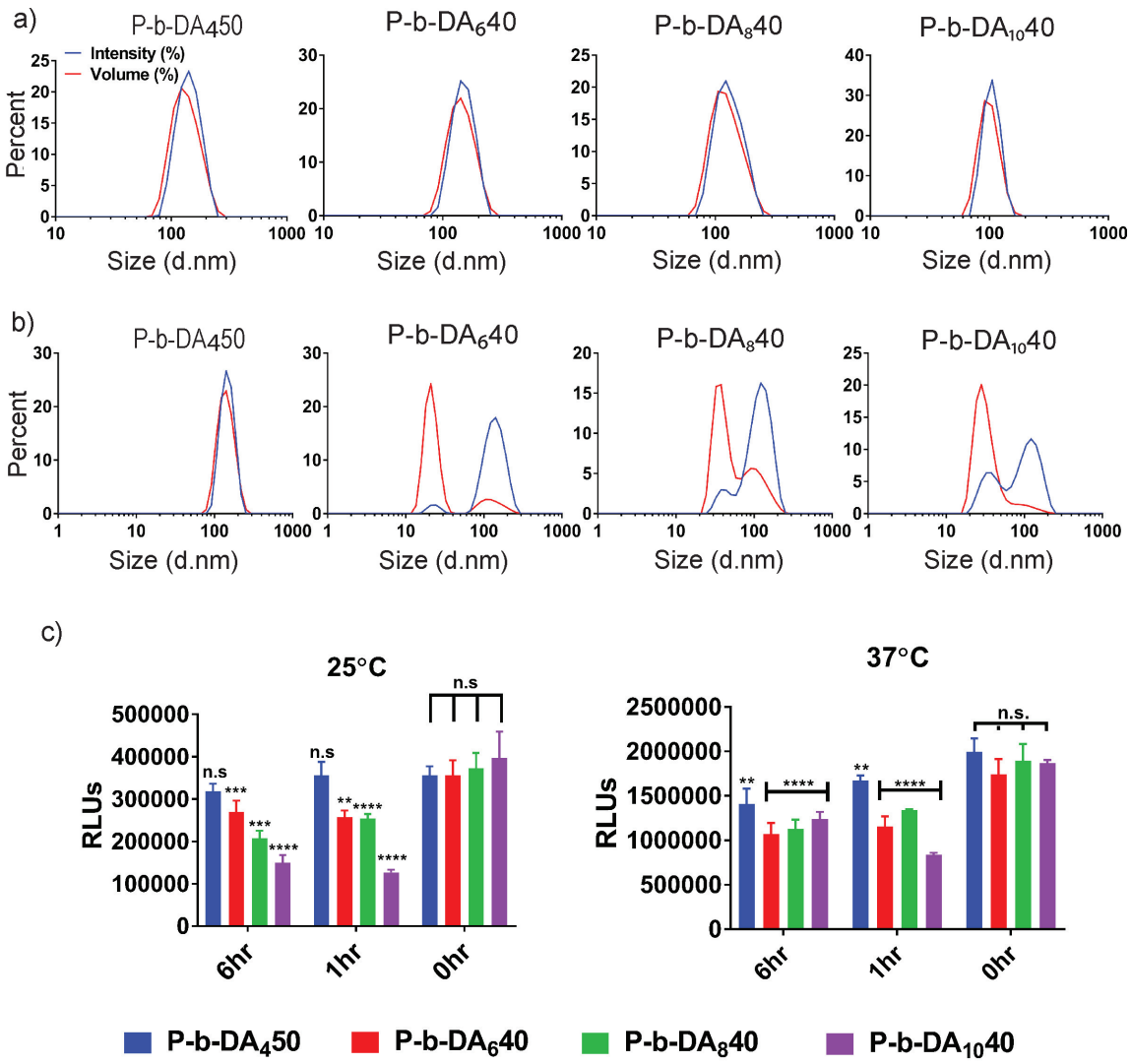

Figure 3.7: **P-b-DA$_4$50 maintains particle size and activity in serum.** a) Particle size distributions for 3pRNA/NPs. 3pRNA was complexed with lead polymers in low pH buffer and raised to a final pH of 7.4 in 100 mM PBS, and particle size distribution was measured using dynamic light scattering. 3pRNA/NP Z-average diameters for lead carriers did not exceed 150 nm for each polymer. b) Particle size distributions for 3pRNA/NPs suspended in 50% serum for 15 minutes (n=3) c) 3pRNA/NPs were incubated in 50% serum at 25^{o}C (left) and 37^{o}C (right) for 0 h, 1 h, or 6 h before treating ISG reporter A549 cells at 5.0 nM RNA . Statistics at t=0 h reference P-b-DA$_4$50. All statistics for t=1 h and t=6 h are calculated in comparison to the same polymer 3pRNA/NP activity at t=0 h using one-way ANOVA with post-hoc analysis.

of 3pRNA/NPs to overcome this delivery barrier, we evaluate the size and activity of 3pRNA/NPs comprised of lead polymers P-b-$DA_4$50, P-b-$DA_6$40, P-b-$DA_8$40, and P-b-$DA_1$040 that are exposed 50% adult bovine serum. Using dynamic light scattering, we evaluate the intensity percent and volume percent size distributions of 3pRNA/NP comprised of 3pRNA and the four lead polymer carriers incubated in either pH 7.4 PBS (Figure 7a) or in 50% adult bovine serum at room temperature (Figure 7b) or at 37^oc(Figure 7c). Protection from RNA degradation is critical for 3pRNA/NP efficacy *in vivo*. In order to assess RNA degradation *in vitro*, we incubated 3pRNA/NPs comprised of lead carrier polymers complexed with 3pRNA in 50% serum for 0 h, 1 h, or 6h at room temperature as well as 37^oC to evaluate loss of efficacy due to RNA degradation. A549 reporter cells were treated with these formulations at 25 nM final RNA dose for 24 h before evaluation. We uncovered that without incubation, all four 3pRNA NPs are roughly equivalent. However, incubation in 50% serum at room temperature results in significant loss of activity loss due to RNA degradation for all 3pRNA/NPs except those comprising P-b-$DA_4$50, at 1 h and 6 h. Furthermore, at 37^oC, all 3pRNA/NPs experiences a significant reduction of activity. NPs comprising P-b-$DA_4$50, however, retain significantly more activity than other 3pRNA/NPs. This loss causes significant differences in activity between 3pRNA/NPs comprised of P-b-$DA_4$50 and the other lead carriers in this study at the 1 h and 6 h timepoints. These results demonstrate that P-b-$DA_4$50 maintains a particulate structure in serum that protects 3pRNA from degradation compared to other formulations comprised of 3pRNA and lead polymeric carriers.

Systemic administration of 3pRNA/NPs comprised of lead carriers and 3pRNA activate ISGs increase type-I IFN production in serum and organs. We evaluated the ability of 3pRNA/NPs comprised of lead polymeric

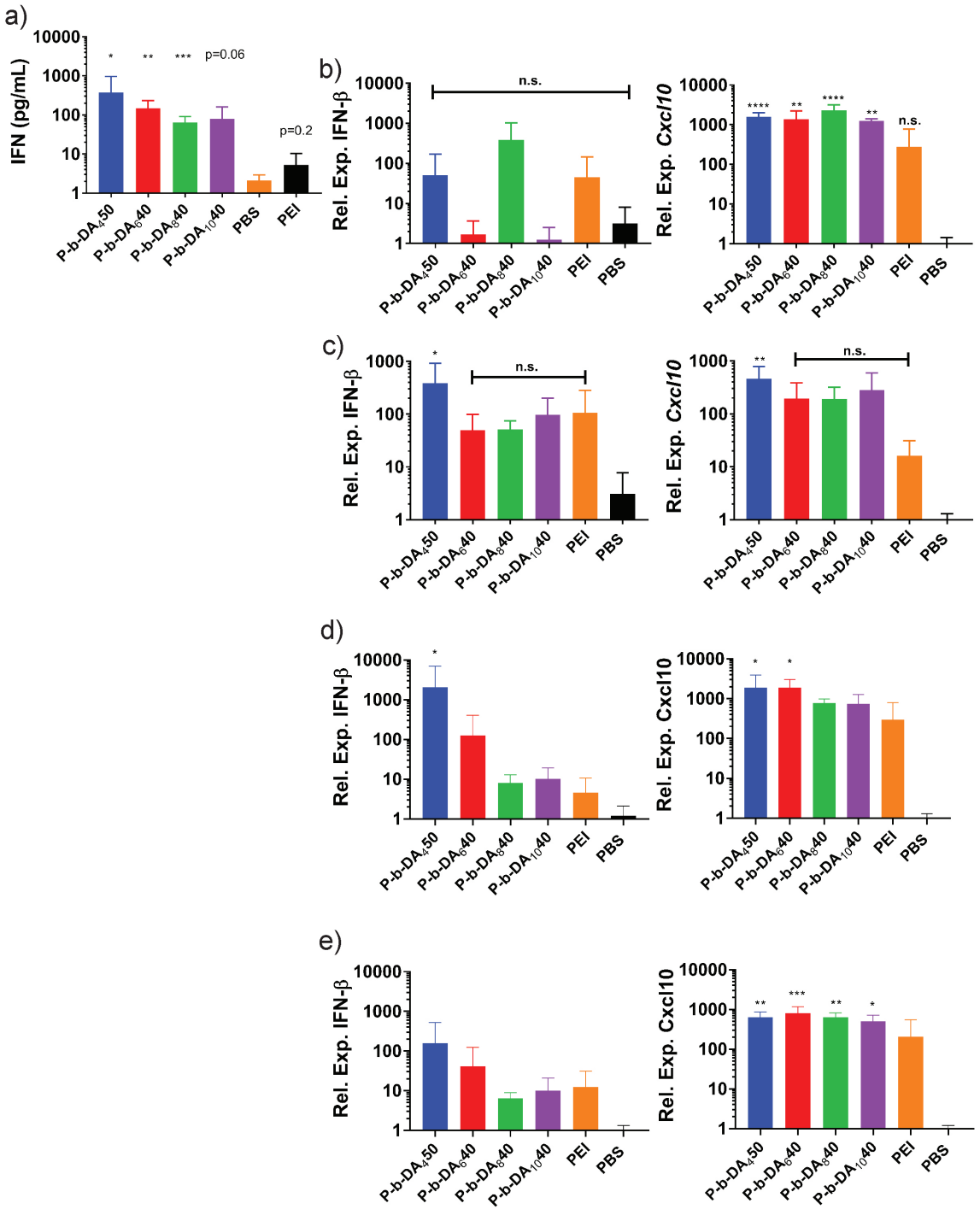

Figure 3.8: **Systemic administration of NP comprised of lead carriers and 3pRNA activate ISGs and increase type-I IFN production in serum and organs.**

a) Serum IFN-α concentration, and b) liver c) spleen d) lung e) kidney *IFN-β* and *cxcl10* expression 6 h after tail vein injection of 0.625 mg/kg 3pRNA/NPs. All statistics were calculated compared to PBS using one-way ANOVA with post-hoc analysis.

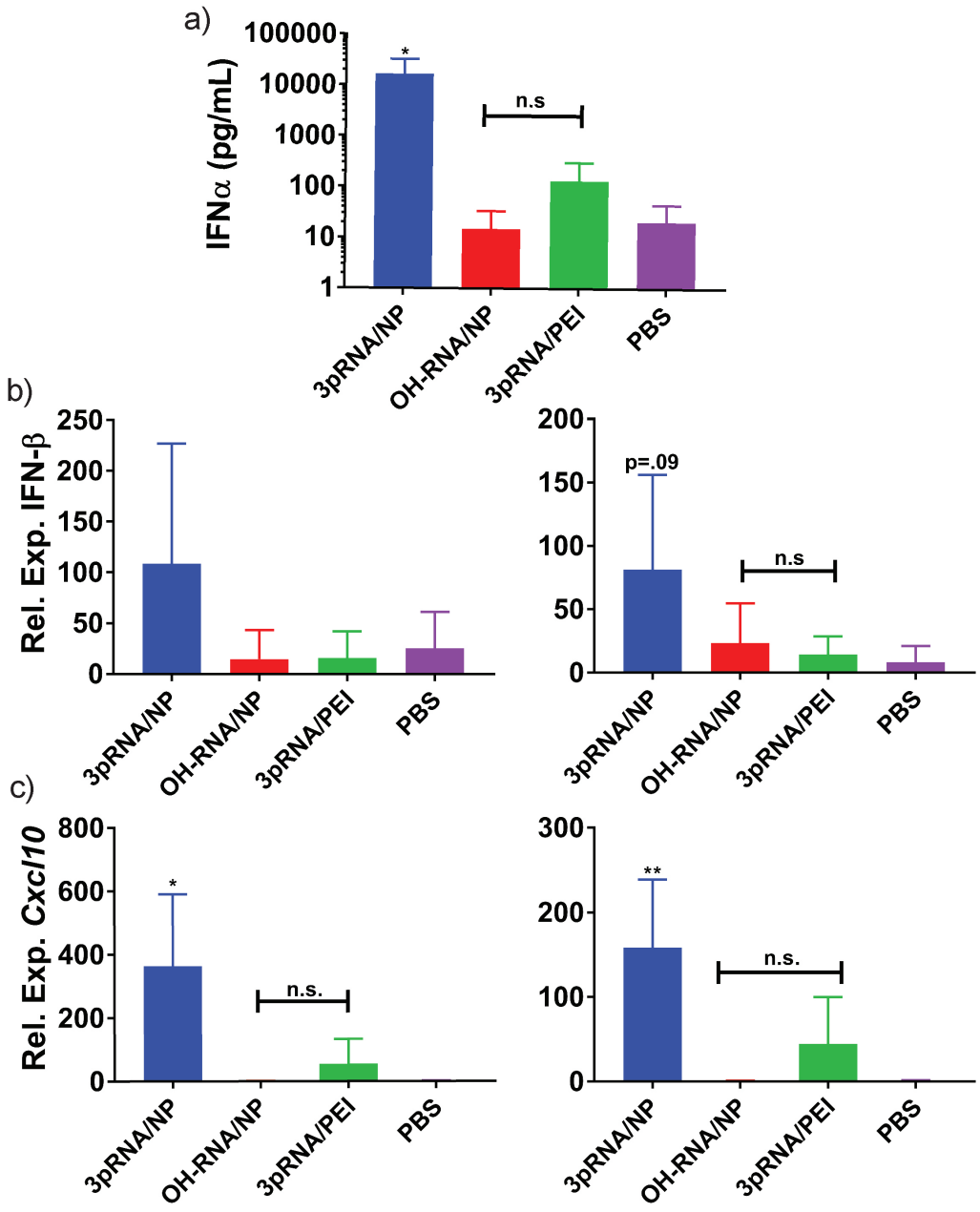

Figure 3.9: **Systemic administration of OH-RNA/NPs comprised of P-b-DA$_4$50 and 3pRNA do not activate ISGs or increase type-I IFN production in serum and organs.**
a) Serum IFN-α concentration 6 h after tail vein injection of 3pRNA/NPs and OH-RNA/NPs at 1.25 mg/kg (n=6) b) Liver (left) and spleen (right) *IFN-β* expression 6 h after tail vein injection c) Liver (left) and spleen (right) *CXCL10* expression 6 h after tail vein injections

carriers complexed to 3pRNA to induce type-I IFN and other ISGs *in vivo* utilizing an intravenous route. BL/6 mice were administered 3pRNA/NPs comprised of lead polymeric carriers complexed 12.5 μg of 3pRNA, 3pRNA/PEI comprised of *in vivo* jetPEI complexed to 3pRNA, OH-RNA/NPs comprised of P-b-$DA_4$50 complexed with OH-RNA, or PBS at 0.625 mg/kg. Mice were euthanized 5 hrs after injection, blood was harvested through cardiac puncture, and organs harvested and digested for qRT-PCT analysis. Serum was further extracted from whole blood before analysis using ELISA. We find that 3pRNA/NPs comprised of lead polymer carriers are capable of inducing serum IFNα expression significantly above baseline (Figure 8a). The four lead carriers, however, did not result in significantly different serum IFNα concentrations. We find that 3pRNA/NPs comprising P-b-$DA_4$50 Moreover, 3pRNA/PEI NP treatment not able to induce significantly increased serum IFNα, we also analyzed expression of *IFNβ* as well as *CXCL10* using qRT-PCR for digested murine livers (Figure 8b), spleens (Figure 8c), lungs (Figure 8d), and kidneys (Figure 8e). Here, there was no significant IFNβ expression in murine livers and kidneys after i.v. administration of 3pRNA/NPs. However, in spleens and lungs, we observed a robust expression of CXCL10 over the baseline for mice treated with 3pRNA/NPs comprised of P-b-$DA_4$50. Expression of CXCL10 in the liver and kidney is significantly increased over the baseline for all 3pRNA/NPs comprised of polymeric lead carriers, but not for mice injected with 3pRNA/PEI NPs. For analyzed spleens and lungs, once more, we observed gene expression of CXCL10 significantly over baseline for 3pRNA/NPs comprised of P-b-$DA_4$50. Additionally, we evaluated the ability of 3pRNA/NPs comprised of lead polymeric carriers complexed to 3pRNA to induce type-I IFN and other ISGs *in vivo* in a murine breast cancer model directly at the tumor site utilizing an intravenous route (Figure

A.8) and found that only mice injected with 3pRNA/NPs comprising P-b-$DA_4$50 induced expression of *IFNβ* as well as *CXCL10* in the tumor microenvironment. We confirmed that this effect was independent of polymer toxicity or immune related effects by comparing OH-RNA/NPs comprising OH-RNA complexed to P-b-$DA_4$50 with 3pRNA/NPs comprising 3pRNA complexed to P-b-$DA_4$50 (Figure 9). Here, we find that intravenous injection of OH-RNA/NPs in non-tumor bearing BL/6 female mice do not induce ISG activation in murine organs, and do not result in increased serum IFNα concentration, while 3pRNA/NPs, as previously observed, do induce both organ ISG activation and increased serum IFNα concentration. Ultimately, serum and organs from mice administered i.v. using 3pRNA/NPs comprised of P-b-$DA_4$50 complexed with 3pRNA resulted in increased expression of ISGs, and injection of either 3pRNA/NPs comprised of other lead polymers with *in vivo* jetPEI were either partially effective or were not significantly above baseline for both serum IFNβ and organ ISG expression.

Discussion

Overcoming drug delivery challenges is a critical factor towards development of novel 3pRNA therapeutics critical to revolutionizing cancer immunotherapy. Drug delivery of current therapeutics can lead to poor cellular uptake, susceptibility to nuclease degradation, and very low cytosolic bioavailability. Research completed in this chapter has demonstrated that polymeric nanoparticles (NP) with pH-responsive, endosome-releasing activity can enhance the intracellular delivery of 3pRNA to potently activate the RIG-I pathway, and that this property is dependent on the second block composition of series polymers. In order to optimize 3pRNA/NPs, a series of novel polymeric carriers were developed to further

elucidate the relationships between polymeric composition, pH-responsiveness, and 3pRNA/NP RIG-I pathway activation.

RAFT polymerization was used to synthesize a series of block copolymers, P-b-DA_n[%], with values of n, representing polymeric hydrophobic monomer chain length equal to 2, 4, 6, 8, 10, and 12, and values of [%] representing polymeric hydrophobic monomer composition equal to 20%, 30%, 40%, 50%, and 60%. Specific polymer series were shown to exhibit pH-responsive size change and hemolytic potential. Moreover, four polymers from the series, P-b-$DA_4$50, P-b-$DA_6$40, P-b-$DA_8$40, and P-b-$DA_1$040, potently activate ISGs when complexed with 3pRNA. Results of extensive copolymer characterization and testing revealed that the polymer hemolytic potential moderately correlates to n, the hydrophobic monomer chain length, while 3pRNA/NP activity for each series polymer moderately correlates to [%]. Taken together, this indicates that the hydrophobic monomer chain length is an important factor driving the pH-responsive polymer properties, and that the polymeric hydrophobic monomer composition of the polymer is critical for determining NP activity. Four lead carriers were selected for further investigation, ultimately leading to identification of polymers that would form suitable 3pRNA/NPs for *in vivo* therapy studies. Next, several properties of 3pRNA/NPs were investigated, including inflammasome activation, serum stability, size, and immunogenic activity. This research revealed that 3pRNA/NPs activated cancer cells and myeloid cells to a similar degree. Additionally, none of the polymers activated the inflammasome using active dosing, however, when applied systemically in mice, induced a robust increase of type-I IFN and CXCL10 in serum, liver, spleen, lung, kidney, and tumor.

While complexed with 3pRNA, P-b-$DA_4$50 was found to uniquely retain its particle size and activity after incubating in serum, thus offering an explanation as to why

the polymeric hydrophobic monomer composition correlates more to 3pRNA/NP activity than it does to pH-responsive polymer properties. It also demonstrates that P-b-$DA_4$50 comprised 3pRNA/NPs may be effective for systemic *in vivo* therapy studies. Overall, these studies demonstrate the influence of hydrophobic block chain length and hydrophobic alkyl chain length of amphiphilic block in these designed copolymers on the pH dependent behavior of these delivery systems, offering insight into choosing a lead carrier in future studies.

Materials and Methods

RAFT Polymerization of PEG-b-(DMAEMA-co-A_nMA). For these reversible addition-fragmentation chain transfer (RAFT) polymerizations, the following reagents were used: Poly(ethylene glycol) 4-cyano-4-(phenylcarbonothioylthio)pentanoate (10,000 kDa, Sigma), was used as the chain transfer agent (CTA), Diethyl Aminoethyl methacrylate (DMAEMA, Sigma Aldrich) and variable hydrophobic side chain length methacrylates (A_nMA), including ethyl methacrylate (EMA, Sigma Aldrich), butyl methacrylate (BMA, Sigma Aldrich), hexyl methacrylate (HMA, Sigma Aldrich), octyl methacrylate (OMA, Polysciences), decyl methacrylate (DeMA, Polysciences), and lauryl methacrylate (LMA, Sigma Aldrich) were used as monomers, 4,4'-Azobis(4-cyanovaleric acid) (V-501, Wako Chemicals) was used as a free-radical initiator, and 60:40 mixture of 1,4-dioxane (Sigma Aldrich) and dimethylformamide (Sigma Aldrich) was used as the solvent. Briefly, inhibitor was removed from monomer solutions using gravity filtration through aluminum oxide (Sigma) packed columns. Initiator, CTA, and monomers were mixed into solvent at a ratio of 0.2 I_o : 1 CTA_o : 300 M_o. Monomers were 20 wt% of the final solution, and a ratio of 0:100, 20:80, 30:70, 40:60, 50:50, or

60:40 DMAEMA:A_nMA. The mixture was polymerized under a nitrogen atmosphere for 20 h at 70 ^{o}C. The resultant diblock copolymers were diluted in acetone and isolated using dialysis (3kDa MWCO, Thermo) against acetone with a final dialysis against molecular grade water (HyClone). After polymer isolation, the purified polymer solution was frozen and lyophilized. Polymer molecular weight (Mn) as well as polydispersity (PDI) were determined using GPC using a dimethylformamide mobile phase with 0.1 M LiBr with inline light scattering (Wyatt) and refractive index (Agilent) detectors. Polymer composition, the concentration of any unreacted contaminants, and polymer molecular weight were determined using ^{1}H NMR (CDCl3) spectroscopy (Figure A.8).

Synthesis of 5'-Triphosphate RNA. 5'-ppp- CGUUAAUCGCGUAUAAUACGCCUAU-3' was generously synthesized and provided by the laboratory of Dr. Anna M. Pyle at Yale University.[160] 5'-OH-CGUUAAUCGCGUAUAAUACGCCUAU-3' as well as the complement strand 5'-AUAGGCGUAUUAUACGCGAUUAACG-3' was purchased from Integrated DNA technologies (IDT) and resuspended in RNAse free water. To generate double stranded RNA, equimolar amounts of top strand with a triphosphorylated or OH 5' terminus top strand, and the complement strand were suspended in 0.3 M NaCl, transferred to a 0.25mL PCR tube and annealed using a thermocycler by setting the temperature to 90^{o}C and slowly cooling to 35^{o}C over 1 h. The resulting duplexes were diluted to 100μM RNA in RNAse free water and agarose gel (2%) electrophoresis was used to confirm hybridization.

Formulation of NP/3pRNA complexes for *in vitro* investigations. A series of amphiphilic diblock copolymers were synthesized as described above. Lyophilized copolymers were dissolved into ethanol at 50 mg/mL and stored at 4^{o}C.

This stock was further diluted to 3.33 mg/mL in citric acid buffer (pH 4, 100 mM) and rapidly mixed with either RNA at charge ratios (N:P) between 20:1 and 1:1. After incubating at room temperature for 30 min, 1.24x volume of a high pH buffer comprising phosphate buffer (pH 8, 100 mM, PB) containing 20 nM NaOH and mixing rapidly to form nanoparticles (NPs). After 15 min, the solution was further diluted into PBS (pH 7.4, Gibco) before use. The second block DMAEMA content is estimated to have 50% protonation for the purposes of determining N:P ratios. A charge ratio of 20:1 was selected for all *in vitro* cell culture studies.

Dynamic Light Scattering. Series polymers were diluted from ethanol stocks to 1 mg/mL in either lysosomal pH range (pH 5.8) and physiological pH range (pH 7.4) PBS. For each series polymer, NP particle size distribution and polydispersity index (PDI) was analyzed via dynamic light scattering (Malvern Zetasizer Nano ZS). Fold pH responsive size change was determined using the following formula: $(Diameter(pH7.4))/(Diameter(pH5.8)) - 1$.

Erythrocyte Hemolysis assay. The ability of NPs comprising different series polymers to disrupt lipid bilayer membranes at various pH was performed as previously described. Briefly, whole blood from de-identified patients was acquired from the Vanderbilt Technologies for Advanced Genomics (VANTAGE) core. Blood was centrifuged to pellet erythrocytes, and plasma was aspirated, and erythrocytes were resuspended in pH 7.4 PBS (Gibco) 3x. After the final rinse, erythrocytes were resuspended in pH 7.4, 7.0, 6.6, 6.2, or 5.8 PBS (150 nM). Polymers were mixed with suspended erythrocytes to a concentration of 1 μg/mL in a 96-well V-bottom plate. The plates were incubated for 1 h at 37^{o}C and centrifuged to pellet intact erythrocytes, and the supernatant was transferred to a 96-well flat bottom plate. Membrane disruption was quantified through hemoglobin leakage, which can

be measured using absorbance spectroscopy at 575 nm.

Cell lines. The human lung carcinoma IRF and NF-κB reporter cell line A549-Dual (Invivogen), murine Lewis lung carcinoma cell line (ATCC), the murine metastatic lung cancer cell line CMT64 (Sigma), the human kidney IL-1β reporter HEK-293-blue cell type (Invivogen), and the murine macrophage cell line RAW 264.7 (ATCC) were cultured in DMEM (Gibco) supplemented with 2mM L-glutamine, 4.5 g/L D-glucose, 10% heat inactivated fetal bovine serum (HI FBS, Gibco), and 100 U/mL penicillin/100 μg/mL streptomycin (Gibco). The murine colon carcinoma CT26 cell type (ATCC), the murine breast cancer cell line 4T1 (ATCC) as well as modified luciferase expression 4T1 cells generously provided by the Advanced therapeutics Laboratory at Vanderbilt university, and the murine melanoma cell line B16-F10 (ATCC) were cultured in RPMI 1640 (Gibco) supplemented with 2 mM L-glutamine, 10% fetal bovine serum (FBS, Gibco), and 100 U/mL penicillin/100 μg/mL streptomycin (Gibco). The FVB derived mmtv-PyMT breast cancer cell line was generously provided by the Cook lab at Vanderbilt University, and was cultured in F-12/DMEM 1:1 (Gibco) supplemented with 2 mM L-glutamine, 10% fetal bovine serum (FBS, Gibco), and 100 U/mL penicillin/100 μg/mL streptomycin (Gibco). The human monocytes THP1 and THP1-defNLRP3 cell lines that we generously donated by the Balko laboratory at Vanderbilt University were cultured in RPMI 1640 (Gibco) supplemented with 2 mM L-glutamine, 10% fetal bovine serum (FBS, Gibco), 10 mM Hepes buffer (Gibco), and 100 U/mL penicillin/100 μg/mL streptomycin (Gibco). The murine dendritic cell line DC2.4 (H-2Kb-positive) was kindly provided by K. Rock (University of Massachusetts Medical School) and cultured in RPMI 1640 (Gibco) supplemented with 10% fetal bovine serum (HI FBS; Gibco), 2 mM L-glutamine, 100 U/mL penicillin/100 μg/mL streptomycin (Gibco),

50 μM 2-mercaptoethanol (Gibco), 1 x nonessential amino acids (Cellgro), and 10 mM HEPES (Invitrogen). All cell types were grown at 37^{o}C in 5% CO_2.

***in vitro* Evaluation of NP/3pRNA Delivery.** For all cell lines, cells were suspended at 50,000 cells/mL and plated at 200μL in 96-well plates. Cells were allowed to adhere overnight for reporter cell activity or IFN-α secretion at multiple doses. 1 mL of suspended cells were plated in 12-well plates and allowed to adhere overnight for qRT-PCR and flow cytometry experiments. After 24 h, the cell supernatant was collected for analysis and stored at -80 ^{o}C until used. IFN-α concentrations in cell supernatant were determined using a Lumikine mIFN-α kit (Invivogen) according to the manufacturer's instructions.

For flow cytometry, cells were detached from plates using 0.25% Trypsin EDTA buffer, washed in PBS, and incubated with labeled antibodies for CD80, CD86, and MHC-I (BioLegends) following the manufacturer's protocols. After 24 h of treatment, supernatant was collected and cells were removed using 0.05% Trypsin-EDTA (Gibco). Cells and supernatant were spun down and washed 3x in FACS buffer (0.5% BSA in PBS), pelleted via centrifugation (850 rcf, 5 min), and stained with a cocktail of anti-MHC-I-(FITC), CD80 (APC), and CD-86 (PE/Cy7) antibodies (BioLegend) in FACS buffer (0.5% BSA in PBS). DAPI staining was used to discriminate live from dead cells. Samples were kept on ice and analyzed using a BD-LSR Fortessa flow cytometer. All flow cytometry data were analyzed using FlowJo version 10 (Tree Star Inc).

To determine the half maximal response concentration (EC_{50}) of indicated formulation, RNA dose sweeps between 0.05-50 nM final RNA concentration were performed in A549-Dual cells. Values for EC_{50} were extrapolated from dose-response curve fits using GraphPad Prism software. NPs were formulated as

detailed above and treated with P-b-DA$_n$[%] and 3pRNA (NP/3pRNA), or OH-RNA as a control, as well as PBS. Luminescent reporter assays were performed using QUANTI-Luc (Invivogen) following the manufacturer's instructions. Luminescence was quantified using a Synergy H1 microplate reader (BioTek, Winooski, VT). All measurements were normalized after baselining to the average value of the PBS-treated negative control group. EC_{50} ratios were determined using the following formula:$EC_50min/EC_50sample$.

For qRT-PCR analyses, cells were washed and 700 μL of RLT lysis buffer (Qiagen) was added to each well. Lysates were stored at -80 ^{o}C until used. mRNA was extracted from cell lysates using an RNA isolation kit (RNeasy mini kit, Qiagen). cDNA was synthesized for each sample using a cDNA synthesis kit (iScript, Bio-Rad) and analyzed using qRT-PCR using SybrGreen (Thermo Fischer) with CFX real time PCR detection system (Bio-Rad) following the manufacturer's instructions. Primers for *Ifnb1* (Mm.PT.58.30132453.g), *Cxcl10* (Mm.PT.58.4357827), *Il6* (Mm.PT.58.10005566), *PD-L1* (Mm.PT.58.12575861), and *PPIB* (Mm.PT.58.29807961) were purchased from Integrated DNA Technologies.

Serum 3pRNA/NP activity reduction assay. Lead carriers P-b-DA$_4$50, P-b-DA$_6$40, P-b-DA$_8$40, and P-bDA$_1$040, were complexed with 3pRNA to create 3pRNA/NPs, following steps detailed above, except that formulations are diluted into a solution of PBS (Gibco) and adult bovine serum (Gibco) to a final serum volume concentration of 50% instead of PBS alone, in addition to being formulated without serum as detailed above. Formulations were incubated at 37^{o}C for 15 min, 1 h, or 6 h. Particle size for formulations that were incubated in serum for 15 min were analyzed as described above, and A549-dual reporter cells were treated with

formulations incubated for 15 min, 1 h, and 6 h, and EC_{50} values were calculated as described above.

NP Inflammasome Activation. THP-1 and THP1-Def-NLRP3 cells were plated in 96-well plates as described above in the presence of 100 nM PMA for 24 h. After, media was then replaced with fresh media containing 100 ng/mL LPS for 3 h. The media was replaced and cells were treated using 3pRNA/NPs comprising 3pRNA complexed with series polymers as well as PBS as a control. HEK-293-blue reporter cells were played and allowed to adhere overnight, as described above. After 24 hr treatment, the supernatant was collected and added 1:10 to plated HEK-293 blue cells for another 24 hr. Supernatant was collected, and 20 μL of supernatant was added to 180 μL of suspended QuantiBlue (Invivogen) reagent and incubated for 1 hr at 37^{o}C. Relative inflammasome activation was quantified using a Synergy H1 microplate reader (BioTek, Winooski, VT).

Preparation of 3pRNA/NP for *in vivo* studies. All buffers used for this protocol were pre-filtered using a 0.22 μm syringe filter (Pall corporation). 3pRNA/NPs were formulated as descried above, except polymers were suspended at 10 mg/mL in citric acid buffer instead of 3.33 mg/mL, and PB buffer was added at a ratio of 1:1.26. A charge ratio of 15:1 was selected for all *in vivo* cell culture studies.

Animal Care and Experimentation. Female C57BL/6J mice (7 weeks old) were obtained from The Jackson Laboratory (Bar Harbor, ME). All animals were maintained at the animal facilities of Vanderbilt University under specific pathogen-free conditions. All animal experiments were approved by the Vanderbilt University Institutional Animal Care and Use Committee (IACUC). Tumor volume, as well as mouse weight, was measured every other day via caliper measurements and a balance.

Tumor volume was calculated using the equation $V = 1/2(L * W * H)$.[161]

qRT-PCR and ELISA Analysis of Murine Organs and Serum. Female C57BL/6J mice (9 weeks old mice) were inoculated with 100 μL of E0771 cells suspended in cold PBS (pH 7.4, Gibco), at 2.5x105 cells/mL. Once tumor volumes reached approximately 100 mm^3, Mice were intravenously administered 150 μL of indicated formulation or vehicle (PBS) containing 15 μg of either 3pRNA or OH-RNA and 600 μg of polymer in buffer using a 0.5 cc syringe and a 27 gauge needle (n=7 for each group). After 5 h, mice from each group were euthanized, blood was collected using cardiac puncture, and lungs, livers, spleens, and kidneys were surgically removed and stored at -20^{o}C in RNA later. Blood was kept at 4^{o}C and centrifuged at 8000g for 5 minutes. Supernatant for each blood sample was collected and serum IFN-α were determined using a Lumikine mIFN-α kit (Invivogen) according to the manufacturer's instructions. Tumors and organs stored in RNA later were transferred into 1 mL of RLT lysis buffer in gentleMACs P tubes (Miltenyi Biotec) and digested using gentleMACS Octo dissociator (Miltenyi Biotec). Supernatant was transferred to RNeasy mini columns for mRNA purification following the manufacturer's instructions. mRNA was extracted from cell lysates using an RNA isolation kit (RNeasy mini kit, Qiagen). cDNA was synthesized for each sample using a cDNA synthesis kit (iScript, Bio-Rad) and analyzed using qRT-PCR using TAQMAN (Thermo Fischer) with CFX real time PCR detection system (Bio-Rad) following the manufacturer's instructions. Primers for Ifnb1 (Mm00439552_s1), Cxcl10 (Mm00445235_m1), and HMBS (Mm01143545_m1) were purchased from ThermoFisher Scientific.

Statistics. Significance was determined using one-way ANOVA with Tukey's multiple comparisons test unless otherwise noted. Values represent experimental

means, and error bars represent S.D. unless otherwise noted. **** p¡0.0001, *** p¡0.005, **p¡0.01, * p¡0.05. Spearman's rank coefficients for linear and nonlinear n and [%] were calculated using JMP data analysis software.

Acknowledgements

We gratefully acknowledge Prof. Kenneth Rock (University of Massachusetts Medical School) for providing DC2.4 cells, Prof. Anna M. Pyle and Dr. Olga Fedorova (Yale University) for synthesizing and providing 5' triphosphate RNA, and Prof. Craig Duvall (Vanderbilt University) for use of gel permeation chromatography and IVIS equipment. We thank the core facilities of the Vanderbilt Institute of Nanoscale Sciences and Engineering (VINSE) for the use of their Malvern Zetasizer for dynamic light scattering, the VUMC Flow Cytometry Shared Resource, supported by the Vanderbilt Ingram Cancer Center (P30 CA68485) and the Vanderbilt Digestive Disease Research Center (DK058404), for the usage of the BD LSR Fortessa flow cytometer, and the Vanderbilt Technologies for Advanced Genomics (VANTAGE) for providing blood for hemolysis experiments. This research was supported by grants to JTW from the American Cancer Society (Institutional Research Grant IRG-58-009-56), the Alex's Lemonade Stand Foundation (SID924), and the Congressionally-Directed Medical Research Program (W81XWH-161-0063).

Table 2: **Design of experiments factors and levels**

Factor name	Formula Representation	Number of levels	Low	High
Alkyl chain length	n	6	2	12
Composition	[%]	5	20	60

Table 3: **Series polymer properties**

PEG Mn	Block 2 DP	Cationic monomer	Hydrophobe	Hydrophobe composition
10000	160	DMAEMA	A_nMA	20%-60%

Table 4: **Spearman's correlations.**
This table represents both the likelihood and strength of a non-parametric correlation between the established factors n or [%], pH responsive polymer properties, and EC_{50} ratio. Green = no correlation ($|x| < .2$), Blue = weak correlation ($.2 < |x| < .4$), and Red = moderate correlation ($.4 < |x| < .6$)

Property	n	prob $>\|\rho\|$	%	prob $>\|\rho\|$	Non-linear n	prob $>\|\rho\|$	Non-linear [%]	prob $>\|\rho\|$
Size ratio	-0.025	0.630	0.360	0.035	-0.33	0.046	-0.357	0.037
Hemolysis	0.055	0.547	0.269	0.002	-0.524	<.0001	-0.433	0.0001
EC_{50} ratio	-0.110	0.299	0.375	0.0003	-0.280	0.0074	-0.463	<.0001

Chapter 4

Systemic Delivery of 5'-Triphosphate RNA Challenged by Dose-Limiting Toxicity

Chapter Summary

In chapter 3, we have demonstrated four lead carriers for systemic 3pRNA delivery. In this chapter, we treat mice with 3pRNA/NPs. We find that therapeutically relevant doses of 3pRNA/NPs comprising lead carriers are toxicity limited, and that assays using non-immunogenic RNA to evaluate potential 3pRNA/NP efficacy *in vivo* were not sensitive enough. Ultimately, we find that these specific carriers could be improved upon, using what we learned about polymer structure and 3pRNA/NP activity, and redesigned for improved *in vivo* results.

Introduction

RIG-I agonist efficacy is hindered by barriers to drug delivery such as nuclease degradation, poor intracellular uptake, and minimal access to the cytosol where RIG-I is localized.[21] In the previous chapter, we have demonstrated that pH-responsive endosomolytic polymer NPs enhance the cytosolic delivery and immunostimulatory activity of 3pRNA, the ligand for RIG-I. In chapter 2, we demonstrated that: 1) D-PDB, a polymer previously used for delivery of siRNA and subunit vaccines, is capable of 3pRNA delivery, 2) that 3pRNA/NPs comprised of D-PDB complexed to 3pRNA activate RIG-I, and 3) that this activity induces production of anti-tumor cytokines and T cell chemokines causing cancer cells to undergo immunogenic cell death. This significantly enhances survival of 4T1 bearing mice when treated in

tandem with ICB. In chapter 3, we demonstrated that diblock copolymers with a hydrophilic first block made of 10 kDa PEG and a tunable hydrophobic second block are capable of 3pRNA delivery. Here, 3pRNA forms a potent and stable complex with P-b-$DA_4$50 block copolymer nanoparticles suitable for *in vivo* studies. In this chapter, we explore the efficacy of 3pRNA complexed to lead series block copolymer nanoparticles in a therapeutic regimen.

First, we administer 3pRNA/NPs through local and systemic administration at 1.25 mg/kg which was the same dose used for the therapy study in chapter 2. Unexpectedly, the mice that had been give this dose experienced unexpected deaths. In order to better evaluate 3pRNA/NP dosage, we delivered other small RNAs, including siRNA, to evaluate models utilizing NP delivery of non-immunogenic RNA, then we systemically administered a reduced RNA dose of 0.625 mg/kg to evaluate the ability of 3pRNA/NPs comprised of polymeric lead carrier P-b-$DA_4$50 to improve response to PD-L1 immune checkpoint blockade. Details and results are presented in the next section.

Results

3pRNA/NP buffer exchange and concentration does not affect particle size, particle loading, or reduce particle efficacy. Complexing 3pRNA to polymeric lead carriers, in addition to providing a platform to improve cellular uptake and RIG-I activation, also serves to shield precious RNA cargo from nuclease degradation. In chapter 3, we demonstrated that 3pRNA/NPs comprised of P-b-$DA_4$50 complexed with 3pRNA can protect RNA cargo from nuclease degradation in serum. Here, we prepare additional formulation steps to prepare 3pRNA/NPs for *in vivo* application. Formulations of 3pRNA/NPs for *in vitro* studies require additional

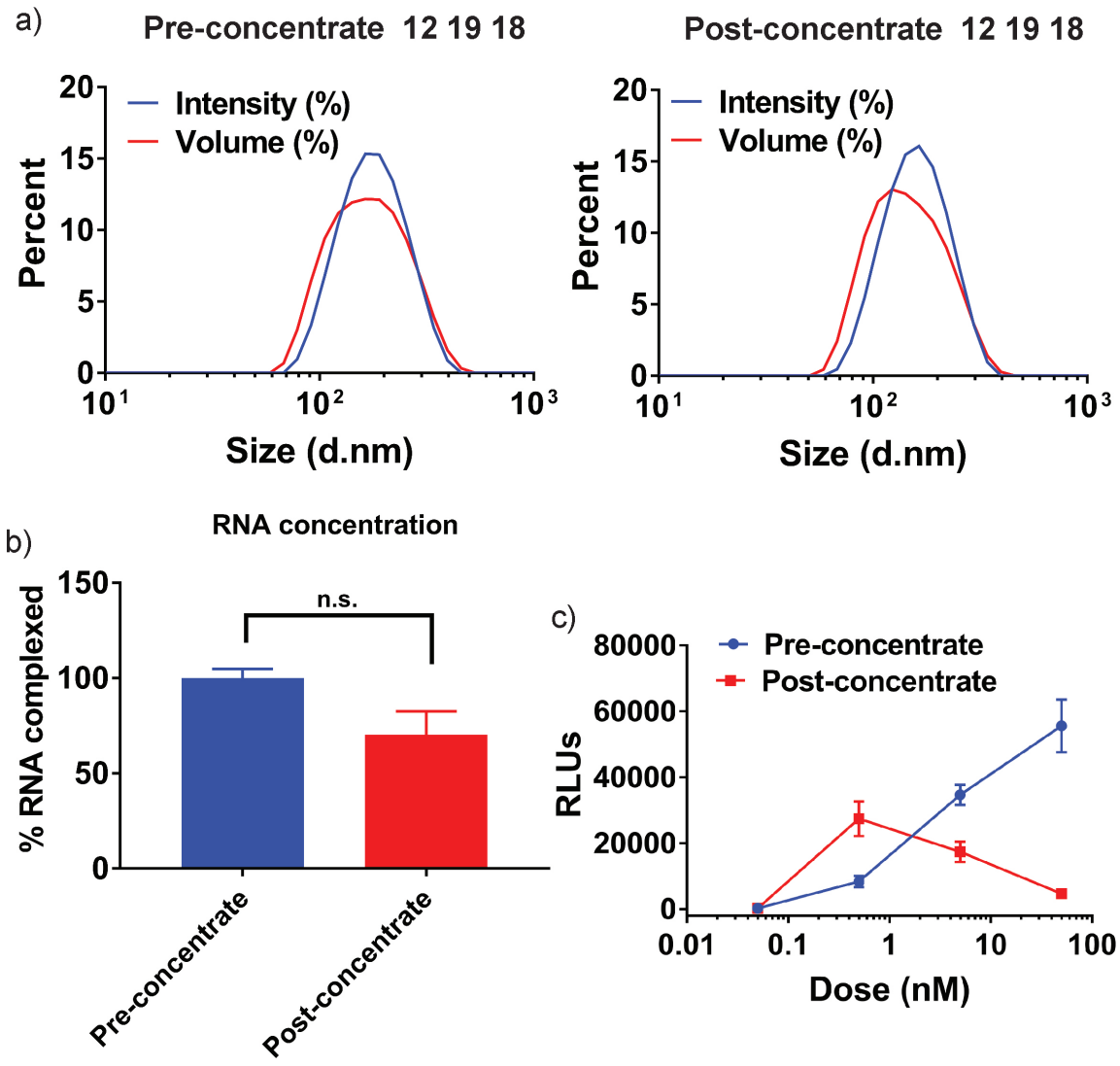

Figure 4.1: **3pRNA/NP buffer exchange and concentration does not affect particle size, particle loading, or reduce particle efficacy.**
a) Intensity and volume percent particle size distribution before (left) and after (right) 3pRNA/NP concentration was evaluates using a Malvern Zetasizer. b) 3pRNA/NP loading efficiency was determined using fluorescence spectroscopy. Free RNA, pre-concentrated 3pRNA/NPs, and post-concentrated 3pRNA/NPs were incubated in 1% SDS for 5 minutes, then with Ribogreen, to achieve fluorescence. Values are relative to Free RNA. c) A549 dual reporter cells were transfected with pre-concentrated 3pRNA/NPs and post-concentrated 3pRNA/NPs were at 0.05, 0.5, 5, and 50 nM. ISG activation was determined using luminescence.

steps to meet dose and injection volume requirements. We utilize tangential flow filtration to concentrate formulated 3pRNA/NPs for *in vivo* use. We measured particle size distributions before concentration (left) and after concentration (right) of 3pRNA/NPs to find that particles are similarly sized (Figure 1a). We also dissociate 3pRNA/NPs formulations before and after concentration steps using 1% sodium dodecyl sulfate and incubate formulations with RNA intercalating dye Ribogreen to determine relative quantities of RNA (Figure 1b). There is no significant difference in RNA concentrations indicating insignificant RNA loss from the formulation process itself. A549 ISG reporter cells were treated with originally formulated 3pRNA/NPs or concentrated 3pRNA/NPs comprised of 3pRNA complexed to P-b-$DA_4$50 diluted to final RNA doses of 50 nM, 5 nM, 0.5 nM, and 0.05 nM (Figure 1c). For concentrated samples, we discovered that although 3pRNA/NP formulations retain their low dose requirement for RIG-I activation, concentrated samples exhibit dose-limiting toxicity whereas the 3pRNA/NP formulations without concentration do not. This difference could be caused by a small population of aggregate particles exhibiting increased cytotoxicity that were not detected by DLS analysis or small morphological changes that exposed membrane disruptive groups to cell membranes before endocytosis, causing increased cytotoxicity. This dose-limiting toxicity can lead to complications for *in vivo* therapy.

NP delivery of 3pRNA in mice bearing 4T1 tumors is complicated by dose-limiting toxicity. While NP delivery of 3pRNA has been shown to improve efficacy for 3pRNA by overcoming nuclease degradation and improving cellular uptake, thus reaching a lysosomal fate, the efficacy of polymeric NP carriers is also subject to similar difficulties. For example, the most established polymer for NP formulation, PEI, is notorious for cytotoxicity caused by large amounts of positively

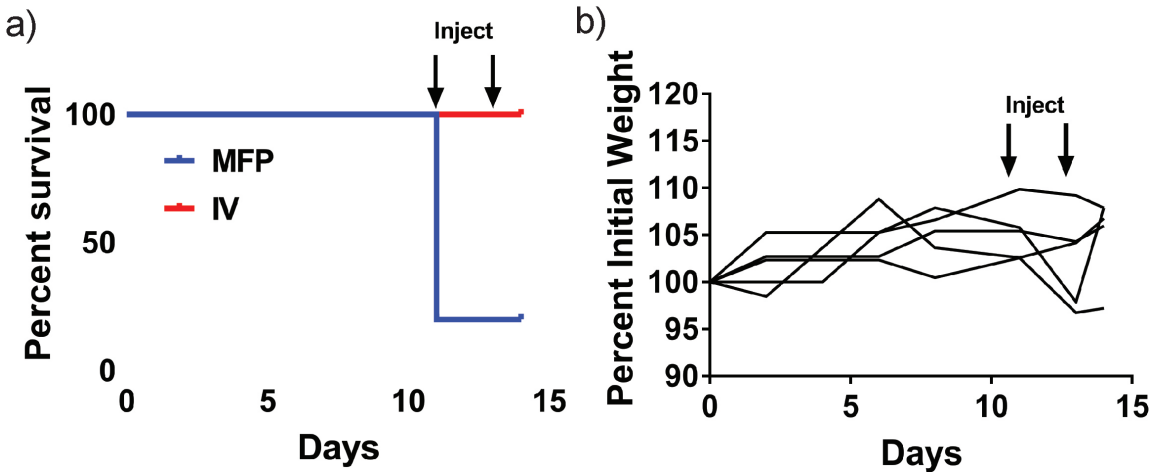

Figure 4.2: **Intratumoral administration of 3pRNA/NPs results in immediate mouse deaths.**
a) Kaplan-Meier survival curves of mice treated with indicated formulation. MFP mice were administered 3pRNA/NP formulations directly into the mammary fat pad, and i.v. mice were administered 3pRNA/NP formulations through an intravenous route. b) Percent weight curve for all i.v. administered mice over the course of two i.v. injections of 3pRNA/NP.

charged monomer groups. In addition, high dosing of particles can result in immune related adverse effects, leading to a cytokine storm effect that can ravage mice, possibly even causing death. This research demonstrated revealed that 3pRNA/NPs utilizing 3pRNA and lead polymeric carrier P-b-$DA_4$50 caused mouse death over the course of three injections. After observing near instantaneous death for 4T1 bearing mice that were administered 3pRNA/NPs through an intratumoral route (Figure 2), we treated mice with 3pRNA/NPs comprised of 3pRNA complexed to P-b-$DA_4$50, OH-RNA/NPs comprised of OH-RNA complexed to P-b-$DA_4$50, and PBS in conjunction with αPD-L1 monoclonal antibodies, once every three days for a total three intravenous injections. Tumor volumes (Figure 3a) and mouse weights (Figure 3b) were recorded for mice that survived all three injections. Unfortunately, we did not find significant differences in tumor burden or survival for each group. Treatment

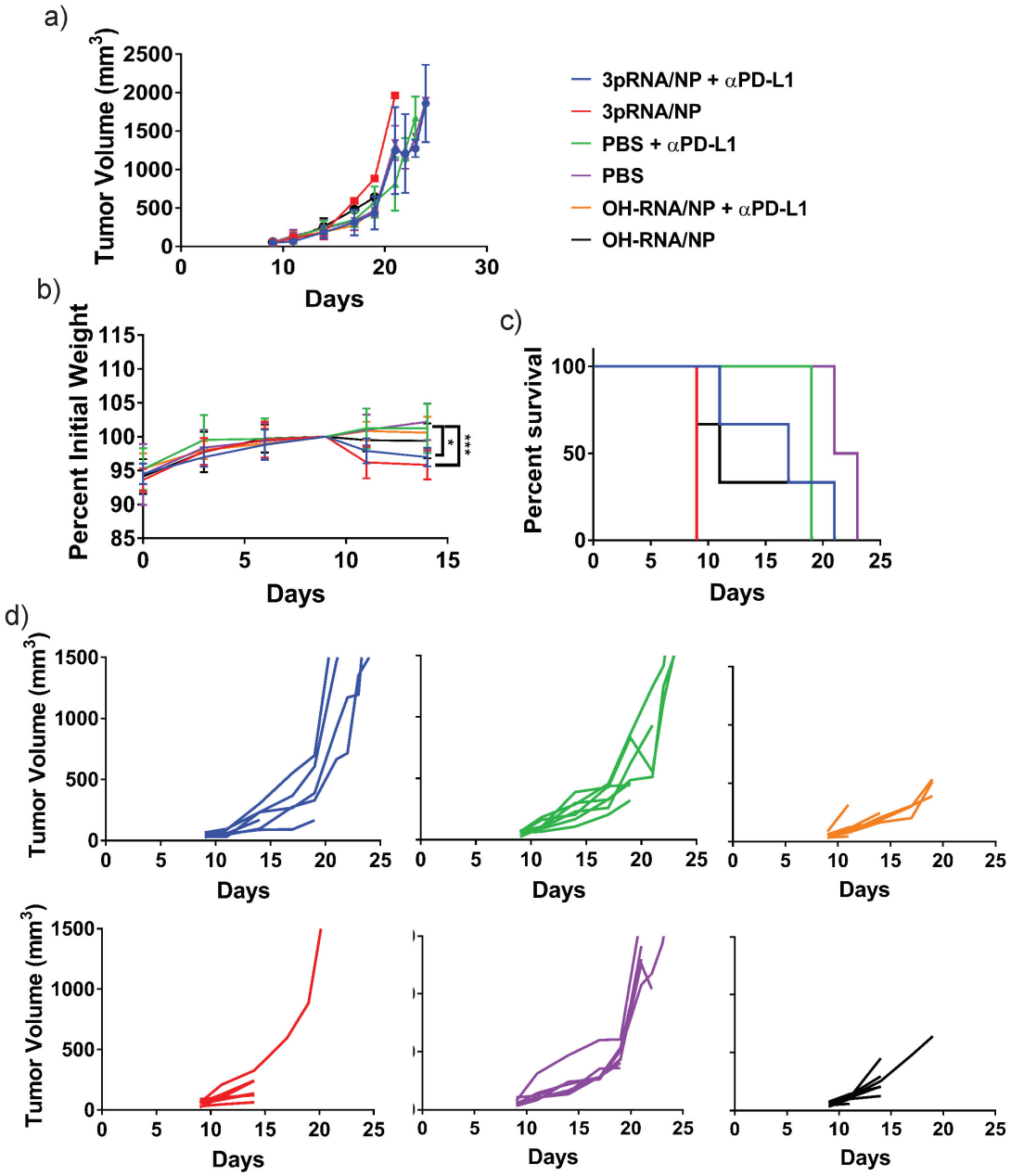

Figure 4.3: **NP delivery of 3pRNA in mice bearing 4T1 tumors is complicated by dose limiting toxicity.**
a) Average tumor volumes for mice treated with 3pRNA/NPs + αPD-L1, 3pRNA/NPs, PBS, PBS + αPD-L1, OH-RNA/NPs, and OH-RNA/NPs + αPD-L1. (n=8) b) Mouse weight monitored over the course of the study for each group. Differences in weight were analyzed compared to PBS using two-way ANOVA with post-hoc analysis. c) Kaplan-Meier survival curves of mice treated with indicated formulation using 1500 mm^3 tumor volume as endpoint criteria (n=8) d) Spider plots of individual growth curves up to day 24.

with 3pRNA/NPs and OH-RNA/NPs caused significant weight loss compared to mice treated with PBS alone. Mice began to recover weight after the final treatment. Mouse tumor progression for each group, as well as mouse death, is illustrated for each group using spider plots representing individual mice for each group (Figure 3c). We find that although only a few mice treated with 3pRNA/NPs died during early injections, over the course of the study, 26 out of 32 mice injected intravenously with either 3pRNA/NPs or OH-RNA/NPs died before tumor endpoint. Moreover, all mice injected with OH-RNA/NPs died before reaching tumor endpoint volumes of 1500 mm^3, indicating either immune mediated adverse effects from delivery of 3pRNA, or polymer toxicity related inflammation resulting in mouse death.

NP delivery of siRNA in 4T1 luciferase cells suppresses luciferase expression. siRNA is a small RNA sequence capable of suppressing specific gene expression. There are attractive targets for gene silencing in cancer therapy, including cytokines such as TGF-β and immune checkpoint genes such as PD-L1. Moreover, siRNA is not inherently immunogenic, therefore siRNA/NPs comprised of siRNA complexed to polymeric lead carriers could exhibit reduced toxicity when administered in murine models. In order to determine whether the design of the polymer second block effects siRNA delivery in a similar fashion to 3pRNA delivery, we treated 4T1 luciferase expressing cells with 50 nM, 5 nM, 0.5 nM, and 0.05 nM final RNA doses of siRNA/NPs comprised of each unique series polymer. NPs made from Lipofectamine 2000 complexed with luciferase siRNA were used as a positive control. The luminescence of scrRNA/NPs comprised of each unique series polymer, or Lipofectamine 2000 as a positive control, complexed with scrambled RNA for 24 h, followed by adding D-luciferin to each sample, were measured using an *in vivo* imaging system (IVIS) (Figure 4a). Through comparisons to untreated

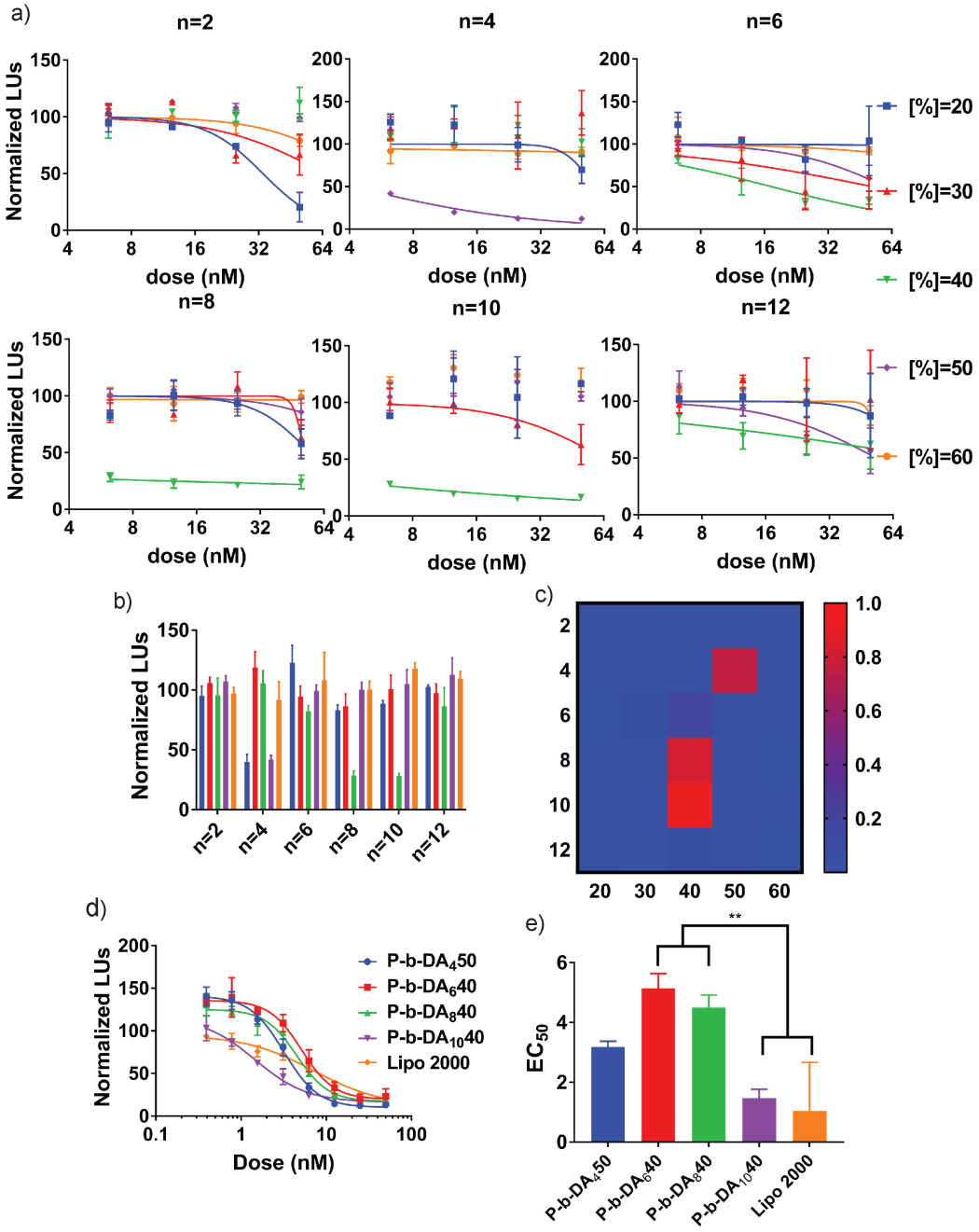

Figure 4.4: **NP delivery of siRNA in 4T1 luciferase cells suppresses luciferase expression.**
a) Series polymers were complexed with siRNA and 4T1 luciferase expressing cells were treated with siRNA/NPs to a final siRNA concentration of 50 nM, 25 nM, 12.5 nM, and 6.25 nM. b) Percent luminescence of samples treated with siRNA/NPs at 6 nM. c) A heat map demonstrating siRNA/NP silencing. The colorbar represents the fraction of cells silenced at 6 nM. d) 4T1 cells were treated with siRNA/NPs comprising lead carriers and siRNA to a final siRNA concentration of 50 nM, 25 nM, 12.5 nM, 6.25 nM, 3.125 nM, 1.5625 nM, and 0.78125 nM. e) EC_{50} values for siRNA/NPs comprising lead carriers.

cells and scrRNA/NPs, we was able to calculate relative luciferase expression for each polymer (Figure 4b) and visualize fraction silencing using a heatmap, colorbar representing the fraction of cells silenced (Figure 4c). Interestingly, the same four lead carriers described in chapter 3, including P-b-$DA_4$50, P-b-$DA_6$40, P-b-$DA_8$40, and P-b-$DA_1$040, form the most potent siRNA/NPs in this study.

In order to further compare these four polymeric lead carriers, we treated 4T1 luciferase expressing cells with siRNA/NPs comprised of polymeric lead carriers, or Lipofectamine 2000 as a positive control, complexed with luciferase siRNA or scrRNA/NPs comprised of polymeric lead carriers, or Lipofectamine 2000 as a positive control, complexed with scrambled RNA at a two-fold dose sweep starting at 50 nM for 24 h, followed by addition of D-luciferin to each sample and measurement of sample luminescence using an IVIS (Figure 4d). We calculated EC_{50} values for each dose response curve. This data reveals differences between the efficacy of siRNA/NPs comprised of the four polymeric lead carriers (Figure 4e). Here, we demonstrate that siRNA/NPs comprised of siRNA complexed to P-b-$DA_1$040 are significantly more potent than siRNA/NPs comprised of other lead polymers. While the overall trends observed from analyzing siRNA/NP formulation potency for each series polymer are consistent with 3pRNA/NPs, the activity of siRNA/NPs with the lead carriers are slightly different. With regards to 3pRNA/NP activity, P-b-$DA_4$50 and P-b-$DA_6$40 outperform P-b-$DA_8$40 and P-b-$DA_1$040. For siRNA/NPs, however, P-b-$DA_4$50 and P-b-$DA_1$040 form more portent NPs than when formulated using P-b-$DA_6$40 and P-b-$DA_8$40. Overall, these studies demonstrate that polymeric lead carriers are capable of enhancing delivery of robust RNA populations, including siRNA, and that studies utilizing NPs comprising non-immunogenic RNA would be a good indicator of 3pRNA/NP potency.

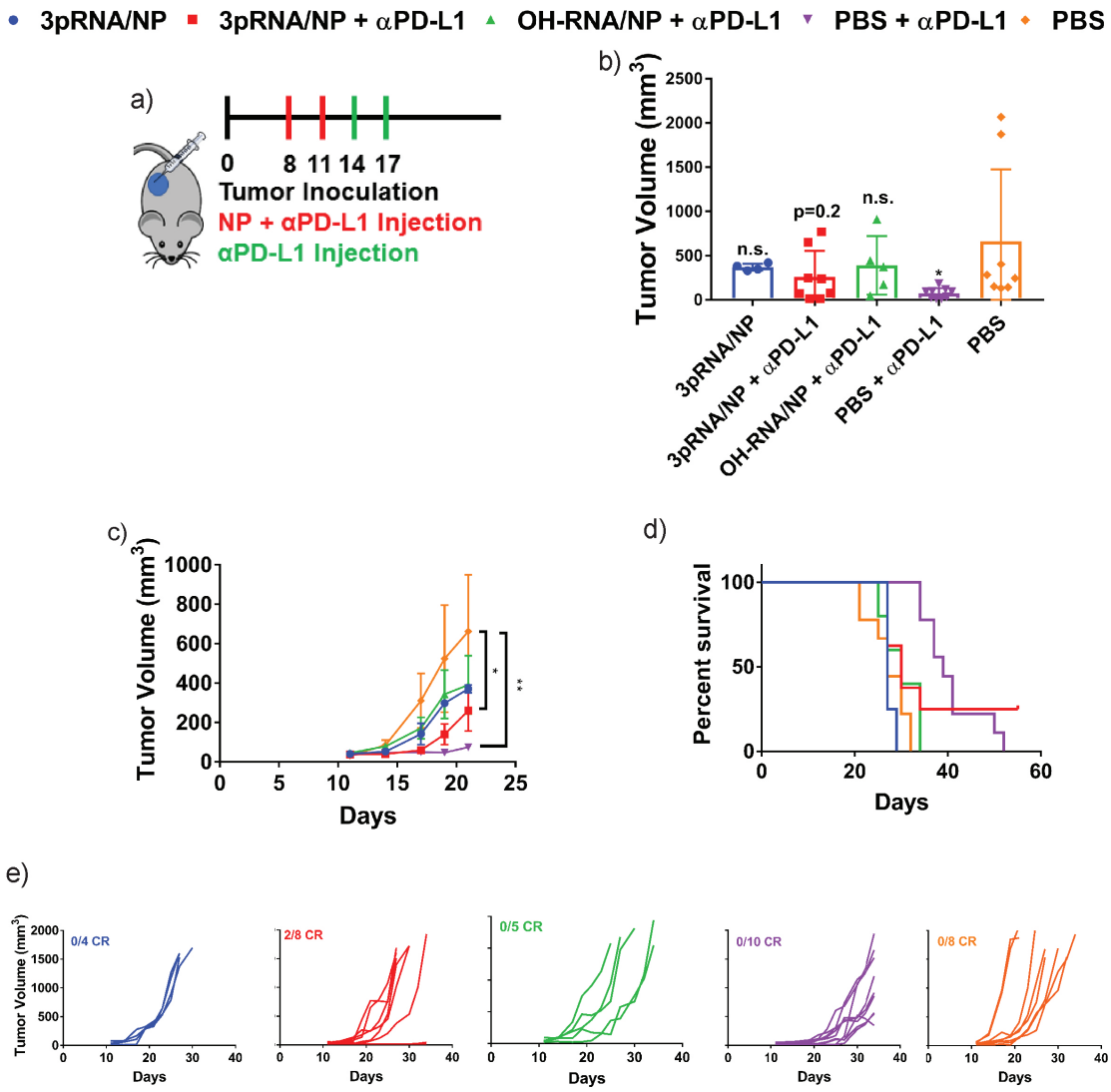

Figure 4.5: **Systemic NP delivery of 3pRNA comprising P-b-DA$_4$50 in tandem with PD-L1 checkpoint blockade inhibits tumor growth and extends survival.**
a) Schematic summarizing tumor formation and treatment schedule used for evaluating efficacy of NP/3pRNA in combination with PD-L1 blockade. Mice bearing E0771 tumors were treated i.v. two times with NP/3pRNA, NP/OH-RNA, or PBS. Mice were injected with αPD-1 every 3 days intraperitoneally. b) Average tumor volume at day 21, corresponding to the first incidence of euthanize in any treatment or control cohort. Error bars represent S.D. c) Kaplan-Meier survival curves of mice treated with indicated formulation using 1500 mm3 tumor volume as endpoint criteria (n=10). d) Spider plots of individual growth curves truncating at a tumor volume of 1500 mm^3 up to day 36.

Systemic NP delivery of 3pRNA comprised of P-b-DA$_4$50 in tandem with PD-L1 immune checkpoint blockade inhibits tumor growth and extends survival. Due to 3pRNA/NP ISG activation *in vitro* and capability to induce organ and serum type-I IFN expression *in vivo*, we decided to administer 3pRNA/NPs comprised of 3pRNA and P-b-DA$_4$50, OH-RNA/NPs comprised of OH-RNA complexed with P-b-DA$_4$50, and formulation buffer in tandem with PD-L1 checkpoint blockade intravenously in mice inoculated with E0771 breast tumors in right mammary fat pads. Since my previous study administering 1.25 mg/kg of 3pRNA had exhibited mouse deaths, we administered two 3pRNA/NP treatments for this study. The first NP treatment administered 0.6125 mg/kg 3pRNA, and the second administered 0.30625 mg/kg 3pRNA. Groups that were administered αPD-L1 intraperitoneally were injected four total times (Figure 5a). Mice that were administered 0.30625 mg/kg did not experience 3pRNA/NP-mediated mouse death. Mice administered with 3pRNA/NPs and αPD-L1 as well as PBS and αPD-L1 exhibited reduced tumor burden compared to mice treated with PBS (Figure 5b-5c). Moreover, although the effect of treatment on reducing tumor burden was modest, 2/8 mice administered both 3pRNA/NPs and αPD-L1 demonstrated complete response (CR) without any further evidence of tumor growth, and 0/10 mice administered PBA and αPD-L1 resulted in tumor free CRs. This study demonstrates that systemic administration of 3pRNA/NPs is capable of enhancing the efficacy of αPD-L1 for cancer therapy.

Discussion

Chapters 2 and 3 have demonstrated that 3pRNA agonists of RIG-I when delivered using endosomolytic nanoparticles are strong potentiators of type-I IFN, enhancing

the therapeutic efficacy of αPD-1 ICB to yield significant improvement in survival while resulting in a 30% complete response rate in a CT26 murine colon cancer model. A series of block copolymers were synthesized, characterized and found to exhibit significant pH-responsive behavior, suggesting that this custom designed polymer could be developed to offer significant drug delivery improvement. This research found that 3pRNA/NPs comprising a lead polymer defined in chapter 2 exhibited enhanced *in vivo* activity; however, when accounting for *in vitro* serum stability and activity, P-b-$DA_4$50 emerged as a potentially stronger candidate for formulating 3pRNA/NPs for cancer immunotherapy. This chapter described the continuation of my work towards developing systemic 3pRNA/NPs to enhance ICB efficacy, which focused on studies involving local injections of the lead series polymers 3pRNA/NPs, in concert with αPD-L1 in a 4T1 breast cancer mouse model.

This research revealed that local injection and systemic injection of 3pRNA/NPs at 4 mg or higher in tumor models led to unexpected mouse mortality. This could be related to NP uptake by Kupffer cells, which has also occurred with similar nanoparticles.[101] Briefly, 3pRNAs that accumulate in the liver can be endocytosed by Kupffer cells, resulting in the production of adverse related immune effects mediated by Platelet activating factors.[163] In order to show the efficacy of the 3pRNA/NP system, 3pRNA/NPs, comprised of P-b-$DA_4$50 and 3pRNA, were administered in combination with αPD-L1 checkpoint in E0771 tumor models. While murine treatment with 3pRNA/NP and PD-L1 checkpoint blockade did not result in significant reduction of tumor burden or survival compared to PD-L1 checkpoint blockade alone, 3pRNA/NP treatment in conjunction with 3pRNA resulted in 2/8 tumor free complete responses (CRs). These results could indicate that 3pRNA/NPs may be critical to the development of anti-tumor immunity in this model but will

need to be further evaluated. We studied the behavior of the same polymers in a model that utilized siRNA *in vitro* as an alternative application of these NPs that may be effective at low doses *in vivo*. Correspondingly, we complexed a series of polymers with firefly luciferase siRNA to form siRNA/NPs. These studies found that all four of the lead polymers previously discovered in Chapter 2 formed potent siRNA/NPs, and therefore could be evaluated using a 4T1-luciferase silencing model. While not part of this thesis, *in vivo*, my result suggest the potential to also leverage these carriers for siRNA delivery applications at lower polymer doses, and would be an exciting use of these carriers that merits further evaluation.

The juxtaposition of 3pRNA/NP's potent activity *in vitro* and NP dose limiting toxicity *in vivo* was unexpected in this delivery system. Nevertheless, this work provided critical results towards an effective treatment and lays a strong foundation for future studies in this area, supporting NP delivery of 3pRNA as a powerful addition to ICB for cancer therapy. We believe that using small polymer modifications and novel 3pRNA oligos to reduce the polymer dose per NP will lead to a powerful systemic formulation that improves the success rate of ICB.

Materials and Methods

Synthesis and Preparation of 5'-Triphosphate RNA, siRNA, and 5'-A647-RNA. 5'-ppp-CGUUAAUCGCGUAUAAUACGCCUAU-3' (5'ppp Scr top) and 5'-ppp-AACAAUUGCACU GAUAAUGAAUUCC - 3' (5'ppp Luc top) was generously synthesized and provided by the laboratory of Dr. Anna M. Pyle at Yale University. 5'-OH-CGUUAAUCGCGUAUAAUACGCCUAU-3' (Scr top) and 5'- AACAAUUGCACU GAUAAUGAAUUCC - 3' (Luc top) as well as the complement strands 5'-AUAGGCGUAUUAUACGCGAUUAACG-3' (Scr bot)

and 5' -GGAAUUCAUUAUCAGUGCAAUUGUU - 3' (Luc bot) was purchased from Integrated DNA technologies (IDT) and resuspended in RNAse free water. Equimolar amounts of 5'ppp Scr top, 5'ppp Luc top, Scr top, or luc top were mixed with the matching complement strand and were suspended in 0.3 M NaCl and transferred to a 0.25mL PCR tube. The top and bottom strands were annealed using a thermocycler, setting the temperature to 90^{o}C and slowly cooling to 35^{o}C for 1 h in order to generate hybridized RNA. The resulting duplexes for 3pRNA, 3p-Luc-RNA, OH-RNA, and OH-Luc-RNA were diluted to 100μM RNA in RNAse free water and agarose gel (2%) electrophoresis used to confirm hybridization. In addition, more traditional luciferase silencing and scrambled RNA controls were provided by Meredith Jackson from the advanced therapeutics laboratory at Vanderbilt University.

Formulation of NP/3pRNA complexes for *in vitro* investigations. Lyophilized copolymers were dissolved into ethanol at 50 mg/mL and stored at 4^{o}C. This stock was further diluted to 3.33 mg/mL in citric acid buffer (pH 4, 100 mM) and rapidly mixed with either RNA at charge ratios (N:P) between 20:1 and 1:1. After incubating at room temperature for 30 min, 1.24x volume of a high pH buffer comprising phosphate buffer (pH 8, 100 mM, PB) containing 20 nM NaOH and mixing rapidly to form nanoparticles (NPs). After 15 min, the solution was further diluted into PBS (pH 7.4, Gibco) before use. The second block DMAEMA content is estimated to have 50% protonation for the purposes of determining N:P ratios. A charge ratio of 20:1 was selected for all *in vitro* cell culture studies.

Cell lines. The murine breast cancer cell line 4T1 (ATCC) as well as modified luciferase expression 4T1 cells generously provided by the Advanced therapeutics Laboratory at Vanderbilt university were cultured in RPMI 1640

(Gibco) supplemented with 2 mM L-glutamine, 10% fetal bovine serum (FBS, Gibco), and 100 U/mL penicillin/100 μg/mL streptomycin (Gibco). The murine breast cancer cell line E0071s that was kindly provided by the Balko lab at Vanderbilt University were cultured in RPMI 1640 (Gibco) supplemented with 2 mM L-glutamine, 10% fetal bovine serum (FBS, Gibco), 10 mM Hepes buffer (Gibco), and 100 U/mL penicillin/100 μg/mL streptomycin (Gibco). All cell types were grown at 37^{o}C in 5% CO_2.

***in vitro* Evaluation of NP Delivery of Luciferase siRNA.** 4T1-luciferase expressing cells were seeded in clear, flat bottom, black walled 96 well plates (Grenier Bio-One) at 2000 cells/well and permitted to adhere overnight at 37^{o}C. The next day, siRNA/NPs were formulated using luciferase siRNA or scrambled RNA complexed to lead carriers as described above and treated at a final RNA concentration of 0.5-50 nM. After 24 hours, the media was removed and replaced with media containing 150 μg/mL D-luciferin, and bioluminescence was measured with an IVIS Lumina III imaging system. Percent gene silencing was calculated using the following formula: $\frac{RLU_{scr}-RLU_{luc}}{RLU_{PBS}-RLU_{bgd}}x100\%$, where RLUs are the raw luciferase expression of samples, scr represents cells transfected with NPs comprising scr RNA, luc represents cells transfected with NPs comprising luciferase siRNA, PBS represents untransfected controls, and bgd represents the fluorescence of luciferin containing media without the presence of 4T1-luciferase cells.

Preparation of NP/3pRNA for *in vivo* studies. All buffers used for this protocol were pre-filtered using a 0.22 μm syringe filter (Pall corporation). 3pRNA/NPs were formulated as descried above, except polymers were suspended at 10 mg/mL in citric acid buffer instead of 3.33 mg/mL, and PB buffer was added at a ratio of 1:1.26. A charge ratio of 15:1 was selected for all *in vivo* cell culture studies.

If the treatment required a higher RNA concentration than possible using these parameters, the formulation was then diluted into 10 mL of sterile, biological grade PBS. The NP solution was then drawn into a 10 mL syringe and passed through a 5 kD tangential flow column (C02-E05-05-S, Spectrum Labs). The solution was washed 3x in sterile, biological grade PBS, and the pH of the effluent stream was confirmed to be 7.4 before concentrating the NP solution to the required concentration for treatment.

Animal Care and Experimentation. Female C57BL/6J mice (7 weeks old) were obtained from The Jackson Laboratory (Bar Harbor, ME). All animals were maintained at the animal facilities of Vanderbilt University under specific pathogen-free conditions. All animal experiments were approved by the Vanderbilt University Institutional Animal Care and Use Committee (IACUC). Tumor volume, as well as mouse weight, was measured every other day via caliper measurements and a balance. Tumor volume was calculated using the equation$V = 1/2(L * W * H)$.[161]

qRT-PCR and ELISA Analysis of Murine Organs and Serum. Female C57BL/6J mice (9 weeks old mice) were inoculated with 100 μL of E0771 cells suspended in cold PBS (pH 7.4, Gibco), at 2.5x10^5 cells/mL. Once tumor volumes reached approximately 100 mm^3, Mice were intravenously administered 150 μL of indicated formulation or vehicle (PBS) containing 15 μg of either 3pRNA or OH-RNA and 600 μg of polymer in buffer using a 0.5 cc syringe and a 27 gauge needle (n=7 for each group). After 5 h, mice from each group were euthanized, blood was collected using cardiac puncture, and lungs, livers, spleens, and kidneys were surgically removed and stored at -20^{o}C in RNA later. Blood was kept at 4^{o}C and centrifuged at 8000g for 5 minutes. Supernatant for each blood sample was collected and serum IFN-α were determined using a Lumikine mIFN-α kit (Invivogen) according

to the manufacturer's instructions. Tumors and organs stored in RNA later were transferred into 1 mL of RLT lysis buffer in gentleMACs P tubes (Miltenyi Biotec) and digested using gentleMACS Octo dissociator (Miltenyi Biotec). Supernatant was transferred to RNeasy mini columns for mRNA purification following the manufacturer's instructions. mRNA was extracted from cell lysates using an RNA isolation kit (RNeasy mini kit, Qiagen). cDNA was synthesized for each sample using a cDNA synthesis kit (iScript, Bio-Rad) and analyzed using qRT-PCR using TAQMAN (Thermo Fischer) with CFX real time PCR detection system (Bio-Rad) following the manufacturer's instructions. Primers for *Ifnb1* (Mm00439552_s1), *CXCL10* (Mm00445235_m1), and *HMBS* (Mm01143545_m1) were purchased from ThermoFisher Scientific.

Evaluation of NP/3pRNA in 4T1 and E0771 breast cancer model. Female C57BL/6J mice (7 weeks old) were inoculated with 100 μL of E0771 or 4T1 cells suspended in cold PBS (pH 7.4, Gibco), at 2.5x10^5 cells/mL on day 0 in the right mammary fat pad. Once tumors reached 50mm^3, mice were administered NPs and checkpoint antibodies. In some cohorts, mice were administered 100 μg αPD-L1 (RMP1-14, BioXCell) in 100 μL Antibody Diluent (1x, Perkin Elmer) intraperitoneally on the same day as intravenous injections. Mice bearing 4T1 tumors were treated with 100 μL of NP/3pRNA, NP/OH-RNA, or PBS at a dose corresponding to 25 μg RNA and 900 μg polymer in buffer. Mice were treated every three days for four total treatments. Mice bearing E0771 tumors were treated with 150 μL of NP/3pRNA, NP/OH-RNA, or vehicle control at a dose corresponding to 15 μg RNA for the first injection, 7.5 μg RNA for the second injection, and 0 μg RNA for the third and fourth injections. Mixed low pH citric acid buffer and high pH PB buffer was used as the vehicle control. First, The groups for this study were

the following: NP/3pRNA + αPD-L1 (n=10), NP/3pRNA (n=10), NP/OH-RNA + αPD-L1 (n=10), PBS + αPD-L1 (n=10), and PBS (n=10). Mice were euthanized when tumor volumes exceeded 1500 mm^3.

Statistics. Significance was determined using one-way ANOVA with Tukey's multiple comparisons test unless otherwise noted. Values represent experimental means, and error bars represent S.E.M. unless otherwise noted. **** p¡0.0001, *** p¡0.005, **p¡0.01, * p¡0.05.

Acknowledgements

We gratefully acknowledge Prof. Kenneth Rock (University of Massachusetts Medical School) for providing DC2.4 cells, Prof. Anna M. Pyle and Dr. Olga Fedorova (Yale University) for synthesizing and providing 5' triphosphate RNA, and Prof. Craig Duvall (Vanderbilt University) for use of the IVIS equipment. We thank the core facilities of the Vanderbilt Institute of Nanoscale Sciences and Engineering (VINSE) for the use of their Malvern Zetasizer for dynamic light scattering. This research was supported by grants to JTW from the Congressionally-Directed Medical Research Program (W81XWH-161-0063).

Chapter 5

Conclusions and Future Work

The recent clinical success of immune checkpoint blockade (ICB) in treating some cancer provides an opportunity for further research and develop of new immunotherapies that could revolutionize cancer treatment. One important issue that has emerged with increased use of ICB in the clinic is the need for a deeper understanding as to why only a small fraction of patients respond remarkably to ICB, while most patients do not. While greater appreciation for the importance of the innate immune system in eliciting and supporting effective anti-tumor T cell immunity has prompted the expansion of the immunotherapeutic arsenal to include innate immune agonists, many promising nucleic acid therapeutics remain limited by critical drug delivery challenges, including poor cellular uptake and therefore diminished delivery, susceptibility to nuclease degradation, and very low cytosolic bioavailability.

Within the emergent family of nucleic acid immunomodulators, 3pRNA agonists of RIG-I hold considerable promise owing to the robust and ubiquitous expression pattern of RIG-I, their capacity to stimulate a strong type-I IFN-driven inflammatory program, and their ability to induce immunogenic cell death in multiple cancer cell types. My work, presented in this thesis, focused on developing polymeric carriers to improve the efficacy of the innate immune agonist 3pRNA, which binds to the cytosolic recognition receptor RIG-I, with the ultimate goal of utilizing 3pRNA/NPs for *in situ* cancer vaccination. In order to optimize nanoparticles (NP) to deliver 3pRNA, new copolymer NPs (D-PDB polymers) were complexed with 3pRNA and

found to significantly enhance biological activity. More specifically, I saw enhanced expression of ISGs in multiple cell types represented in the TME as well as induction of immunogenic cell death in murine colon cancer cell line CT26 after treatment with pH-responsive amphiphilic diblock copolymers complexed with 3pRNA. Further, I demonstrated that local treatment of s.c. CT26 tumors *in vivo* led to increased infiltration of CD8+ T-cells and reduced cancer cell viability. Finally, a local regimen of 3pRNA/NPs reduced tumor burden and enhanced survival in tumor bearing mice, resulting in three complete responses. Results showed that non-pH-responsive carriers did not enhance activity, thereby confirming the importance of an active endosomal escape mechanism that enhances delivery in the design of 3pRNA delivery systems. This work also demonstrates the utility of NPs for 3pRNA delivery, with data indicating that NP/3pRNA can trigger RIG-I signaling and downstream immunostimulatory effects in macrophages, dendritic cells, and several cancer cell lines in a 3pRNA-dependent manner. Moreover, this 3pRNA/NP is also capable of inducing immunogenic cell death and activating myeloid cells. Treating mice growing CT26 murine colon cancer tumors with both αPD-1 immune checkpoint blockade and 3pRNA/NPs led to an increased infiltration of CD8+ T cells and decreased tumor burden with 30% complete responses showing no tumors after treatment. Furthermore, complete responses were able to completely resist tumor growth when re-challenged in the contralateral flank, indicating that mice without tumors had indeed developed anti-tumor immunity capable of eliminating cancer cell growth. Ultimately, I use an established polymeric carrier to form potent 3pRNA/NPs, indicating that amphiphilic diblock copolymers are capable of significantly enhancing 3pRNA efficacy for *in situ* vaccination.

In order to further optimize 3pRNA/NPs for enhanced activity and systemic

distribution, I synthesized a series of novel polymeric carriers and investigated the relationship between polymeric composition, pH-responsive properties, and 3pRNA/NP RIG-I pathway activation. Here, I found that RIG-I pathway activation showed a moderate non-linear correlation with polymer carrier alkyl chain length value n, and to a lesser extent non-linear polymer carrier hydrophobic monomer composition [%]. These results indicate that polymers with a specific range of n and [%] for more active 3pRNA/NPs, whereas steadily increasing or decreasing hydrophobic monomer composition or alkyl chain length does not result in more active 3pRNA/NPs. Four of these polymeric carriers successfully induced the expression of ISGs, including type-I IFNs, chemokines, and other cytokines, as well as activated murine myeloid cells, thereby enhancing the intracellular delivery of 3pRNA to potently activate the RIG-I pathway. I also evaluated 3pRNA/NPs comprising lead polymers in breast tumor models. First, I determined that systemic injection of 3pRNA/NPs at a reduced dose resulted in activation of ISGs in breast cancer tumors, while also increasing ISG expression in organs as and serum concentration of type-I IFN. I also evaluated the effects of a systemic regimen of 3pRNA/NPs in combination with αPD-L1, but ultimately found that 3pRNA/NP in this breast cancer model, as well as a number of other models, resulted in acute toxicity in the dose ranges evaluated in chapter 4.

While D-PDB was effective for murine local therapy, it exhibits a positively charged corona that would not facilitate systemic therapy and could lead to systemic toxicity. I synthesized novel polymer for 3pRNA/NPs; however, these formulations encountered dose related toxicity. Future studies will investigate new formulations that would not just overcome the dose-related toxicity challenges that arose from the *in vivo* studies presented in this thesis with the lead polymers, but also have

the potential to enhance other delivery vehicles, improving the delivery of other immunotherapeutic compounds. For example, there are efforts for developing a modified second block that would break apart in the endosome, potentially curbing the membrane disruptive potential of 3pRNA/NPs in the late endosome, reducing lysosomal leakage into the cytosol. Another possible system that is currently being investigated by our lab group involves covalently bonding nucleic acids to polymer carriers in addition to other formulation techniques to reduce the amount of polymer required for 3pRNA/NP formulations, reduce 3pRNA/NP size, and potentially improve NP shielding. He has also developed 3pRNA pro-drugs, which could reduce off target immune related adverse effects, reducing 3pRNA/NP toxicity.[164] Finally, working closely with the Pyle lab at Yale university, I am running studies using 3pRNA/NPs comprising various compositions of 3pRNAs to better understand the relationship between 3pRNA structure and 3pRNA/NP activity.

While NP properties, RIG-I ligand design, and NP/3pRNA dose and treatment regimen remain to be optimized for maximum therapeutic benefit, these studies demonstrate the importance of carrier design in immunotherapeutic targeting and set the stage for future investigation into the development of new delivery technologies for this promising class of innate immune agonist.

Appendix

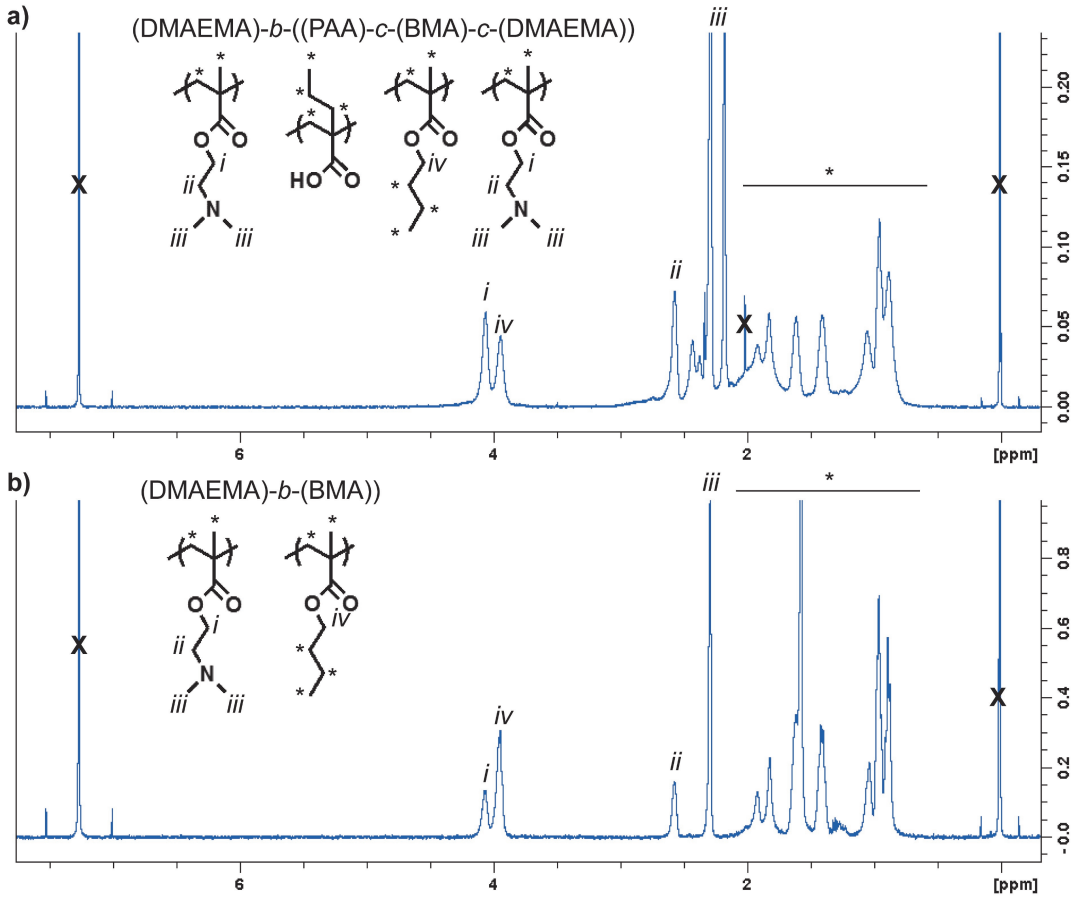

Figure A.1: **^{1}H NMR Characterization of diblock copolymers.** (a) DMAEMA-b-(PAA-c-BMA-c-DMAEMA) and (b) DMAEMA-b-BMA were characterized using NMR. Peaks denoted with an X originate from solvent or TMS.

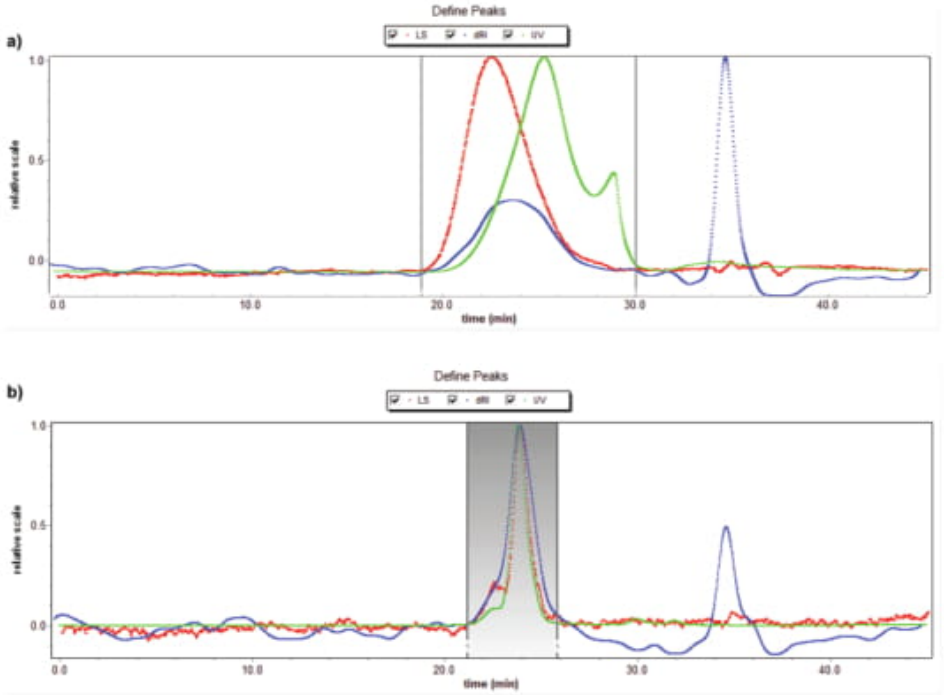

Figure A.2: **GPC spectra of diblock copolymers**
(a) DMAEMA-b-(PAA-c-BMA-c-DMAEMA) and (b) DMAEMA-b-BMA were characterized using GPC.

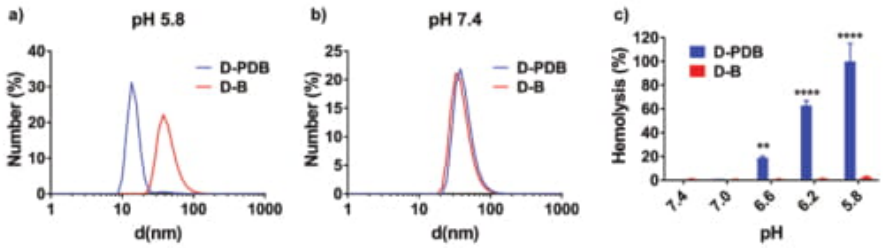

Figure A.3: **DMAEMA-b-BMA (D-B) is not pH-responsive or membrane disruptive.**
D-PDB and D-B were suspended in (a) pH 5.8 or (b) pH 7.4 PBS and particle size distribution was measured using DLS. (c) Erythrocytes were incubated with 10 μg/mL D-PDB or D-B in PBS at pH 5.8, pH 6.2, pH 6.6, pH 7.0, or pH 7.4 and membrane disruption was quantified using spectrophotometric determination of hemoglobin leakage as an indicator of hemolysis. Significance is between D-PDB and D-B treatment at the same pH.

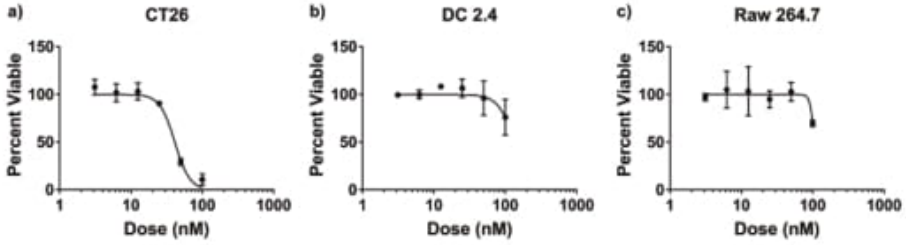

Figure A.4: **3pRNA without a transfection agent or other carrier does not activate RIG-I.**
A549-dual reporter cells were treated with Lipofectamine complexed with 3pRNA or 3pRNA only at doses ranging from 0.05 nM to 50 nM 3pRNA.

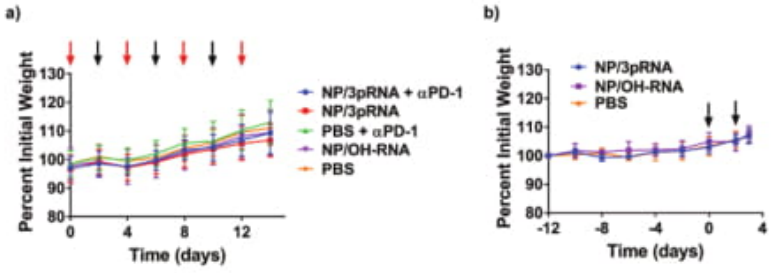

Figure A.5: **D-PDB is not cytotoxic at relevant concentrations *in vitro*.** (a) CT26 cells, (b) DC 2.4 cells, and (c) RAW 264.7 cells were treated with OH-RNA/NP at doses between 1.5 nM-100 nM RNA.

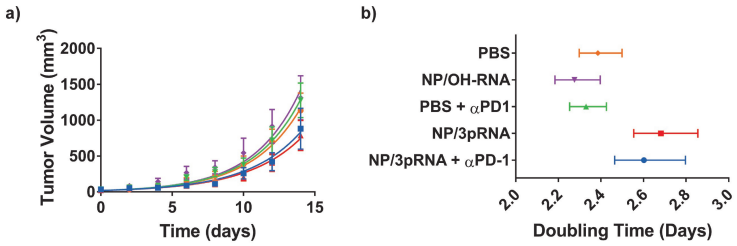

Figure A.6: ***In vivo* treatment regimens do not result in toxicity-related weight loss.**
Mice were weighed every two days following CT26 cell injection. (a) Mice from studies detailed in Figure 4 were weighed after tumor cell injection. The mice exhibited no weight loss from any of the treatment regimens. Mice were treated with NPs only at days indicated by the black arrow. (b) Mice from the study detailed in Figure 2.5 were weighed after tumor cell injection (d-12). The mice exhibited no weight loss from any of the treatment regimens. Mice were injected with αPD1 and NPs at days indicated by the red arrow. Mice were treated with NPs only at days indicated by the black arrow.

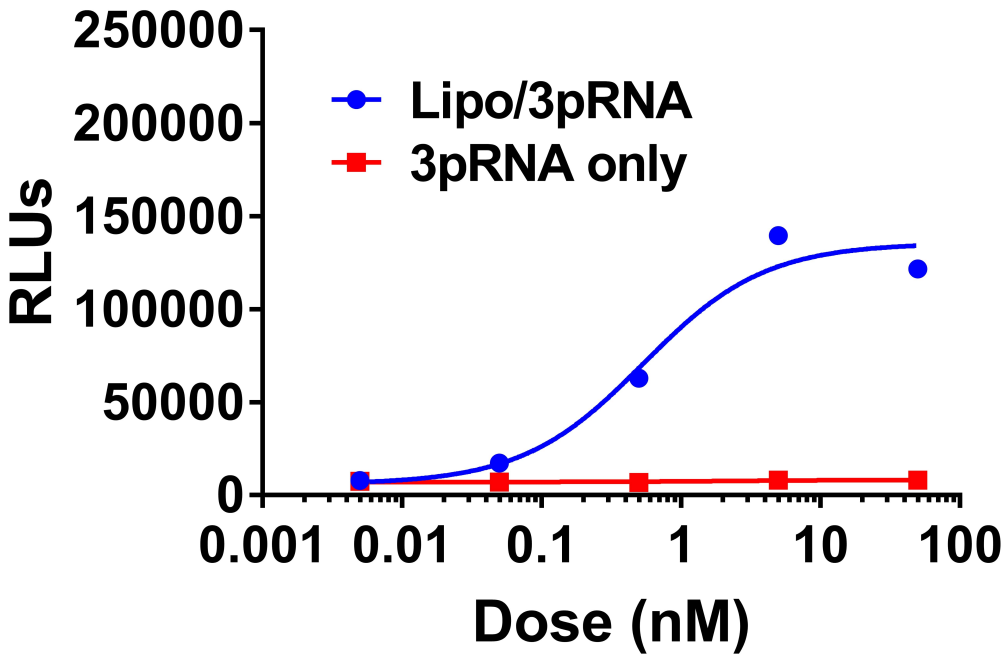

Figure A.7: **Intratumoral administration of NP/3pRNA + αPD-1 and NP/3pRNA results in an increased average tumor volume doubling time in CT26 colon cancer model.**
(a) Tumor growth plots were fit using an exponential curve. Initial tumor volume was assumed to be the minimum measured in the study for each group. (b) Tumor doubling time derived from exponential fits for each group plotted with 95% confidence intervals.

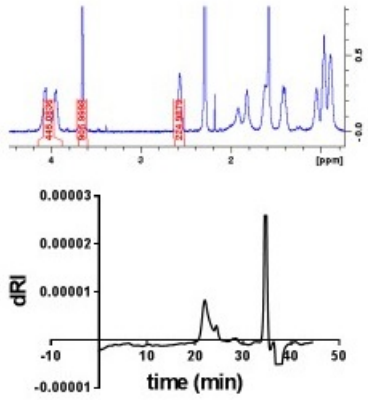

Figure A.8: **Example traces for P-b-DA$_4$50.**
NMR (top) and GPC (bottom) trace of P-b-DA$_4$50. Experimental molecular weights and polymer compositions were determined through this analysis.

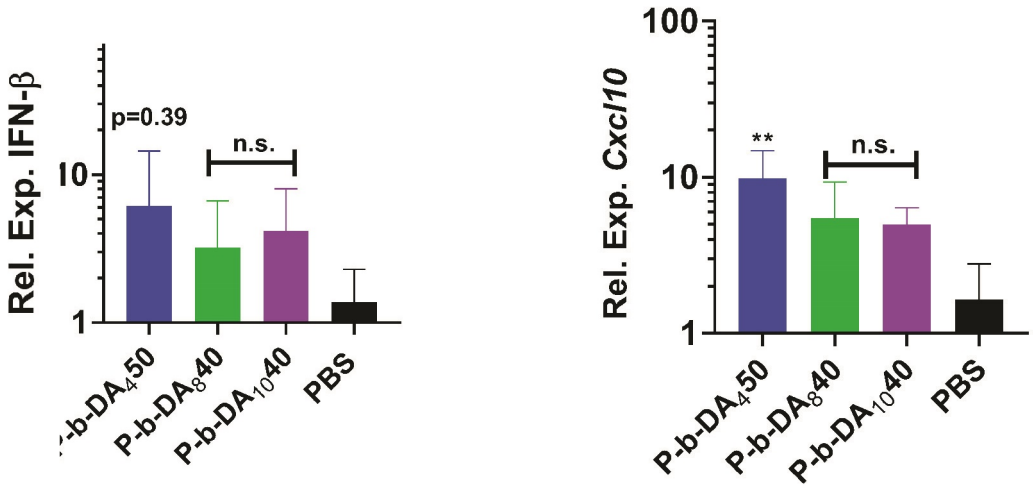

Figure A.9: **Systemic administration of NP comprised of lead carriers and 3pRNA activate ISGs and increase type-I IFN production in tumors.** Tumor *IFN-β* and *cxcl10* expression 6 h after tail vein injection of 0.625 mg/kg 3pRNA/NPs . All statistics were calculated compared to PBS using one-way ANOVA with post-hoc analysis.

Table 5: **Summary of D-PDB polymer properties.**
1^st block Mn, 2^{nd} block Mn, 2^{nd} block composition, and PDI of both polymers were determined from ^{1}H NMR and GPC analysis.

Polymer	Mn Block 1	Mn Block 2	PAA(%)	BMA%	DMAEMA(%)	PDI
D-PDB	10300	31000	28	39	33	1.24
D-B	9900	34122	0	100	0	1.09

Table 6: **Summary of doubling time analysis.**
Mean doubling time in days derived from each exponential fit as well as the 95% upper and lower confidence limits (CL).

Doubling Time	3pRNA/NP+αPD-1$	3pRNA/NP	PBS+αPD-1	OH-RNA/NP	PBS
Mean	2.602	2.682	2.330	2.276	2.386
Upper 95% CL	2.797	2.855	2.436	2.397	2.499
Lower 95% CL	2.465	2.544	2.253	2.184	2.298

References

[1] Charles A Dinarello. Proinflammatory cytokines. *Chest*, 118(2):503–508, 2000.

[2] Steven M Opal and Vera A DePalo. Anti-inflammatory cytokines. *Chest*, 117(4):1162–1172, 2000.

[3] Parris Kidd. Th1/th2 balance: the hypothesis, its limitations, and implications for health and disease. *Alternative medicine review*, 8(3):223–246, 2003.

[4] Stephan Halle, Olga Halle, and Reinhold Förster. Mechanisms and dynamics of t cell-mediated cytotoxicity in vivo. *Trends in immunology*, 38(6):432–443, 2017.

[5] Margaret K Callahan and Jedd D Wolchok. At the bedside: Ctla-4-and pd-1-blocking antibodies in cancer immunotherapy. *Journal of Leukocyte Biology*, 94(1):41–53, 2013.

[6] Drew M Pardoll. The blockade of immune checkpoints in cancer immunotherapy. *Nature Reviews Cancer*, 12(4):252–264, 2012.

[7] Mizuki Nishino, Nikhil H Ramaiya, Hiroto Hatabu, and F Stephen Hodi. Monitoring immune-checkpoint blockade: response evaluation and biomarker development. *Nature reviews Clinical Oncology*, 14(11):655, 2017.

[8] Mark J Smyth, Shin Foong Ngiow, Antoni Ribas, and Michele WL Teng. Combination cancer immunotherapies tailored to the tumour microenvironment. *Nature Reviews Clinical Oncology*, 2015.

[9] Daniel S Chen and Ira Mellman. Oncology meets immunology: the cancer-immunity cycle. *Immunity*, 39(1):1–10, 2013.

[10] Daniel Sanghoon Shin and Antoni Ribas. The evolution of checkpoint blockade

as a cancer therapy: whats here, whats next? *Current Opinion in Immunology*, 33:23–35, 2015.

[11] Carol DeSantis, Rebecca Siegel, Priti Bandi, and Ahmedin Jemal. Breast cancer statistics, 2011. *CA: a Cancer Journal for Clinicians*, 61(6):408–418, 2011.

[12] RM Clark, T Whelan, M Levine, R Roberts, A Willan, P McCulloch, M Lipa, RH Wilkinson, and LJ Mahoney. Randomized clinical trial of breast irradiation following lumpectomy and axillary dissection for node-negative breast cancer: an update. *Journal of the National Cancer Institute*, 88(22):1659–1664, 1996.

[13] Ibiayi Dagogo-Jack and Alice T Shaw. Tumour heterogeneity and resistance to cancer therapies. *Nature reviews Clinical Oncology*, 15(2):81, 2018.

[14] Giampaolo Bianchini, Justin M Balko, Ingrid A Mayer, Melinda E Sanders, and Luca Gianni. Triple-negative breast cancer: challenges and opportunities of a heterogeneous disease. *Nature reviews Clinical Oncology*, 13(11):674, 2016.

[15] Joseph A Sparano, Robert J Gray, Della F Makower, Kathleen I Pritchard, Kathy S Albain, Daniel F Hayes, Charles E Geyer Jr, Elizabeth C Dees, Matthew P Goetz, John A Olson Jr, et al. Adjuvant chemotherapy guided by a 21-gene expression assay in breast cancer. *New England Journal of Medicine*, 379(2):111–121, 2018.

[16] Lynn AG Ries, D Harkins, M Krapcho, Angela Mariotto, BA Miller, Eric J Feuer, Limin X Clegg, MP Eisner, Marie-Josèphe Horner, Nadia Howlader, et al. Seer cancer statistics review, 1975-2003. 2006.

[17] Emma Nolan, Peter Savas, Antonia N Policheni, Phillip K Darcy, François Vaillant, Christopher P Mintoff, Sathana Dushyanthen, Mariam Mansour, Jia-Min B Pang, Stephen B Fox, et al. Combined immune checkpoint blockade as

a therapeutic strategy for brca1-mutated breast cancer. *Science translational medicine*, 9(393):eaal4922, 2017.

[18] Duane A Mitchell and Smita K Nair. Rna-transfected dendritic cells in cancer immunotherapy. *The Journal of Clinical Investigation*, 106(9):1065–1069, 2000.

[19] Jean-Rémi Bertrand, Catherine Pioche-Durieu, Juan Ayala, Tristan Petit, Hugues A Girard, Claude P Malvy, Eric Le Cam, François Treussart, and Jean-Charles Arnault. Plasma hydrogenated cationic detonation nanodiamonds efficiently deliver to human cells in culture functional sirna targeting the ewing sarcoma junction oncogene. *Biomaterials*, 45:93–98, 2015.

[20] Roman Barbalat, Sarah E Ewald, Maria L Mouchess, and Gregory M Barton. Nucleic acid recognition by the innate immune system. *Annual Review of Immunology*, 29:185–214, 2011.

[21] Gaurav Sahay, William Querbes, Christopher Alabi, Ahmed Eltoukhy, Sovan Sarkar, Christopher Zurenko, Emmanouil Karagiannis, Kevin Love, Delai Chen, Roberto Zoncu, et al. Efficiency of sirna delivery by lipid nanoparticles is limited by endocytic recycling. *Nature biotechnology*, 31(7):653–658, 2013.

[22] Fu-Sheng Du, Yang Wang, Rui Zhang, and Zi-Chen Li. Intelligent nucleic acid delivery systems based on stimuli-responsive polymers. *Soft Matter*, 6(5):835–848, 2010.

[23] Jeffrey A Hubbell, Susan N Thomas, and Melody A Swartz. Materials engineering for immunomodulation. *Nature*, 462(7272):449–460, 2009.

[24] Jacqueline Parkin and Bryony Cohen. An overview of the immune system. *The Lancet*, 357(9270):1777–1789, 2001.

[25] Ruslan Medzhitov and Charles A Janeway. Innate immunity: the virtues of a nonclonal system of recognition. *cell*, 91(3):295–298, 1997.

[26] Taro Kawai and Shizuo Akira. The role of pattern-recognition receptors in innate immunity: update on toll-like receptors. *Nature immunology*, 11(5):373–384, 2010.

[27] Osamu Takeuchi and Shizuo Akira. Pattern recognition receptors and inflammation. *Cell*, 140(6):805–820, 2010.

[28] Akiko Iwasaki and Ruslan Medzhitov. Regulation of adaptive immunity by the innate immune system. *science*, 327(5963):291–295, 2010.

[29] Francisco A Bonilla and Hans C Oettgen. Adaptive immunity. *Journal of Allergy and Clinical Immunology*, 125(2):S33–S40, 2010.

[30] Susan M Kaech, E John Wherry, and Rafi Ahmed. Effector and memory t-cell differentiation: implications for vaccine development. *Nature Reviews Immunology*, 2(4):251–262, 2002.

[31] Greg T Motz and George Coukos. Deciphering and reversing tumor immune suppression. *Immunity*, 39(1):61–73, 2013.

[32] Flaubert Mbeunkui and Donald J Johann Jr. Cancer and the tumor microenvironment: a review of an essential relationship. *Cancer chemotherapy and pharmacology*, 63(4):571–582, 2009.

[33] Johanna A Joyce. Therapeutic targeting of the tumor microenvironment. *Cancer cell*, 7(6):513–520, 2005.

[34] Minna Allinen, Rameen Beroukhim, Li Cai, Cameron Brennan, Jaana Lahti-Domenici, Haiyan Huang, Dale Porter, Min Hu, Lynda Chin, Andrea Richardson, et al. Molecular characterization of the tumor microenvironment in breast cancer.

Cancer cell, 6(1):17–32, 2004.

[35] Uzma Shamim, Sarmad Hanif, Abdulmajeed Albanyan, Frances WJ Beck, Bin Bao, Zhiwei Wang, Sanjeev Banerjee, Fazlul H Sarkar, Ramzi M Mohammad, Sheikh M Hadi, et al. Resveratrol-induced apoptosis is enhanced in low ph environments associated with cancer. *Journal of cellular physiology*, 227(4):1493–1500, 2012.

[36] David H Munn and Vincenzo Bronte. Immune suppressive mechanisms in the tumor microenvironment. *Current Opinion in Immunology*, 39:1–6, 2016.

[37] Ira Mellman, George Coukos, and Glenn Dranoff. Cancer immunotherapy comes of age. *Nature*, 480(7378):480–489, 2011.

[38] Michael A Postow, Robert Sidlow, and Matthew D Hellmann. Immune-related adverse events associated with immune checkpoint blockade. *New England Journal of Medicine*, 378(2):158–168, 2018.

[39] KiBem Kim, Andrew D Skora, Zhaobo Li, Qiang Liu, Ada J Tam, Richard L Blosser, Luis A Diaz, Nickolas Papadopoulos, Kenneth W Kinzler, Bert Vogelstein, et al. Eradication of metastatic mouse cancers resistant to immune checkpoint blockade by suppression of myeloid-derived cells. *Proceedings of the National Academy of Sciences*, 111(32):11774–11779, 2014.

[40] Teresa Kim, Rodabe N Amaria, Christine Spencer, Alexandre Reuben, Zachary A Cooper, and Jennifer A Wargo. Combining targeted therapy and immune checkpoint inhibitors in the treatment of metastatic melanoma. *Cancer Biology & Medicine*, 11(4):237, 2014.

[41] Jarushka Naidoo, DB Page, BT Li, LC Connell, K Schindler, ME Lacouture, MA Postow, and JD Wolchok. Toxicities of the anti-pd-1 and anti-pd-l1 immune

checkpoint antibodies. *Annals of Oncology*, 26(12):2375–2391, 2015.

[42] J-M Michot, R Pruvost, C Mateus, S Champiat, A-L Voisin, A Marabelle, and O Lambotte. Fever reaction and haemophagocytic syndrome induced by immune checkpoint inhibitors. *Annals of Oncology*, 29(2):518–520, 2017.

[43] H Picchi, C Mateus, C Chouaid, B Besse, A Marabelle, JM Michot, S Champiat, AL Voisin, and O Lambotte. Infectious complications associated with the use of immune checkpoint inhibitors in oncology: reactivation of tuberculosis after anti pd-1 treatment. *Clinical Microbiology and Infection*, 24(3):216–218, 2018.

[44] Padmanee Sharma, Siwen Hu-Lieskovan, Jennifer A Wargo, and Antoni Ribas. Primary, adaptive, and acquired resistance to cancer immunotherapy. *Cell*, 168(4):707–723, 2017.

[45] Jesse M Zaretsky, Angel Garcia-Diaz, Daniel S Shin, Helena Escuin-Ordinas, Willy Hugo, Siwen Hu-Lieskovan, Davis Y Torrejon, Gabriel Abril-Rodriguez, Salemiz Sandoval, Lucas Barthly, et al. Mutations associated with acquired resistance to pd-1 blockade in melanoma. *New England Journal of Medicine*, 375(9):819–829, 2016.

[46] JM Taube, RA Anders, GD Young, H Xu, R Sharma, TL McMiller, S Chen, AP Klein, DM Pardoll, SL Topalian, et al. Colocalization of inflammatory response with b7-h1 expression in human melanocytic lesions supports an adaptive resistance mechanism of immune escape. 4 (127): 127ra137, 2012.

[47] Peter Schmid, Sylvia Adams, Hope S Rugo, Andreas Schneeweiss, Carlos H Barrios, Hiroji Iwata, Véronique Diéras, Roberto Hegg, Seock-Ah Im, Gail Shaw Wright, et al. Atezolizumab and nab-paclitaxel in advanced triple-negative breast cancer. *New England Journal of Medicine*, 379(22):2108–2121, 2018.

[48] Kun Zhou, Ji Lu, Xiaoxin Yin, Han Xu, Longzhi Li, and Baojin Ma. Structure-based derivation and intramolecular cyclization of peptide inhibitors from pd-1/pd-l1 complex interface as immune checkpoint blockade for breast cancer immunotherapy. *Biophysical Chemistry*, page 106213, 2019.

[49] Sasha E Stanton, Sylvia Adams, and Mary L Disis. Variation in the incidence and magnitude of tumor-infiltrating lymphocytes in breast cancer subtypes: a systematic review. *JAMA oncology*, 2(10):1354–1360, 2016.

[50] Susan B Manoff, Sarah L George, Andrew J Bett, Michele L Yelmene, Govindarajan Dhanasekaran, Linda Eggemeyer, Michele L Sausser, Sheri A Dubey, Danilo R Casimiro, David E Clements, et al. Preclinical and clinical development of a dengue recombinant subunit vaccine. *Vaccine*, 33(50):7126–7134, 2015.

[51] Francisco J Esteva, Vanessa M Hubbard-Lucey, Jun Tang, and Lajos Pusztai. Immunotherapy and targeted therapy combinations in metastatic breast cancer. *The Lancet Oncology*, 20(3):e175–e186, 2019.

[52] P Schmid, S Adams, HS Rugo, A Schneeweiss, CH Barrios, H Iwata, V Dieras, R Hegg, SA Im, GS Wright, et al. Lba1_pr impassion130: Results from a global, randomised, double-blind, phase iii study of atezolizumab (atezo)+ nab-paclitaxel (nab-p) vs placebo+ nab-p in treatment-naive, locally advanced or metastatic triple-negative breast cancer (mtnbc). *Annals of Oncology*, 29(suppl_8):mdy424–008, 2018.

[53] D Miles, F André, J Gligorov, S Verma, B Xu, D Cameron, CH Barrios, A Schneeweiss, V Easton, Y Ghazi, et al. Abstract ot1-01-01: Impassion131: A phase iii study comparing 1l atezolizumab with paclitaxel vs placebo with

paclitaxel in treatment-naive patients with inoperable locally advanced or metastatic triple negative breast cancer (tnbc), 2018.

[54] Charles E Geyer, Sibylle Loibl, Priya Rastogi, Sabine Seiler, Joseph P Costantino, Namrata Vijayvergia, Patricia Cortazar, Peter C Lucas, Carsten Denkert, Eleftherios P Mamounas, et al. Nsabp b-59/gbg 96-gepardouze: A randomized double-blind phase iii clinical trial of neoadjuvant chemotherapy (nac) with atezolizumab or placebo in patients (pts) with triple negative breast cancer (tnbc) followed by adjuvant atezolizumab or placebo., 2018.

[55] Trevor T Hansel, Harald Kropshofer, Thomas Singer, Jane A Mitchell, and Andrew JT George. The safety and side effects of monoclonal antibodies. *Nature reviews Drug discovery*, 9(4):325–338, 2010.

[56] Peter Savas, Roberto Salgado, Carsten Denkert, Christos Sotiriou, Phillip K Darcy, Mark J Smyth, and Sherene Loi. Clinical relevance of host immunity in breast cancer: from tils to the clinic. *Nature reviews Clinical Oncology*, 13(4):228, 2016.

[57] Martina Schmittnaegel, Nicolò Rigamonti, Ece Kadioglu, Antonino Cassará, Céline Wyser Rmili, Anna Kiialainen, Yvonne Kienast, Hans-Joachim Mueller, Chia-Huey Ooi, Damya Laoui, et al. Dual angiopoietin-2 and vegfa inhibition elicits antitumor immunity that is enhanced by pd-1 checkpoint blockade. *Science translational medicine*, 9(385):eaak9670, 2017.

[58] Javier Cortés, Zifang Guo, Vassiliki Karantza, and Gursel Aktan. Keynote-355: Randomized, double-blind, phase iii study of pembrolizumab (pembro)+ chemotherapy (chemo) vs placebo (pbo)+ chemo for previously untreated, locally recurrent, inoperable or metastatic triple-negative breast cancer (mtnbc)., 2018.

[59] Peter Schmid, Javier Cortes, Jonas CS Bergh, Lajos Pusztai, Carsten Denkert, Sunil Verma, Heather L McArthur, Sherko Kummel, Yu Ding, Vassiliki Karantza, et al. Keynote-522: Phase iii study of pembrolizumab (pembro)+ chemotherapy (chemo) vs placebo+ chemo as neoadjuvant therapy followed by pembro vs placebo as adjuvant therapy for triple-negative breast cancer (tnbc)., 2018.

[60] Eric P Winer, Thao Dang, Vassiliki Karantza, and Shu-Chih Su. Keynote-119: A randomized phase iii study of single-agent pembrolizumab (mk-3475) vs single-agent chemotherapy per physicianś choice for metastatic triple-negative breast cancer (mtnbc)., 2016.

[61] Mitsutoshi Yoneyama and Takashi Fujita. Rna recognition and signal transduction by rig-i-like receptors. *Immunological reviews*, 227(1):54–65, 2009.

[62] Hinh Ly Morgan Brisse. Comparative structure and function analysis of the rig-i-like receptors: Rig-i and mda5. *Frontiers in immunology*, 10, 2019.

[63] Elizabeth Thompson, Janis M Taube, Hillary Elwood, Rajni Sharma, Alan Meeker, Hind Nassar Warzecha, Pedram Argani, Ashley Cimino-Mathews, and Leisha A Emens. The immune microenvironment of breast ductal carcinoma in situ. *Modern Pathology*, 29(3):249, 2016.

[64] Kanjiro Miyata, Nobuhiro Nishiyama, and Kazunori Kataoka. Rational design of smart supramolecular assemblies for gene delivery: chemical challenges in the creation of artificial viruses. *Chemical Society Reviews*, 41(7):2562–2574, 2012.

[65] Michelle MA Fernando, Christine R Stevens, Emily C Walsh, Philip L De Jager, Philippe Goyette, Robert M Plenge, Timothy J Vyse, and John D Rioux. Defining the role of the mhc in autoimmunity: a review and pooled analysis. *PLoS genetics*, 4(4):e1000024, 2008.

[66] Seng-Ryong Woo, Mercedes B Fuertes, Leticia Corrales, Stefani Spranger, Michael J Furdyna, Michael YK Leung, Ryan Duggan, Ying Wang, Glen N Barber, Katherine A Fitzgerald, et al. Sting-dependent cytosolic dna sensing mediates innate immune recognition of immunogenic tumors. *Immunity*, 41(5):830–842, 2014.

[67] Xu Zhang, Heping Shi, Jiaxi Wu, Xuewu Zhang, Lijun Sun, Chuo Chen, and Zhijian J Chen. Cyclic gmp-amp containing mixed phosphodiester linkages is an endogenous high-affinity ligand for sting. *Molecular cell*, 51(2):226–235, 2013.

[68] Pu Gao, Manuel Ascano, Yang Wu, Winfried Barchet, Barbara L Gaffney, Thomas Zillinger, Artem A Serganov, Yizhou Liu, Roger A Jones, Gunther Hartmann, et al. Cyclic [g (2, 5) pa (3, 5) p] is the metazoan second messenger produced by dna-activated cyclic gmp-amp synthase. *Cell*, 153(5):1094–1107, 2013.

[69]

[70] Leticia Corrales, Sarah M McWhirter, Thomas W Dubensky, and Thomas F Gajewski. The host sting pathway at the interface of cancer and immunity. *The Journal of clinical investigation*, 126(7):2404–2411, 2016.

[71] Hua Wang, Shuiqing Hu, Xiang Chen, Heping Shi, Chuo Chen, Lijun Sun, and Zhijian J Chen. cgas is essential for the antitumor effect of immune checkpoint blockade. *Proceedings of the National Academy of Sciences*, 114(7):1637–1642, 2017.

[72] Hiroki Ishikawa, Zhe Ma, and Glen N Barber. Sting regulates intracellular dna-mediated, type i interferon-dependent innate immunity. *Nature*, 461(7265):788–792, 2009.

[73] Melissa M Linehan, Thayne H Dickey, Emanuela S Molinari, Megan E Fitzgerald,

Olga Potapova, Akiko Iwasaki, and Anna M Pyle. A minimal rna ligand for potent rig-i activation in living mice. *Science advances*, 4(2):e1701854, 2018.

[74] Mike W Helms, Kerstin Jahn-Hofmann, Felix Gnerlich, Christiane Metz-Weidmann, Monika Braun, Gabriele Dietert, Petra Scherer, Kaj Grandien, Joachim Theilhaber, Hui Cao, et al. Utility of the rig-i agonist triphosphate rna for melanoma therapy. *Molecular Cancer Therapeutics*, pages molcanther–1262, 2019.

[75] Lionel B Ivashkiv. Ifnγ: signalling, epigenetics and roles in immunity, metabolism, disease and cancer immunotherapy. *Nature Reviews Immunology*, 18(9):545, 2018.

[76] Taeko Matsushima-Miyagi, Koji Hatano, Motonari Nomura, Liu Li-Wen, Tomoyuki Nishikawa, Kotaro Saga, Takashi Shimbo, and Yasufumi Kaneda. Trail and noxa are selectively upregulated in prostate cancer cells downstream of the rig-i/mavs signaling pathway by nonreplicating sendai virus particles. *Clinical Cancer Research*, 18(22):6271–6283, 2012.

[77] Robert Besch, Hendrik Poeck, Tobias Hohenauer, Daniela Senft, Georg Häcker, Carola Berking, Veit Hornung, Stefan Endres, Thomas Ruzicka, Simon Rothenfusser, et al. Proapoptotic signaling induced by rig-i and mda-5 results in type i interferon–independent apoptosis in human melanoma cells. *The Journal of Clinical Investigation*, 119(8):2399–2411, 2009.

[78] Yueh-Ming Loo and Michael Gale Jr. Immune signaling by rig-i-like receptors. *Immunity*, 34(5):680–692, 2011.

[79] Hiroki Kato, Osamu Takeuchi, Shintaro Sato, Mitsutoshi Yoneyama, Masahiro Yamamoto, Kosuke Matsui, Satoshi Uematsu, Andreas Jung, Taro Kawai, Ken J Ishii, et al. Differential roles of mda5 and rig-i helicases in the recognition of rna

viruses. *Nature*, 441(7089):101–105, 2006.

[80] Simon Heidegger, Alexander Wintges, Florian Stritzke, Sarah Bek, Katja Steiger, Paul-Albert Koenig, Sascha Göttert, Thomas Engleitner, Rupert Öllinger, Tatiana Nedelko, et al. Rig-i activation is critical for responsiveness to checkpoint blockade. *Science Immunology*, 4(39):eaau8943, 2019.

[81] Sowmya Pattabhi, Courtney R Wilkins, Ran Dong, Megan L Knoll, Jeffrey Posakony, Shari Kaiser, Chad E Mire, Myra L Wang, Renee C Ireton, Thomas W Geisbert, et al. Targeting innate immunity for antiviral therapy through small molecule agonists of the rlr pathway. *Journal of Virology*, 90(5):2372–2387, 2016.

[82] Nadine S Jahchan, Adriana M Mujal, Joshua L Pollack, Mikhail Binnewies, Venkataraman Sriram, Leonard Reyno, and Matthew F Krummel. Tuning the tumor myeloid microenvironment to fight cancer. *Frontiers in Immunology*, 10, 2019.

[83] MR Middleton, M Wermke, E Calvo, E Chartash, H Zhou, X Zhao, M Niewel, K Dobrenkov, and V Moreno. Lba16 phase i/ii, multicenter, open-label study of intratumoral/intralesional administration of the retinoic acid–inducible gene i (rig-i) activator mk-4621 in patients with advanced or recurrent tumors. *Annals of Oncology*, 29(suppl_8):mdy424–016, 2018.

[84] Rosemary Kanasty, Joseph Robert Dorkin, Arturo Vegas, and Daniel Anderson. Delivery materials for sirna therapeutics. *Nature materials*, 12:967–77, 2013.

[85] Daniel W Pack, Allan S Hoffman, Suzie Pun, and Patrick S Stayton. Design and development of polymers for gene delivery. *Nature Reviews Drug Discovery*, 4(7):581–593, 2005.

[86] K. J. Kauffman, M. J. Webber, and D. G. Anderson. Materials for non-viral

intracellular delivery of messenger rna therapeutics. *J Control Release*, 240:227–234, 2016.

[87] Khalid A. Hajj and Kathryn A. Whitehead. Tools for translation: non-viral materials for therapeutic mrna delivery. *Nature Reviews Materials*, 2:17056, 2017.

[88] Thomas A Werfel, Meredith A Jackson, Taylor E Kavanaugh, Kellye C Kirkbride, Martina Miteva, Todd D Giorgio, and Craig Duvall. Combinatorial optimization of peg architecture and hydrophobic content improves ternary sirna polyplex stability, pharmacokinetics, and potency in vivo. *Journal of Controlled Release*, 255:12–26, 2017.

[89] Melissa M Linehan, Thayne H Dickey, Emanuela S Molinari, Megan E Fitzgerald, Olga Potapova, Akiko Iwasaki, and Anna M Pyle. A minimal rna ligand for potent rig-i activation in living mice. *Science Advances*, 4(2):e1701854, 2018.

[90] Hendrik Poeck, Robert Besch, Cornelius Maihoefer, Marcel Renn, Damia Tormo, Svetlana Shulga Morskaya, Susanne Kirschnek, Evelyn Gaffal, Jennifer Landsberg, Johannes Hellmuth, Andreas Schmidt, David Anz, Michael Bscheider, Tobias Schwerd, Carola Berking, Carole Bourquin, Ulrich Kalinke, Elisabeth Kremmer, Hiroki Kato, Shizuo Akira, Rachel Meyers, Georg Häcker, Michael Neuenhahn, Dirk Busch, Jürgen Ruland, Simon Rothenfusser, Marco Prinz, Veit Hornung, Stefan Endres, Thomas Tüting, and Gunther Hartmann. 5'-triphosphate-sirna: turning gene silencing and rig-i activation against melanoma. *Nature Medicine*, 14(11):1256–1263, 2008.

[91] Jonathan Ellermeier, Jiwu Wei, Peter Duewell, Sabine Hoves, Mareike R Stieg, Tina Adunka, Daniel Noerenberg, Hans-Joachim Anders, Doris Mayr, and Hendrik Poeck. Therapeutic efficacy of bifunctional sirna combining tgf-β1

silencing with rig-i activation in pancreatic cancer. *Cancer research*, page canres. 3850.2011, 2013.

[92] Cong-fei Xu and Jun Wang. Delivery systems for sirna drug development in cancer therapy. *Asian Journal of Pharmaceutical Sciences*, 10(1):1–12, 2015.

[93] M Laird Forrest, James T Koerber, and Daniel W Pack. A degradable polyethylenimine derivative with low toxicity for highly efficient gene delivery. *Bioconjugate chemistry*, 14(5):934–940, 2003.

[94] Otmane Boussif, Frank Lezoualch, Marla Antonietra Zanta, Mogjan Djavaheri Mergny, Daniel Scherman, Barbara Demeneix, and Jean-Paul Behr. A versatile vector for gene and oligonucleotide transfer into cells in culture and in vivo: polyethylenimine. *Proceedings of the National Academy of Sciences*, 92(16):7297–7301, 1995.

[95] Rikke V Benjaminsen, Maria A Mattebjerg, Jonas R Henriksen, S Moein Moghimi, and Thomas L Andresen. The possible "proton sponge" effect of polyethylenimine (pei) does not include change in lysosomal ph. *Molecular Therapy*, 21(1):149–157, 2013.

[96] Beichu Guo, Shunjun Fu, Jinyu Zhang, Bei Liu, and Zihai Li. Targeting inflammasome/il-1 pathways for cancer immunotherapy. *Scientific reports*, 6:36107, 2016.

[97] John T Wilson, Salka Keller, Matthew J Manganiello, Connie Cheng, Chen-Chang Lee, Chinonso Opara, Anthony Convertine, and Patrick S Stayton. ph-responsive nanoparticle vaccines for dual-delivery of antigens and immunostimulatory oligonucleotides. *ACS nano*, 7(5):3912–3925, 2013.

[98] Christopher E Nelson, James R Kintzing, Ann Hanna, Joshua M Shannon,

Mukesh K Gupta, and Craig L Duvall. Balancing cationic and hydrophobic content of pegylated sirna polyplexes enhances endosome escape, stability, blood circulation time, and bioactivity in vivo. *ACS nano*, 7(10):8870–8880, 2013.

[99] Anthony J Convertine, Danielle SW Benoit, Craig L Duvall, Allan S Hoffman, and Patrick S Stayton. Development of a novel endosomolytic diblock copolymer for sirna delivery. *Journal of Controlled Release*, 133(3):221–229, 2009.

[100] Niren Murthy, Jean Campbell, Nelson Fausto, Allan S Hoffman, and Patrick S Stayton. Design and synthesis of ph-responsive polymeric carriers that target uptake and enhance the intracellular delivery of oligonucleotides. *Journal of Controlled Release*, 89(3):365–374, 2003.

[101] Meredith A Jackson, Sean K Bedingfield, Fang Yu, Mitchell E Stokan, Rachel E Miles, Elizabeth J Curvino, Ella N Hoogenboezem, Rachel H Bonami, Shrusti S Patel, Peggy L Kendall, et al. Dual carrier-cargo hydrophobization and charge ratio optimization improve the systemic circulation and safety of zwitterionic nano-polyplexes. *Biomaterials*, 192:245–259, 2019.

[102] A. Ribas and J. D. Wolchok. Cancer immunotherapy using checkpoint blockade. *Science*, 359(6382):1350–1355, 2018.

[103] S. L. Topalian, C. G. Drake, and D. M. Pardoll. Immune checkpoint blockade: a common denominator approach to cancer therapy. *Cancer Cell*, 27(4):450–61, 2015.

[104] P. Sharma and J. P. Allison. Immune checkpoint targeting in cancer therapy: toward combination strategies with curative potential. *Cell*, 161(2):205–14, 2015.

[105] P. Gotwals, S. Cameron, D. Cipolletta, V. Cremasco, A. Crystal, B. Hewes, B. Mueller, S. Quaratino, C. Sabatos-Peyton, L. Petruzzelli, J. A. Engelman, and

G. Dranoff. Prospects for combining targeted and conventional cancer therapy with immunotherapy. *Nat Rev Cancer*, 17(5):286–301, 2017.

[106] Michael A Postow, Margaret K Callahan, and Jedd D Wolchok. Immune checkpoint blockade in cancer therapy. *Journal of Clinical Oncology*, 33(17):1974, 2015.

[107] Nicholas McGranahan, Andrew JS Furness, Rachel Rosenthal, Sofie Ramskov, Rikke Lyngaa, Sunil Kumar Saini, Mariam Jamal-Hanjani, Gareth A Wilson, Nicolai J Birkbak, and Crispin T Hiley. Clonal neoantigens elicit t cell immunoreactivity and sensitivity to immune checkpoint blockade. *Science*, 351(6280):1463–1469, 2016.

[108] R. Zappasodi, T. Merghoub, and J. D. Wolchok. Emerging concepts for immune checkpoint blockade-based combination therapies. *Cancer Cell*, 33(4):581–598, 2018.

[109] M. Binnewies, E. W. Roberts, K. Kersten, V. Chan, D. F. Fearon, M. Merad, L. M. Coussens, D. I. Gabrilovich, S. Ostrand-Rosenberg, C. C. Hedrick, R. H. Vonderheide, M. J. Pittet, R. K. Jain, W. Zou, T. K. Howcroft, E. C. Woodhouse, R. A. Weinberg, and M. F. Krummel. Understanding the tumor immune microenvironment (time) for effective therapy. *Nat Med*, 24(5):541–550, 2018.

[110] D. S. Chen and I. Mellman. Elements of cancer immunity and the cancer-immune set point. *Nature*, 541(7637):321–330, 2017.

[111] A. Iwasaki and R. Medzhitov. Toll-like receptor control of the adaptive immune responses. *Nat Immunol*, 5(10):987–95, 2004.

[112] K. D. Moynihan and D. J. Irvine. Roles for innate immunity in combination immunotherapies. *Cancer Res*, 77(19):5215–5221, 2017.

[113] L. Corrales, V. Matson, B. Flood, S. Spranger, and T. F. Gajewski. Innate immune signaling and regulation in cancer immunotherapy. *Cell Res*, 27(1):96–108, 2017.

[114] D. L. Elion and R. S. Cook. Harnessing rig-i and intrinsic immunity in the tumor microenvironment for therapeutic cancer treatment. *Oncotarget*, 9(48):29007–29017, 2018.

[115] A. Mullard. Can innate immune system targets turn up the heat on 'cold' tumours? *Nat Rev Drug Discov*, 17(1):3–5, 2018.

[116] Siamon Gordon. Pattern recognition receptors: doubling up for the innate immune response. *Cell*, 111(7):927–930, 2002.

[117] P. Kamath, E. Darwin, H. Arora, and K. Nouri. A review on imiquimod therapy and discussion on optimal management of basal cell carcinomas. *Clin Drug Investig*, 2018.

[118] J. D. Campbell. Development of the cpg adjuvant 1018: A case study. *Methods Mol Biol*, 1494:15–27, 2017.

[119] K. Iribarren, N. Bloy, A. Buque, I. Cremer, A. Eggermont, W. H. Fridman, J. Fucikova, J. Galon, R. Spisek, L. Zitvogel, G. Kroemer, and L. Galluzzi. Trial watch: Immunostimulation with toll-like receptor agonists in cancer therapy. *Oncoimmunology*, 5(3):e1088631, 2016.

[120] M. Kiss, S. Van Gassen, K. Movahedi, Y. Saeys, and D. Laoui. Myeloid cell heterogeneity in cancer: not a single cell alike. *Cell Immunol*, 330:188–201, 2018.

[121] Roman Barbalat, Sarah E Ewald, Maria L Mouchess, and Gregory M Barton. Nucleic acid recognition by the innate immune system. *Annual Review of Immunology*, 29:185–214, 2011.

[122] X. Cao. Self-regulation and cross-regulation of pattern-recognition receptor signalling in health and disease. *Nat Rev Immunol*, 16(1):35–50, 2016.

[123] Laurence Zitvogel, Lorenzo Galluzzi, Oliver Kepp, Mark J Smyth, and Guido Kroemer. Type i interferons in anticancer immunity. *Nature Reviews Immunology*, 15(7):405, 2015.

[124] Antonella Sistigu, Takahiro Yamazaki, Erika Vacchelli, Kariman Chaba, David P Enot, Julien Adam, Ilio Vitale, Aicha Goubar, Elisa E Baracco, and Catarina Remédios. Cancer cell–autonomous contribution of type i interferon signaling to the efficacy of chemotherapy. *Nature medicine*, 20(11):1301, 2014.

[125] George Kassiotis and Jonathan P Stoye. Immune responses to endogenous retroelements: taking the bad with the good. *Nature Reviews Immunology*, 16(4):207, 2016.

[126] Katherine B Chiappinelli, Pamela L Strissel, Alexis Desrichard, Huili Li, Christine Henke, Benjamin Akman, Alexander Hein, Neal S Rote, Leslie M Cope, and Alexandra Snyder. Inhibiting dna methylation causes an interferon response in cancer via dsrna including endogenous retroviruses. *Cell*, 162(5):974–986, 2015.

[127] Delphine Goubau, Martin Schlee, Safia Deddouche, Andrea J Pruijssers, Thomas Zillinger, Marion Goldeck, Christine Schuberth, Annemarthe G Van der Veen, Tsutomu Fujimura, and Jan Rehwinkel. Antiviral immunity via rig-i-mediated recognition of rna bearing 5'-diphosphates. *Nature*, 514(7522):372, 2014.

[128] V Hornung, J Ellegast, S Kim, K Brzózka, A Jung, H Kato, H Poeck, S Akira, K K Conzelmann, M Schlee, S Endres, and G Hartmann. 5'-triphosphate rna is the ligand for rig-i. *Science*, 314(5801):994–997, 2006.

[129] Andreas Schmidt, Tobias Schwerd, Wolfgang Hamm, Johannes C Hellmuth,

Sheng Cui, Michael Wenzel, Franziska S Hoffmann, Marie-Cecile Michallet, Robert Besch, Karl-Peter Hopfner, Stefan Endres, and Simon Rothenfusser. 5'-triphosphate rna requires base-paired structures to activate antiviral signaling via rig-i. *Proceedings of the National Academy of Sciences of the United States of America*, 106(29):12067–12072, 2009.

[130] Reneé C Ireton and Michael Gale. Rig-i like receptors in antiviral immunity and therapeutic applications. *Viruses*, 3:906–19, 2011.

[131] Andrew Kohlway, Dahai Luo, David C Rawling, Steve C Ding, and Anna Marie Pyle. Defining the functional determinants for rna surveillance by rig-i. *EMBO reports*, 14:772–9, 2013.

[132] Veit Hornung and Eicke Latz. Intracellular dna recognition. *Nature reviews. Immunology*, 10:123–30, 2010.

[133] Jasper G van den Boorn, Winfried Barchet, and Gunther Hartmann. Nucleic acid adjuvants: toward an educated vaccine. *Advances in Immunology*, 114:1–32, 2012.

[134] Taeko Matsushima-Miyagi, Koji Hatano, Motonari Nomura, Liu Li-Wen, Tomoyuki Nishikawa, Kotaro Saga, Takashi Shimbo, and Yasufumi Kaneda. Trail and/or noxa are selectively up-regulated in prostate cancer cells downstream of the rig-i/mavs signaling pathway by non-replicating sendai virus particles. *Clinical Cancer Research*, page clincanres. 1595.2012, 2012.

[135] Robert Besch, Hendrik Poeck, Tobias Hohenauer, Daniela Senft, Georg Häcker, Carola Berking, Veit Hornung, Stefan Endres, Thomas Ruzicka, and Simon Rothenfusser. Proapoptotic signaling induced by rig-i and mda-5 results in type i interferon–independent apoptosis in human melanoma cells. *The Journal of Clinical Investigation*, 119(8):2399–2411, 2009.

[136] P Duewell, A Steger, H Lohr, H Bourhis, H Hoelz, SV Kirchleitner, MR Stieg, S Grassmann, S Kobold, and JT Siveke. Rig-i-like helicases induce immunogenic cell death of pancreatic cancer cells and sensitize tumors toward killing by cd8+ t cells. *Cell Death and Differentiation*, 21(12):1825, 2014.

[137] Tatyana O Kabilova, Aleksandra V Sen'kova, Valeriy P Nikolin, Nelly A Popova, Marina A Zenkova, Valentin V Vlassov, and Elena L Chernolovskaya. Antitumor and antimetastatic effect of small immunostimulatory rna against b16 melanoma in mice. *PloS one*, 11(3):e0150751, 2016.

[138] Attila Szabo, Tunde Fekete, Gabor Koncz, Brahma V Kumar, Kitti Pazmandi, Zsofia Foldvari, Balazs Hegedus, Tamas Garay, Attila Bacsi, and Eva Rajnavolgyi. Rig-i inhibits the mapk-dependent proliferation of braf mutant melanoma cells via mkp-1. *Cellular signalling*, 28(5):335–347, 2016.

[139] John T Wilson, Salka Keller, Matthew J Manganiello, Connie Cheng, Chen-Chang Lee, Chinonso Opara, Anthony Convertine, and Patrick S Stayton. ph-responsive nanoparticle vaccines for dual-delivery of antigens and immunostimulatory oligonucleotides. *ACS Nano*, 7:3912–25, 2013.

[140] A J Convertine, D S W Benoit, C L Duvall, A S Hoffman, and P S Stayton. Development of a novel endosomolytic diblock copolymer for sirna delivery. *Journal of Controlled Release*, 133(3):221–229, 2009.

[141] A J Convertine, C Diab, M Prieve, A Paschal, A S Hoffman, P H Johnson, and P S Stayton. ph-responsive polymeric micelle carriers for sirna drugs. *Biomacromolecules*, 11(11):2904–2910, 2010.

[142] Craig L Duvall, Anthony J Convertine, Danielle S W Benoit, Allan S Hoffman, and Patrick S Stayton. Intracellular delivery of a proapoptotic peptide via conjugation

to a raft synthesized endosomolytic polymer. *Molecular Pharmaceutics*, 7(2):468–476, 2010.

[143] Salka Keller, John T Wilson, Gabriela I Patilea, Hanna B Kern, Anthony J Convertine, and Patrick S Stayton. Neutral polymer micelle carriers with ph-responsive, endosome-releasing activity modulate antigen trafficking to enhance cd8(+) t cell responses. *Journal of Controlled Release*, 191:24–33, 2014.

[144] Christopher E Nelson, James R Kintzing, Ann Hanna, Joshua M Shannon, Mukesh K Gupta, and Craig L Duvall. Balancing cationic and hydrophobic content of pegylated sirna polyplexes enhances endosome escape, stability, blood circulation time, and bioactivity in vivo. *ACS Nano*, 7:8870–80, 2013.

[145] Dongmei Yuan, Mao Xia, Gang Meng, Chun Xu, Yong Song, and Jiwu Wei. Anti-angiogenic efficacy of 5'-triphosphate sirna combining vegf silencing and rig-i activation in nsclcs. *Oncotarget*, 6(30):29664, 2015.

[146] Xian-Yang Li, Lin-Jia Jiang, Lei Chen, Meng-Lei Ding, He-Zhou Guo, Wu Zhang, Hong-Xin Zhang, Xiao-Dan Ma, Xiang-Zhen Liu, and Xiao-Dong Xi. Rig-i modulates src-mediated akt activation to restrain leukemic stemness. *Molecular cell*, 53(3):407–419, 2014.

[147] Kirsten Kübler, Nadine Gehrke, Soheila Riemann, Volker Böhnert, Thomas Zillinger, Evelyn Hartmann, Martin Pölcher, Christian Rudlowski, Walther Kuhn, Gunther Hartmann, and Winfried Barchet. Targeted activation of rna helicase retinoic acid-inducible gene-i induces proimmunogenic apoptosis of human ovarian cancer cells. *Cancer Research*, 70(13):5293–5304, 2010.

[148] Dengzhe Li, Robert Peter Gale, Yanfeng Liu, Baoxia Lei, Yuan Wang, Dongmei Diao, and Mei Zhang. 5'-triphosphate sirna targeting mdr1 reverses multi-drug

resistance and activates rig-i-induced immune-stimulatory and apoptotic effects against human myeloid leukaemia cells. *Leukemia research*, 58:23–30, 2017.

[149] James J Lee and Edward Chu. Recent advances in the clinical development of immune checkpoint blockade therapy for mismatch repair proficient (pmmr)/non-msi-h metastatic colorectal cancer. *Clinical Colorectal Cancer*, 2018.

[150] Suruchi N Schock, Neha V Chandra, Yuefang Sun, Takashi Irie, Yoshinori Kitagawa, Bin Gotoh, Laurent Coscoy, and Astar Winoto. Induction of necroptotic cell death by viral activation of the rig-i or sting pathway. *Cell Death and Differentiation*, 24(4):615, 2017.

[151] Attila Szabo and Eva Rajnavolgyi. Collaboration of toll-like and rig-i-like receptors in human dendritic cells: triggering antiviral innate immune responses. *American journal of clinical and experimental immunology*, 2:195–207, 2013.

[152] L. Galluzzi, A. Buque, O. Kepp, L. Zitvogel, and G. Kroemer. Immunogenic cell death in cancer and infectious disease. *Nat Rev Immunol*, 17(2):97–111, 2017.

[153] Alice O Kamphorst, Koichi Araki, and Rafi Ahmed. Beyond adjuvants: Immunomodulation strategies to enhance t cell immunity. *Vaccine*, 33 Suppl 2:B21–B28, 2015.

[154] J. I. Andorko and C. M. Jewell. Designing biomaterials with immunomodulatory properties for tissue engineering and regenerative medicine. *Bioeng Transl Med*, 2(2):139–155, 2017.

[155] Frank Wegmann, Kate H Gartlan, Ali M Harandi, Sarah A Brinckmann, Margherita Coccia, William R Hillson, Wai Ling Kok, Suzanne Cole, Ling-Pei Ho, Teresa Lambe, Manoj Puthia, Catharina Svanborg, Erin M Scherer, George Krashias, Adam Williams, Joseph N Blattman, Philip D Greenberg, Richard A

Flavell, Amin E Moghaddam, Neil C Sheppard, and Quentin J Sattentau. Polyethyleneimine is a potent mucosal adjuvant for viral glycoprotein antigens. *Nature Biotechnology*, 30(9):883–888, 2012.

[156] E. C. Carroll, L. Jin, A. Mori, N. Munoz-Wolf, E. Oleszycka, H. B. T. Moran, S. Mansouri, C. P. McEntee, E. Lambe, E. M. Agger, P. Andersen, C. Cunningham, P. Hertzog, K. A. Fitzgerald, A. G. Bowie, and E. C. Lavelle. The vaccine adjuvant chitosan promotes cellular immunity via dna sensor cgas-sting-dependent induction of type i interferons. *Immunity*, 44(3):597–608, 2016.

[157] Saikat Manna, William J. Howitz, Nathan J. Oldenhuis, Alexander C. Eldredge, Jingjing Shen, Fnu Naorem Nihesh, Melissa B. Lodoen, Zhibin Guan, and Aaron P. Esser-Kahn. Immunomodulation of the nlrp3 inflammasome through structure-based activator design and functional regulation via lysosomal rupture. *ACS Central Science*, 4(8):982–995, 2018.

[158] Aurélien Marabelle, Holbrook Kohrt, Christophe Caux, and Ronald Levy. Intratumoral immunization: a new paradigm for cancer therapy. *Clinical Cancer Research : an Official Journal of the American Association for Cancer Research*, 20(7):1747–1756, 2014.

[159] MS Ferritto and DA Tirrell. Poly (2-ethylacrylic acid). 1992.

[160] C. R. Palmer, M. E. Jacobson, O. Fedorova, A. M. Pyle, and J. T. Wilson. Environmentally triggerable retinoic acid-inducible gene i agonists using synthetic polymer overhangs. *Bioconjug Chem*, 29(3):742–747, 2018.

[161] Mary M Tomayko and C Patrick Reynolds. Determination of subcutaneous tumor size in athymic (nude) mice. *Cancer chemotherapy and pharmacology*, 24(3):148–154, 1989.

[162] Attila Szabo and Eva Rajnavolgyi. Collaboration of toll-like and rig-i-like receptors in human dendritic cells: triggering antiviral innate immune responses. *American journal of clinical and experimental immunology*, 2(3):195, 2013.

[163] Parwinder Gill, Nina Lakhani Jindal, Amanda Jagdis, and Peter Vadas. Platelets in the immune response: revisiting platelet-activating factor in anaphylaxis. *Journal of Allergy and Clinical Immunology*, 135(6):1424–1432, 2015.

[164] Christian R Palmer, Max E Jacobson, Olga Fedorova, Anna M Pyle, and John T Wilson. Environmentally triggerable retinoic acid-inducible gene i agonists using synthetic polymer overhangs. *Bioconjugate chemistry*, 29(3):742–747, 2018.